Applications of Ultrasound-targeted Microbubble Cavitation with Nitrite and Nitro-alkenes

by

Gary Yu

B.S. in Biomedical Engineering, University of California, Berkeley, 2015

Submitted to the Graduate Faculty of the

Swanson School of Engineering in partial fulfillment

of the requirements for the degree of

Doctor of Philosophy

University of Pittsburgh

2020

UNIVERSITY OF PITTSBURGH

SWANSON SCHOOL OF ENGINEERING

This dissertation was presented

by

Gary Yu

It was defended on

March 25, 2020

and approved by

Harvey Borovetz, PhD, Professor, Department of Bioengineering

Sanjeev Shroff, PhD, Professor, Department of Bioengineering

Howard Aizenstein, MD, PhD, Professor, Departments of Psychiatry and Bioengineering

Kim Kang, PhD, Associate Professor, Departments of Bioengineering and Medicine

Dissertation Director: John Pacella, MD, MS, Associate Professor, Departments of Medicine and Bioengineering

Applications of Ultrasound-targeted Microbubble Cavitation with Nitrite and Nitro-alkenes

Gary Z. Yu, PhD

University of Pittsburgh, 2020

Microvascular obstruction is a common repercussion of percutaneous coronary intervention in treating acute myocardial infarction, and results from a combination of downstream microembolization, ischemia-reperfusion injury, and inflammation. Ultrasound-targeted microbubble cavitation (UTMC) uses external therapeutic ultrasound pulsation to target intravascularly infused microbubble contrast agents to produce shear stresses which mechanically disrupt obstructing microemboli. This work aims to enhance the therapeutic effects of UTMC through synergistic co-administration of nitrite for enhancement of perfusion and nitric oxide bioavailability (Aim 1) and develop a novel microbubble agent using nitro-alkenes for therapeutic reduction of inflammation after ischemia-reperfusion injury (Aim 2).

For characterization and optimization of nitrite co-therapy with UTMC, a rat gastrocnemius model was used with contrast-enhanced ultrasound imaging. A nitric oxide porphyrinic membrane catheter probe was inserted into the treatment site for real-time measurement of nitric oxide concentration changes. In addition to nitrite co-therapy, effects of administering an endothelial nitric oxide synthase inhibitor as well as varying microbubble concentration and therapeutic ultrasound pressure were studied. Results showed that UTMC and nitrite demonstrated positive synergy for enhancing nitric oxide concentration and perfusion which depended on functional endothelial nitric oxide synthase.

After a novel nitro-alkene microbubble agent was synthesized and characterized, it was applied in both healthy and ischemia-reperfusion injury rat gastrocnemius models. Tissue samples were collected after treatment for quantification of nitro-alkene delivery, changes in inflammatory gene expression, and contrast-enhanced ultrasound imaging was used to quantify changes in hindlimb perfusion after treatment. Results showed that incorporation of the nitro-alkene into a microbubble formulation with UTMC greatly enhanced targeted tissue delivery of the nitro-alkene compared to standard microbubbles co-administered with the nitro-alkene and systemic infusion of the nitro-alkene alone. In addition, nitro-alkene microbubble UTMC resulted in greatly enhanced perfusion as well as decreases in inflammatory gene expression.

In summary, both of these applications of enhancing UTMC therapy demonstrate significant mechanistic interactions with endogenous nitric oxide metabolism and may serve to enhance nitric oxide bioavailability through different pathways. They may also improve the relevance of UTMC in treating the biological sequelae of microvascular obstruction without compromising its mechanical function in disrupting microemboli.

Table of Contents

List of Figures

Preface

Nitro-alkenes and nitro-fatty acids are used interchangeably in this work. Ultrasound-targeted microbubble cavitation is referred to as UTMC.

1.0 Basics of Ultrasound

This chapter serves as a background to the ultrasound (US) component of ultrasound-targeted microbubble cavitation (UTMC). Fundamental principles of ultrasound technology are discussed, with additional details regarding harmonic imaging due to its relevance to microbubble (MB) contrast agents. Use of MB contrast agents in imaging and their characterization and interactions will also be discussed but primarily with an imaging focus. Their various compositions, functionalizations, and applications will be discussed in a later chapter. Applications of US imaging in various clinical contexts will be discussed as well, albeit briefly because of the vast and diverse literature which is ever-expanding. Therapeutic US without the combination of MBs will also be briefly discussed briefly given its differences in mechanisms and applications compared to UTMC.

1.1 Basic Principles of Ultrasound

Sound is at its essence, a longitudinal wave involving the compression and rarefaction of particles. It requires a source, such as a vibrating object, as well as a medium through which to propagate. For example, acoustic speakers that one might find at a musical concert generate sound through vibration of a membrane, which then propagates through air as its medium, before being received in the ears of the audience. Sound waves have general wave properties such as frequency, or the number of cyclical pressure changes occurring at a point in space over a unit of time (with units of cycles per second, or hertz abbreviated Hz), peak pressure, which is the greatest

compressive or rarefactive pressure reached over the course of a cycle of the sound wave (with units of pressure in pascals abbreviated Pa), and propagation speed, which is the speed of the sound wave traveling through the medium itself, which is determined by physical properties of the medium especially density and stiffness (with units of velocity such as meters per second).

As its name implies, ultrasound (US) is sound with frequency in excess of the upper limit of human hearing (approximately 20 kHz), similar to how ultraviolet light is light with frequency greater than that of violet light. In clinical contexts, the overall range of frequencies of US used may vary from 1 MHz to 20 MHz, depending on the source consulted [1, 2]. Additional methods of describing US arise from its application, such as using pulses of US at a time. Descriptions for pulsed US may include the number of cycles, or oscillations of compression and rarefaction, pulse length, or the time needed for a pulse to pass a point in space (which is based on the frequency of the pulse and number of cycles), as well as the pulse period, which is the time from the start of one pulse to the next, given that there may be a pause between pulses. For more complicated US pulses, the term duty cycle may also be used, which refers to the fraction of one pulse period in which the US is active. An example of a full description (and also the US scheme used in many treatments described in this dissertation) is 1.5 MPa at 1 MHz with 5000 cycles and a 3 s period. Additionally, pulse repetition frequency (PRF), or the number of pulses transduced per unit time, is also a measure that may be used. Given that US has both therapeutic and imaging applications, these parameters will affect varying aspects of each application.

1.2 Ultrasound Transducers

US waves are produced by transducers which contain piezoelectric elements that convert electrical signals into vibrations. Modern US transducers favor artificial ferroelectric ceramics, of which lead zirconate titanate (PZT) is the most common. The arrangements of these materials in combination with others such as various plastics including polyvinylidene difluoride (PVDF) have been explored as well. PVDF may be polarized and chemically treated to enhance its piezoelectric properties. More recently, capacitive micromachined US transducers have been developed using micro-electromechanical systems, allowing for a wider range of shapes and dimensions. US transducers may employ a wide range of numbers and arrangements of these elements for various effects, with the simplest being the single-element transducer, with one element for transmitting US and one for receiving. Other designs include the annular array, the linear array, and even curved arrays [3, 4].

Although further detail regarding more complex designs of US transducers will not be covered in this dissertation, the key idea is that many of these designs aspire toward characteristics of an US transducer with ideal compatibility with human imaging, which include having a characteristic acoustic impedance (which is the ratio of pressure to volume flow, and also the density of the medium times the speed of sound, generally representative of the resistance of a material to the transmission of sound) matching that of the human body, being highly efficient in the production of US pulses and highly sensitive in receiving pulses, and having a wide range of amplitude pressures (dynamic range) as well as frequencies.

The majority of work described in this dissertation was performed with a single element transducer for therapeutic US delivery, and a linear array transducer for simultaneous imaging.

1.3 Basic Concepts in Ultrasound Imaging

The basic principles of US imaging have remained relatively unchanged since its earliest developments. Imaging US uses a pulse-echo approach which is coupled with a visual display. In this method, the US transducer transmits pulses into the body, and then receives any reflected waves (echoes) and converts them into an image which may then be interpreted. Reflection of US waves known as echoes occur at the boundary between materials of different acoustic impedances, with the strength of the echo dependent on the difference in acoustic impedances. Conversely, materials with the same acoustic impedance will not generate an echo, and the US waves will merely pass through the boundary [5].

In the context of the human body, impedances of various tissue components and mediums have been calculated and translated into percentages of reflection of US at their boundaries. Soft tissue boundaries and soft tissue to fluid boundaries have very low percentages of reflection (up to 2% reflected), while soft tissue to hard tissue boundaries (such as fat to bone) have very high percentages of reflection (up to 50% reflected). The soft tissue to air boundary, such as from pleural membrane to pleural space, or at the skin surface, will reflect almost all US waves and prevent imaging of more distal structures. It is for this reason that coupling of the US transducer to the skin surface using gel is required, as well as strategic placement of the transducer to avoid unwanted reflection by bones [1, 6].

For these reflections, if the interface between the two mediums is a large, smooth surface orthogonal to the wave propagation direction, the reflection (called specular reflection) will travel directly back to the transducer. However, if the angle of incidence for the US waves is not orthogonal to the surface, the resulting echo will return from the boundary at an angle equal to the angle of incidence. In addition, the remaining transmitted beam will be refracted, or deviated in

direction, in an amount dependent on the difference in velocity of US between the two mediums of the boundary as detailed by Snell's law of refraction. These concepts are especially relevant to the imaging of foreign objects inside the body, as in the case of a needle, which will have a strong reflection against the soft tissue but may be missed by imaging depending on its angle of insertion [1].

Another behavior of US when encountering a rough or irregular surface, or reflectors smaller than the wavelength of the US pulse, is scattering, in which echoes are produced in a wide range of directions which reduces the overall intensity of the signal which returns to the transducer. The signal that does return generates an image of staticky irregularity known as speckle, which is a representation of the texture in various structures of the body such as the organs or muscle, or even red blood cells in vessels. Analysis of the speckle signal in itself is an entire subject of research which will not be further detailed here [4].

In all, these processes of reflection, refraction, and scattering all contribute to the diminishing of the US waves in intensity in a process referred to as attenuation. In addition to those detailed, other processes such as absorption of the US waves by particles (resulting in vibration and the production of heat) in a manner similar to friction, will limit the depth to which US waves may penetrate [1, 7].

Frequency of the US beam is directly related to its attenuation, that is higher frequency US waves will be more susceptible to attenuation than lower frequency waves. This is because high frequency waves consist of more compression and rarefaction events for the same amount of distance than low frequency waves. These events, which we have described will generate heat through absorption of the US energy by particles of the medium, and therefore reduce the energy of the US wave, while lower frequency waves will lose less energy over the same distance. As

such, lower frequency US is used to visualize deeper structures while higher frequency US is limited to more superficial structures [2].

In addition to depth of penetration, frequency also governs axial resolution of imaging US. Axial resolution is defined as the minimum distance between what can be distinguished as two separate points (representing reflectors) in the direction parallel to US wave propagation. In short, higher frequency US will result in greater numbers of compression and rarefaction over a given distance, which will result in a greater capacity to generate distinguishable echoes for each reflector which are separated by more wavelengths (because the wavelengths are shorter). In contrast, lower frequency US (with greater wavelengths given the same velocity) will result in muddied, overlapping echo signals for two closely positioned reflectors, which, when detected by the transducer, will not be distinguishable as two separate echo events, which results in the visualization of a single reflector, rather than two separate reflectors [8].

Another conceptual explanation for this is in terms of time, such that to distinguish between two separate echo events (generated by closely positioned reflectors), an echo separation time is necessary. A lack of an echo separation time results in the detection of only one event, and only one descriptor. Therefore, higher frequency US, with a shorter time between cycles, is capable of generating a smaller time between echo events, and therefore superior echo separation, and is capable of returning distinct signals for smaller distances between axially positioned reflectors. Mathematically, this concept of axial resolution is calculated to be half of the spatial pulse length, which is the product of the number of cycles in a pulse and the wavelength [8].

With these concepts of frequency, attenuation, and axial resolution, it is apparent that there is an exchange between depth of visualization and visual resolution as frequency changes. That is, lower frequency US will have greater depth of visualization due to less attenuation as the waves

travel through tissue, while having poorer resolution due to the longer wavelengths, while higher frequency US will have less depth of visualization but greater axial resolution. This determines what types of US are suitable for different applications, such as visualization of deeper patient organs versus a needle used for superficial vascular access.

In contrast to axial resolution, lateral resolution refers to the minimum distance that two reflectors may be placed apart perpendicular to the direction of the US beam and still be distinguished as separate events. While in general terms the lateral resolution is improved with narrowing of the US beam width, the width itself will vary with distance from the US transducer surface. At the transducer surface, the width of the beam is approximately equal to the transducer width. As distance from the transducer surface increases, the beam will first converge until it is approximately half of the transducer width (this distance is called the near-zone length) and encloses what is referred to as Fresnel's zone. After this distance, the beam will diverge and return to and even possibly exceed the width of the transducer in what is called the far zone (Fraunhofer's zone) which reaches a distance from transducer to reflector that is twice the near-zone length. This phenomenon occurs due to the slightly phase-shifted travel paths of multiple US waves resulting in patterns of constructive and destructive interference. In addition to this pattern of lateral resolution changes which occurs in simple, unfocused US transducers, transducers may be focused as well either by curving their surfaces or through use of multiple element arrays, resulting in a focal zone of decreased width relative to the transducer width [8].

Aside from axial or lateral resolution, temporal resolution refers to the minimum time between consecutive image frames. This is particularly relevant when US is used to image structures in movement, such as the heart. Although temporal resolution, or framerate, may be manually programmed during recordings of US live imaging (referred to as cine-loops), temporal

resolution in general terms may be improved by reducing the depth or distance which pulses must travel, reducing the width of the imaging frame, and reducing the number of scan lines, which are the segments which compose of the final US image.

1.4 Ultrasound Imaging Modes

Brightness-mode imaging (also referred to as B-mode imaging) is the most common mode of medical US imaging. As its name implies, brightness displayed on a screen corresponds to the received signal from the pulse-echo approach previously described. In brief, transmitted pulses of US into the human body are then reflected back to the transducer, which then processes the signal from many pulses in sequence and combine them to generate an image. This image construction occurs in real-time and may produce the appearance of continual movement with the improvements in temporal resolution made in modern equipment, allowing physicians to use US to visualize movement of tissues and medical equipment in imaging-guided procedures. In addition, it is possible to change various parameters of the US pulse to modify the imaging outputs in areas such as depth, which involves changing the focus and time delay in receiving US echoes smoothly. This is also called dynamic focusing, as the US beam is always in focus even as echoes are received from structures of different depths. The US transducer structure and its resulting beam pattern determines the shape and quality of the resulting images. For example, element arrays which create a beam focus allow structures placed at the focal distance to be visualized with greater visual clarity [6].

Doppler US imaging involves characterization of moving reflectors or boundaries relative to the transducer. This is based on the Doppler effect by which the relative direction of movement

of a reflector such as a tissue boundary will affect the frequency of reflected US waves. Many modern Doppler US imaging systems are coupled with a B-mode scan and are referred to as color Doppler or color flow Doppler imaging due to their use of the colors red and blue to represent blood flow away or toward the receiving transducer, respectively. It is noted that these colors may also be used to represent magnitude of flow, with blue representing high and red representing low flow. In brief, B-mode imaging is used to localize a region of interest for Doppler imaging. Echoes from this region are isolated and analyzed for frequency shift. The most common application of Doppler imaging in clinical practice is analysis of blood flow with red blood cells being the moving targets. In those cases, it is important to orient the transducer parallel to the direction of motion to maximize the Doppler shift. Aside from color Doppler imaging, spectral Doppler analyzes a specific region and returns a velocity profile (line tracing) rather than visual indicators of flow. Spectral Doppler analysis may either be pulsed or continuous, with the tradeoff of continuous spectral Doppler analysis being an enhanced threshold for maximum flow detection in exchange for precision in localization of flow [5, 9].

Harmonic imaging, as it is pivotal to the imaging of microbubble contrast agents central to this dissertation, will be described briefly as well. Harmonic frequencies are frequencies which are integer multiples of the original frequency of the transmitted US pulse (which is also referred to as the first harmonic). Accordingly, the second harmonic of an US pulse, or wave, has twice the frequency as the first harmonic. This phenomenon occurs as US waves traveling through tissue become distorted and interact with each other in constructive and destructive interference. Some sources note that this may have been originally discovered by accident, that the pulse-echo technique applied to deeper tissue locations resulted in a significant second harmonic frequency signal. The received signal may then be filtered for specific frequencies of the harmonic

components, resulting in the exclusion of noise, and improvement of various aspects such as lateral resolution, reduced artifacts, and improvement in signal-to-noise ratio. The reason for harmonic imaging's relevance to microbubble contrast agents is that the microbubbles, due to their size, oscillate at a similar frequency to that of the harmonic frequencies of imaging US pulses. This concept will be further discussed in the section on microbubble contrast agents [10-12].

1.5 Summary of US Imaging

In all, US imaging is a versatile, mobile, and highly adaptable mode of imaging which has contributed significantly to the improvement of clinical practice, from diagnosis to intervention. Even now, advances are being made to expand the capacity of US imaging such as super-resolution US imaging, US tissue elastography, among others. In this dissertation, US was utilized in its B-mode imaging and therapeutic capacities (which is also the subject of another section's discussion). Imaging of rat hindlimbs was performed in both B-mode (mainly for transducer alignment) and contrast (harmonic) modes for evaluation of microvascular perfusion using microbubble contrast agents (which also doubled as therapeutic agents). Said microbubble contrast agents will be discussed in a later chapter.

1.6 Therapeutic Ultrasound Without Microbubble Contrast Agents

Although the subject of this dissertation involves therapeutic US applied in conjunction with microbubble (MB) contrast agents referred to as ultrasound-targeted microbubble cavitation

(UTMC), it would be remiss of us to disregard the therapeutic applications of US in absence of said MBs given its role in various fields of physical therapy, rehabilitation, and medical practice. While this is an entire field of study, we will summarize the biophysical mechanisms of therapeutic US and its various applications.

Therapeutic US has typically been classified into two regimes based on intensity. Low intensity (around 0.1 to 3 watts per square centimeter) has applications in facilitating and stimulating various normal physiological processes, usually in response to various soft tissue or superficial injuries, or also to sensitize the skin for superficial delivery of various therapeutic agents. High intensity (usually greater than 5 watts per square centimeter) therapeutic US serves the purpose of selectively destroying target tissues [13-15].

Similarly, the biophysical effects of therapeutic US may be divided into thermal and non-thermal effects. Thermal effects, as the name suggests, are based on heat energy produced by the interaction between US waves and tissue. As we discussed earlier in the various interactions between US and its medium of propagation, loss of energy through heat is a significant component of US attenuation due to the waves causing vibrations of particles in a manner akin to friction. High frequency US, because it entails more compression and rarefaction (both of which cause particle vibration) events per distance, will attenuate over a shorter duration and lose energy in the form of heat more readily than lower frequency US. This phenomenon is called acoustic absorption. As in other contexts of heat transfer from an energy source to a medium, the rate of heat absorption is described by both the intensity of the source as well as a coefficient characteristic of the medium. In this case, additional factors mediating this relationship include density of the tissue and its specific heat capacity. Various types of tissue, with different structural compositions,

will have different heat capacities. An early report estimates absorption to account for the majority of attenuation in the context of biological tissues [13, 16].

This concept of heat transfer to tissues through US waves has historically been thought of being key to its applications, for example in physiotherapy, where the target connective tissues (being highly collagenous) have high heat absorption coefficients and may be targeted selectively by therapeutic US. Other similar targets may include synovium and joint capsules, muscles and their fascia, tendons and tendon sheaths, and major nerves. Benefits thought to arise from this application of heating include improvements in blood flow, decrease in stiffness, decrease in muscle spasms, and overall pain relief in the patient [15, 17].

However, this perspective has been challenged in more contemporary studies of therapeutic ultrasound, which have localized changes in blood flow due to heating to be predominantly in the skin. In addition, increased blood flow has resulted in greater circulation of cooler blood to further diminish the warming effect. Studies involving radioactive tracers in human subjects have shown that the heating effect produced by US is also completely dwarfed by moderate exercise. While it has been proposed that higher intensities of US would also result in greater effects of heating, said intensities would no longer be therapeutically appropriate due to the pain that would likely be elicited in the patient. In addition, the idea of US heating improving flexibility of human connective tissue has not been found to be significant in human studies, and the effect size found in animal trials has led to discrepancies in therapeutic feasibility, leading many to believe that purely thermal effects of US are unlikely to be beneficial [15, 18].

Despite flaws in earlier assumptions made regarding the benefits of therapeutic US, more recent clinical applications have broadened and flourished, possibly in part due to the interest

generated by said earlier studies. Three broad areas of modern therapeutic US include high intensity focused US (HIFU), US-enhanced drug delivery, and shockwave lithotripsy (SWL).

HIFU, as earlier noted in the application of high intensity US to destroy target tissues through heat, has been applied to a wide range of localized pathologies including cancers, benign prostatic hypertrophy, glaucoma, fibroids, and myocardial ischemia, among others. Not only has HIFU been found to cause tissue necrosis, it may also serve a cauterizing purpose for hemostasis, and has found additional use in emergency care for trauma control. In addition to these primary effects, the inflammation and necrosis caused by HIFU has also served as an immunogenic stimulant in eliciting further physiological responses to tissue damage. These immune responses have been thought to additionally contribute to the efficacy of HIFU against various malignancies, specifically in protecting against additional tumor growth. Typical HIFU applications operate in frequencies between 1-10 MHz and at the most common intensities between 1500 to 3000 watts per square centimeter. Certain newer clinical devices are capable of delivering up to 10000 watts per square centimeter. Newer piezoceramic and piezo-composite materials have further enabled development of HIFU therapies, along with array transducers which may further focus the US waves for enhanced effect. Other physical mechanisms of HIFU therapy include development of higher harmonics (as discussed earlier, being multiples in frequency of the base harmonic), which are much more readily absorbed (and therefore generate heat) in target tissues. Whereas previously, development of higher harmonics and therefore increased absorption was seen as undesirable for imaging purposes, the opposite is true for HIFU where absorption is the goal, resulting in a nonlinear conversion between US intensity and heat generation due to these mechanisms [19].

US-enhanced drug delivery involves enhanced transport of drugs over various biological barriers in the human body. These barriers may range from scales including cell membrane disruption and transport, to vascular and extravascular compartments, to even penetration of thrombi for delivery of thrombolytic drugs. Although many studies involving the concept of sonoporation, or poration of membranes by sound, have used MB contrast agents in applications including delivery of genetic molecules to pathologic tissue and delivery of chemotherapeutic drugs to tumor models in animals. Frequencies of US used in these applications are much lower than for HIFU, and typically range around the low to mid kHz, up to 1-2 MHz. Transducers used are also not designed for high intensity performance as in HIFU, and do not necessarily require focusing. However, miniaturization is a direction of future transducer design development, especially for direct intravascular applications. Because many of the mechanisms of US-enhanced drug delivery, such as cavitation and microjetting, are identical to those involving MB contrast agents, these topics will be discussed in a later chapter [18, 20, 21].

Lithotripsy, as the name implies, is the destruction of various types of stones, or accumulated mineralizations, in patient organs, most commonly kidney stones. US regimes for lithotripsy are typically short bursts of high intensity US similar to HIFU, with peak pressures reaching up to 140 MPa. As opposed to HIFU, intensities and durations of US in lithotripsy are limited by potential tissue injury. Many different designs of lithotripters have been implemented clinically, such as piezoceramic spherical lithotripters which employ an array design for the capacity to aim the resulting US beam. While mechanisms such as cavitation are also relevant to lithotripsy, other stone based physical mechanisms have been described including erosion, shear, and compression, due to the interaction between the fluid and stone surfaces. All of these processes are manifestations of the various combination effects of fluid jets resulting from cavitation,

generated cavitational bubbles collapsing and producing shockwaves, and material behaviors of the stones themselves such as fatigue, crack production and propagation, and fragmentation [18].

2.0 Microbubble Contrast Agents and Therapeutics

This chapter will introduce the concept of microbubble (MB) contrast agents used with US imaging. This will include the principles of their physical interactions with US waves and the various MB behaviors induced by said interactions. The physical characterization of MBs will also be discussed such as material properties, composition, and methods of synthesis. Especially relevant to this dissertation will be the various methods and directions in functionalization of these MBs to endow them with therapeutic properties. The directions, therapeutic agents used, and relevant clinical applications will conclude this chapter.

2.1 Contrast-enhanced Ultrasound Imaging

In the previous chapter, the various forms of basic US imaging were discussed, including B-mode imaging and Doppler US imaging. Although the utility of the various modes was described, they have many limitations as well. In clinical scenarios where monitoring of tissue perfusion is the goal, neither of these two broad methods of US imaging are ideal. B-mode imaging is not sensitive to distinguishing change or extent of perfusion. Although larger vessels may be visible in the imaging plane, enabling imaging guided vascular procedures such as catheter placement, tissue perfusion itself is not visible due to both the size limitations of detecting microvascular blood flow, as well as the limited differences in physical properties between the bulk tissue and smaller blood vessels. In addition, Doppler US, while it may detect blood flow and characterize said flow with velocity, is mainly limited to evaluation of larger blood vessels with

higher flow rates. Again, the low volumes and flow rates involved in typical physiologic perfusion are not detectable and are subject to the effects of various imaging artifacts. It is noted that while MB contrast agents were also later used with Doppler US imaging and did result in improved visualization and detection sensitivity for smaller blood vessels due to increased backscattering of the US waves off of contrast agents, visual artifacts such as blooming (over-exaggerated width of the imaged vessel compared to B-mode imaging due to scattering) and motion artifacts (tissue movement producing stronger signals than from the MB contrast), as well as general background noise [1, 7, 22, 23].

In addition to the limitations of the various other modes of US imaging, the desire for enhanced clinical utility was also motivation for the development of more sophisticated contrast-enhanced imaging. For other modalities of medical imaging such as computed tomography and magnetic resonance imaging, contrast utilization to not only observe perfusion but also emphasize focal lesions and other patterns of pathology have greatly assisted in medical diagnosis. It is only relatively recently that US imaging also developed agents which could be administered to patients to improve diagnostic information. Given that US itself is becoming a staple of not only bedside and outpatient point-of-care contexts, but also in intra-operative contexts and in dedicated therapeutic applications, development of US contrast agents, namely MB agents, has become a burgeoning field [23, 24].

2.1.1 Early History of Microbubble Agents

For the MB agents themselves, similar to many other advancements in science, their origin lies in fortunate accidents. The earliest discovery of the utility of MB agents in US imaging was made by Dr. Claude Joyner in the 1960's. Dr. Joyner, a cardiologist, observed transient increases

in US signal intensity when performing a chemical dye injection into a patient's left ventricle. His later investigations showed that these increases were due to the accidental formation and injection of small air bubbles forming at the catheter tip. As such, the earliest MB applications were essentially handmade in the most basic sense, resulting from fluid agitation in the presence of room air. Although these makeshift MBs did function, the inconsistency in their roughshod synthesis limited repeatability and proper scientific study, although these early steps paved the way for later discoveries, such as the stabilization of these bubbles by albumin (which occurred when blood was included in the agitated mixture), leading to the first pharmaceutically officiated contrast agent, Albunex™ [23, 25, 26].

2.1.2 Basic Physical Principles of Contrast-enhanced Ultrasound Imaging

As previously discussed regarding the basis of US reflections being the differential in physical properties at the interface between two mediums, the fundamental source of MB contrast agent utility arises from two main responses of MBs to US waves. One is reflection at the bubble surface arising from the differences in acoustic impedance between the gas inside the MB agent and the surrounding blood or tissue. Generally, MB contrast agents are composed of a gas core stabilized by a shell (although as the earliest and most primitive forms of MB agents were merely agitated saline, those resulting gas particles were extremely short-lived due to the lack of a stabilizing shell). Because the difference in impedance between the MB and surrounding blood is very high, there is a strong, almost complete backscattering effect of US waves when encountering the MBs. However, because of the extremely small MB size and their scarcity in circulation, the actual amount of US which is directly reflected and returns to the transducer is insufficient for strong contrast-enhancing. The other most important aspect of the MBs is that they are echogenic,

meaning they are compressible and will be forced into oscillation along with the US wave itself if the size of the MB is sufficiently smaller than the wavelength of the US wave. In essence, during the compressive positive half cycle of the US wave, the MB will decrease in size, and later increase in size during the rarefactive negative half cycle of the US wave. Similar to a musical instrument, this MB behavior is frequency-dependent and reaches a peak at the resonance frequency, which has been shown to be inversely related to the MB particle size. As a result of this behavior, not only do MBs passively reflect US waves, but they themselves behave as small resonating sources of sound, resulting in a true enhancement of the US signal [27, 28].

With these two main mechanisms in mind, there is a range of MB responses to US waves based on the pressure amplitude of the wave itself. At relatively low amplitudes of US pressure, MB size is linear to the applied acoustic pressure as typically expected. The expansion and compression of the MB is the same in this behavior regime, and the MB shell integrity is relatively stable due to the regular movement it experiences. When US amplitude (pressure) is further increased, MB behavior begins to deviate from the previous pattern. Compression reaches a limit before expansion as smaller bubble volumes begin to resist further compression while further expansion of larger MBs require less energy, and the relative extent of these two phases becomes unequal, resulting in what is referred to as nonlinearity. In addition, the MB size is no longer linearly related to the applied US pressure. Due to this nonlinearity and deviations in MB response, distortions of the original stimulating wave occur, and MB oscillations result in formation of higher multiples of the original base frequency through constructive and destructive interference. This is familiar to us as the development of harmonic frequencies, with the most notable harmonic being the second. Human tissue and blood, being relatively solid and not gas-filled microparticles, do not demonstrate this type of behavior, and therefore the resulting signals produced by MBs may

be separated from that arising from surrounding tissue. Lastly, with even further increases in US amplitude, there has been an abrupt increase in US scattering of the MBs followed by a loss of the MB signal. This occurs as nonlinearity in the MB oscillation is greatly exacerbated, resulting in a loss of the periodic nature of MB behavior when driven by a periodic waveform. This is associated with rupture of the MB shell and release of the gas as well as potential fragmentation of the MB shell and production of smaller daughter MBs. This behavior is also highly nonlinear similar to the prior. The released free gas then proceeds to dissolve in the surrounding liquid (blood) at a rate dependent on the type of gas and its chemical interactions with blood [28-31].

Although there are many forms of terminology for the various behaviors described, for our purposes we will refer to the second behavior as stable cavitation and the last behavior with MB rupture as inertial cavitation. Of course, the change in MB behavior between the various regimes described is continuous depending on the US pressure applied, and there is no all-or-nothing type response in that even at high pressures, only a partial population of circulating MBs may be ruptured depending on the numerous other factors which may affect, distort, or disrupt the applied US signal in a practical application. With these behaviors being the primary basis of the physical behaviors of MBs experiencing US stimulation, other concepts important to discuss are temperature increases, microstreaming and micro-jetting. In Chapter 1, absorption of US energy leading to increases in temperature was discussed as a main component of attenuation. With MBs, this concept still holds true, and excitation of the MBs with US waves results in this absorption and therefore dissipation of energy as a result of friction associated with viscosity and damping forces with oscillation. Generation of higher harmonics, particularly the second harmonic, by MBs, also enhances the heating effect. In addition, this heating effect is distinct from the heat produced during the inertial collapse of the MBs during inertial cavitation. The violent cavitation events may

generate extremely short-lived conditions within the center of the MB reaching up to thousands of degrees Celsius. In these extreme conditions, highly reactive radical chemical species such as hydrogen peroxide may be produced, although said production has been limited to excitation frequencies of 20 to 50 kHz in observation [24, 32].

Microstreaming is the concept of momentum from the oscillating MB transferring to surrounding fluid. This phenomenon may occur on a small scale around MBs undergoing stable cavitation (without collapse) and is of particular interest to clinical application when in close proximity to biological surfaces, such as the vascular endothelial compartment, or red blood cell membranes. In theory, these micro-streams may result in shear stresses along cellular surfaces, which have been though to contribute to not only uptake of extracellular compartment contents by cells, as well as mechanical effects [31, 33].

Micro-jetting on the other hand arises from more violent non-spherical oscillations at large amplitudes of US. During these oscillations, MBs may deform from their normal spherical shape into toroidal shapes when close to a rigid surface, which may produce a high-speed micro-jet directed toward the surface. It has been identified that these micro-jets may puncture and produce transient holes in cellular membranes, termed sonoporation, in *in vitro* studies. It is less clear whether this mechanism occurs *in vivo* given the differences and rigidity of tissue environments. However, recent high-speed microscopy work has shown that these various phenomena of fluid movement around oscillating MBs may produce endothelial invaginations which may be more significant for mechanotransductive pathways [28, 32, 33].

Lastly, two additional phenomena of MBs that have been observed experimentally are primary radiation forces and secondary radiation forces. Primary radiation force is also called the Bjerknes, which describes the tendency of an unfixed object in the path of a propagating US beam

to translate in the direction of the beam. In practice, this may be applied to target MBs into specific tissue areas and even possibly stimulate cellular uptake, although *in vivo* experiments have shown that this is not entirely feasible due to the requirement of having a very high bubble to target (cell) ratio as well as damping effects of blood on MB activity. Secondary radiation force, which is also a Bjerknes force, involves interactions between MBs, nearby particles, and other MBs. This interaction involves MB attachment to a nearby surface which reflects sound radiating from the pulsating bubble, as well as attraction to other nearby particles, resulting in a proximity that may enhance the effectiveness of other behaviors such as micro-jetting and microstreaming. In all, these various behaviors are what dictate the elicited biological effects of targeted MB stimulation on a microscopic level. The various macroscopic physiological effects of the vast aggregation of these miniscule events and their interactions with various pharmacologic agents is the focus of this dissertation [10, 28, 31].

2.1.3 Enhanced Detection of Ultrasound Signals

Previously, the capability of using second-harmonic imaging to detect MBs specifically was discussed. However, to fully isolate the MB signal amidst the scattered tissue signals, additional steps may be taken. One example aside from tuning the US receiver to the specific second harmonic frequency produced by the MBs, is through the use of a narrow band US pulse. Although this will decrease the resulting image resolution due to the decreased range of frequencies, it is specific to MBs in that fewer tissue scattered harmonic signals are generated. In addition, the pulse inversion method of imaging further improves upon the limitations faced by harmonic imaging and allow for lower US power to be used during continuous imaging of MBs. In essence, this technique involves sending two pulses in rapid succession into the tissue, with the

second pulse being an inversion of the first (essentially the opposite such that their sum would cancel each other out). As these two pulses travel through the tissue and eventually encounter the MB agents, they generate echoes which become nonlinear based on the previous principles discussed. Therefore, the echoes are no longer perfect opposites of each other, and their sum is no longer zero. It is this non-zero summation signal which returns to the transducer for detection and is recognized as signal only generated from encountered MBs. In contrast to using a narrow band signal, the pulse inversion method is not restricted to specific frequencies, and as a fuller range of frequencies may be used, a much improved, high-resolution image of the MB echoes may be produced. As such, weaker echoes may also be detected, even at lower US intensities where MBs are not necessarily destroyed. Currently, the pulse inversion method is largely the preferred method of imaging MBs [25, 27, 29].

A different method of imaging, used in the present work in this dissertation, is burst-reperfusion imaging, also called intermittent imaging. This technique relies upon the MB behavior of rupture after stimulation by high pressure US. Essentially, a pulse is applied which bursts all MBs in the imaging field, followed by a wait period to allow for new MBs to replenish the imaging field circulation. It has been established that the speed at which MBs are replenished to an asymptote of maximum brightness is directly correlated to hemodynamic parameters in microvascular perfusion. This technique is unique to US imaging because no other imaging modality has the capacity to instantaneously eliminate all contrast from its visual plane. While this is similar to sensing the technique of detecting the transient echo of destroyed MBs (also known as loss-of-correlation imaging, transient scattering, power-enhanced scattering, and stimulated acoustic emission), typically higher concentrations of MBs are needed for consistent images. Other variations on these techniques, especially pulse inversion or phase inversion mode imaging, have

been recently developed and implemented. Power pulse inversion involves repeating the inverted pulse sequence multiple times and taking the average of the resulting signal, thereby improving the signal-to-noise ratio. Similar to Doppler imaging, the B-mode image may also be displayed in the background for localization of the MB signal. Another technique uses pulse inversion as well as changing the US amplitude pressure, allowing for detection of non-linear signals in the second harmonic at improved sensitivity. This has been implemented as contrast pulse sequences (CPS) and is used in this dissertation work. Yet another approach uses both conventional Doppler imaging as well as the phase inversion pulse sequence to distinguish between slow and stationary MBs as well as indicate the direction of MB flow in larger vessels with conventional red and blue tints and is coined as Vascular Recognition Imaging [24, 27, 29, 31].

2.2 Microbubble Properties and Compositions

After discussing the various physical principles behind the function of MB contrast agents, we will now detail the various properties, characterizations, and compositions of these agents. As the composition and structure of these MB agents, from the types of lipids and gases used, to their size, and shell chemical structure, are all intrinsically tied to their various purposes, function, and enhanced therapeutic potential, the development of novel MB agents is an expansive field of ongoing research.

For all MB contrast agents, survival in the circulating environment is a key optimization parameter. Namely, to enhance longevity, passage through the pulmonary vascular beds was necessary to enable re-circulation of the contrast agent. In addition, stability through the pulmonary environment was also necessary to prevent gas transport of the MB gas component resulting in

patient exhalation of the gas. To address this, a shell was necessary for the MB agent. This was typically a lipid or polymer (or a mixture of both) coat which stabilized the gas core of the MB against dissolving into the surrounding fluid medium. Aside from serving as a stabilizing surfactant, the shell also prevented attachment of the MB to the vascular endothelial compartment of the pulmonary circulation. Another aspect to avoiding entrapment in the pulmonary microcirculation is size, and as such, MB particles were required to be on scale or smaller than red blood cells (around 4-5 microns in diameter). Because with such miniscule size comes an extremely high surface-to-volume ratio, and because room air is highly soluble in the surrounding medium (room air being high in nitrogen content, and patients often having decreased levels of nitrogen gas in their bloodstream due to receiving inhaled oxygen), these early-generation MB shells were highly unstable and short-lived. To address these fundamental issues in stability, two approaches were taken. One was replacing the chemical species of the MB gas core with a more stable alternative. This typically involved fluorocarbon gases rather than air. Fluorocarbon gases have much lower solubility in aqueous mediums compared to room air species, and as such, many later developed clinical agents used some form of fluorocarbon or carbon-species based gas. In addition, high molecular weight gases have greatly reduced tendencies to diffuse through the MB shell membrane and are also biologically inert. The in-house MB agents synthesized in the work of this dissertation followed in this trend, using perfluorobutane as the preferred species for the MB gas core. The other direction of improvement, rather than addressing the contents, was improving on the outer coating, or shell, of the MB. The earliest MBs had crude, simply agitated shells of human albumin mixed with various contaminants from whole blood. Later, synthetic approaches were taken with a mixture of various protein and polymer components. Common polymers used for this application were in the polylactide-co-glycolide family. Due to the

numerous chemical offshoots of these materials, this will be covered in an additional sub-section on coated gas MBs [23, 31, 33].

Despite what seems to be a boundless array of possibilities for MB contrast agents, the general classification of these MB agents into families may be simplified into the following groupings.

2.2.1 Coated Gas Microbubbles

Coated gas MBs are the most common type of MB agent utilized in most imaging and contrast-enhanced US applications. As mentioned earlier, one of the earliest iterations of this form of MB came about by agitating saline with a small amount of human blood mixed in, resulting in air bubbles coated with albumin. This resulted in prolonged contrast enhancement because the albumin barrier increased the MB lifespan considerably due to reducing the interface tension between the gas core of the MB and the surrounding medium (usually blood or saline). Due to commercialization and mass production of these products, newer iterations were developed, although human serum albumin (HSA) remains a popular choice and is used in products such as Albunex and Optison (which are both available for clinical use). Not only is denatured HAS flexible in the shell to allow for sufficient MB response to the US waves and pressure changes when sonicated, but it is also biologically inert due to the denaturation process destroying any immunogenic (antigenic) components of the protein itself. However, as with all protein products, there are always theoretical risks with the transference of viral or prion infections, and therefore the origins of the shell components have been mandated to be disclosed clearly to all patients potentially receiving these agents. Aside from HSA, phospholipids are a popular choice, including in the therapeutic in-house synthesized MB agents used in the work for this dissertation. For

phospholipids, the size and thickness of the shell for the MBs formed are determined by the species of lipids used. Typically, these MB formulations require agitation with a gas-liquid interface present to form the actual MBs, rather than preserving pre-formed MB particles such as with a lyophilized powder which may be frozen and stored. One benefit of using a precise phospholipid mixture is that the resulting MB particles are remarkably stable and consistent in size. In addition, phospholipid coatings are much more stable than protein coatings during sonication as well as during circulation, improving upon MB echogenicity as well as longevity in circulation. Adding a polymer brush layer conjugated to the phospholipid species further improves biocompatibility as well as stability. Due to the various pre-existing conjugation techniques to common polymers such as polyethylene glycol, multiple layers of experimental agents may be added for goals of improving echogenicity, stability, and therapeutic benefit [29, 34].

Another type of MB shell construction involves rigid polymeric species which are superior in creating a leakproof, gas-tight shell which is biodegradable. In comparison with protein or lipid shells, polymer shells are thicker and stiffer. Given that the contrast agent properties of MB agents rely on their response to US sonication and in compression and expansion, these polymer shell MBs are less responsive and therefore less efficient in producing a contrast enhancing effect. However, the benefit of using polymer bubbles is that the shell characteristics are more readily controlled, allowing for specific pressure thresholds of rupture, which may be utilized in a therapeutic context. Other methods of stabilization for these coated MBs include use of a carbohydrate matrix to stabilize the MB in its prepared solution, which then dissolves in the bloodstream, leaving behind a revealed lipid coated MB, such as the case with Echovist and Levovist, which utilize galactose and palmitic acid in these roles. In addition, rather than using physical agitation to form the MBs, hypobaric pressure application with electrical shocks may also

produce phase-changing effects which result in production of particles, such as with EchoGen, which utilizes a liquid-in-liquid emulsion containing a perfluorocarbon gas in the liquid phase [32, 35-37].

Although we have briefly touched upon the most common compositions of coated gas MBs in this section, a later section will expand upon these ideas in further detail and discuss further specifics of the chemical species used.

2.2.2 Other Types of Microbubble Agents

Other categories of MB agents aside from coated gas MBs are phase-shifted emulsions, echogenic liposomes, and cavitation nucleated MBs. Phase-shifted emulsions, as the name implies, consists of an emulsion of volatile fluid droplets and lipid shell components (surfactant molecules). Typically, the volatile component has a boiling/vaporization point close to the normal temperature of the human body (37 degrees Celsius), resulting in formation of the MBs either directly after injection or after sonication at sufficient intensity. The main advantages of this technology include stability during storage and administration, as well as the ability of the agent to diffuse into compartments which are not typically accessible by fully formed MB agents. This type of agent may also be referred to as liquid nanodroplets or nanoparticles, due to the droplet nature of the liquid emulsion while in solution or circulation. The transformation of the phase shift due to US stimulation allows for superior imaging or even therapeutic leverage using these agents for compartments such as the interstitium or tumor masses. Echogenic liposomes are a lipid bilayer (as opposed to a monolayer for the typical coated MBs) which encapsulate both liquid and gas. This type of agent offers enhanced stability compared to phospholipid MBs due to the bilayer, as well as improved delivery of therapeutic agents due to the increased amount of non-aqueous

substances that may be contained. However, these liposomes have decreased gas content compared to conventional MBs, and therefore are less echogenic on imaging as well. Therefore, higher concentrations of liposomes are needed for the equivalent amount of contrast enhancement on imaging and different pulse regimes may be necessary for rupture, although the acoustic qualities themselves of the liposomes (in terms of the efficiency of scattering US rather than directly absorbing US) may actually be superior to conventional MBs [21, 34, 38, 39].

As mentioned in Chapter 1, the concept of cavitation is of itself independent of any MB agents, and therefore the concept of endogenously sourced MBs will also be discussed here. Cavitation, once again, refers to the phenomenon of rarefactive phases of US waves drawing out dissolved gas from the solution medium. This gas may then form MBs, which then behave akin to the agents previously discussed. Various parameters may affect this process, such as temperature, diffusion, and pressure. This cavitation is typically seen only at higher pressures of US than those used for only imaging, and instead at those used for HIFU applications such as surgical ablation. The bubbles may then undergo violent inertial collapse, resulting in damage to the surrounding tissue. In thinking of the development of these bubbles as cascade events of the buildup of gas molecules, the application of MB contrast agents may also be thought of as reducing the threshold necessary for this to occur or reducing the cavitation threshold. Because these MB agents are exogenously seeded into the circulation and provide a basis for the formation of larger bubbles, these MB agents and nanoparticles allow formation of bubbles at much lower US intensities, although the exact mechanisms for this are yet unclear [28, 31, 33, 34].

2.2.3 Microbubble Agent Preparation Methods

Preparation of a MB agent involves whatever steps are necessary to transition from a stock packaged solution to one which is ready for infusion into the patient. The earliest method of preparation involved vigorous agitation of a fluid sample with gas enclosed and remains extremely popular due to its simplicity and lack of technical demands. Nowadays, this may be achieved through either mechanical agitation or through high intensity US dispersal of a gas into a MB coating solution. Characteristics of the agitation including duration, rate, and energy input all affect the resulting MB particles, including concentration and distribution of size. Other methods include simply resuspending particles in solution prior to injection, given pre-formed MBs or liposomes (single-layered membrane preparations). As mentioned before, dissolution of crystalline carbohydrates and phase change of volatile liquids are also methods for MB agent preparation. Other preparation methods include high shear emulsification (which may often be mechanical), or membrane emulsification, which involves extrusion of a liquid through finely sized pores in a membrane and into a suspension of the coat material. However, this method, as well as agitation and sonication, do not produce the most uniform populations of MB particles. More recently developed methods have been designed to offer more control over particle uniformity, and include ink jet printing (which extrudes fluid through mechanical nozzles), which uses only liquid components (therefore requiring additional subsequent steps to evaporate select volatile components resulting in bubble formation), electrohydrodynamic atomization, which involves a stream of fluid being focused in an electrical field, which then breaks the fluid into droplets. Coaxial electrohydrodynamic atomization involves two coaxial streams of fluid, which are placed within one another, resulting in the encapsulation of one fluid stream. Dispersal of the fluid stream into particles then results in formation of MBs and has been successfully demonstrated with

phospholipid and polymer coated gas MBs, as well as liquid filled capsules. Another more recently developed method for MB production which also reports the highest MB particle uniformity is through microfluidic devices, which involves focusing a jet of gas through a microscopic orifice into a flowing stream of fluid. As the gas-liquid interface passes through the orifice, the medium interface becomes unstable, and MB particles are naturally pinched off and deposited into a separate compartment. Addition of therapeutic components through this mean may also be accomplished through positioning various thin layers of oils, drugs, or other aqueous solutions at various positions along the columns of gas and fluid [34, 35, 37].

2.3 Principles of Therapeutic Microbubble Agents

The previous part of Chapter 2 discussed the basic principles behind contrast enhanced US imaging (CEUS), the early development of MB agents, the various behaviors of MBs when targeted by an US field, methods behind enhanced detection of contrast MB signals, and a cursory discussion of the various types of contrast MBs and their methods of preparation. This part of Chapter 2 will trend more toward therapeutic aspects of MBs, including more specific details regarding their chemical composition, previous methods in functionalization of MBs (note that functionalization refers to any sort of modification of a pre-existing MB or design of a MB with therapeutic applications in mind aside from serving as a contrast agent in US imaging), as well as an overview of the general principles behind optimization of MBs and their behaviors. The last topic will delve briefly into molecular chemistry for the various interactions between agents used and their behaviors as part of a membrane, although the focus of this dissertation lies rather in the implementation and application of said therapeutic MBs in an animal model.

2.3.1 Formulations and Methods of Synthesis for Microbubble Shells

As an expansion to the previous section discussing various types of coatings for coated gas MBs, this section will discuss all the compositions mentioned in further detail as well as include a few additions not previously mentioned. In all, these are protein, surfactant, lipid, polymer, and polyelectrolyte types of shells.

2.3.1.1 Protein Shells

Protein shells were the first implemented coatings for gas MBs as discussed, with human albumin being the first formulation that was formally approved by the US Food and Drug Administration under the name Albunex. Albunex MBs were generated by the sonication of a heated albumin solution in an atmosphere of room air, resulting in air MBs ranging from diameters of 1 to 15 microns across. Notably, however, these MBs were stable for up to 2 years with refrigeration. To disrupt the native molecular structure of proteins and to facilitate formation of membranes which would encapsulate air, the albumin solution used was heated to denature its contents [40]. The resulting protein shell is described as a mono-molecular layer of both denatured and native albumin molecules which interact in multiple orientations, mainly deriving its structural stability from the disulfide bonds (formed between cysteine residues) which are built during the cavitation or sonication process [41]. Because disulfide bonds are covalent in nature, they are relatively inflexible, and as a result the albumin gas MBs are also relatively inflexible during US sonication (which would therefore limit their echogenicity as previously discussed) [42, 43]. To improve upon the stability and longevity of the MB, the gas species of the MB core was later replaced with a perfluorocarbon gas as previously discussed, resulting in increased longevity *in vivo*. Present iterations of this form are marketed under the name Optison™, which is approved

for contrast echocardiography, or for the use of delineating the boundaries of the various cardiac cavities as well as observing myocardial perfusion [44].

Aside from albumin, proteins in general perform favorably when used in shells for gas MBs. This is likely due to their amphipathic nature (of having both positive and negative electrical charges on a single molecule), which results in them being highly surface active (which means they have a tendency to reduce the surface tension of any fluid, such as saline, in which they come into contact) [45]. As with albumin MBs, other protein species are typically stabilized by the same disulfide bridges between cysteine residues (which are conveniently found on most proteins). In addition, the protein avidin has also been previously incorporated into the albumin MB, which is notable due to the capacity for avidin to form biotin mediated bonds to other large molecules as a form of loading the MB with various therapeutics [46]. This concept will be discussed later in further detail.

2.3.1.2 Surfactant Shells

Surfactants are a term for a group of organic molecules which generally serve to reduce surface tension between two compartments or mediums, in this context being fluid and gas. These molecules are typically amphiphilic, meaning they have both hydrophobic and hydrophilic structures, which result in their organization at the interface usually between an aqueous compartment and a nonpolar compartment (gas in our case). Organization of these surfactants into micelles (single layer organizations of these molecules usually with the hydrophilic head pointing outward) is common, the behavior of which lends toward their use in coatings for gas MBs.

Two species of synthetic surfactants, SPAN-40 (sorbitan monopalmitate) and TWEEN-40 (polyoxyethylenesorbitan monopalmitate) have been used in combination to form stable MBs with room air. These molecules, as we discussed, are comprised of a sorbitol-derived group (which is a

carbohydrate, and therefore having polar characteristics), as well as a palmitic acid-derived group (which is a fatty acid, and also a main component of palm oil, therefore having nonpolar characteristics). Interestingly, these molecules are also used as industrial emulsifiers for cosmetics and food products. Sonication was once again the method used to generate MBs with these molecules in combination, although interestingly it was tested that the stability of the resulting MB shells after sonication was significantly stronger than the film of the surfactant molecules in solution prior to sonication. Another group had reported stable MBs formed using sucrose stearate (once again, a carbohydrate with a fatty acid), although these MBs were limited in further clinical utility [47-49].

2.3.1.3 Lipid Shells

Lipids are perhaps the most interesting and most useful types of shell formulations for gas MBs both in imaging and drug delivery applications. Lipid bubbles may be found in nature, generated on beaches and in rivers as stabilizations of acyl lipids and glycoproteins, as well as in the human body, as natural lung surfactant which forms stable MBs in extracted lung lavage solution. Phospholipids, being amphiphilic, are an extremely popular choice, and are found in commercial products including Definity™ (Lantheus Medical Imaging) and Sonovue® (Bracco Diagnostics). The orientation of phospholipids around gas MBs are that their acyl chains (nonpolar) face the center with their phosphate headgroups facing outward [50, 51].

In essence, the favorability of phospholipids for MB stabilization arises from two main phenomenon; one is their ability to exist in a liquid-crystalline state with behavior similar to the fluid phase (in a manner akin to the fluid mosaic model of cellular membranes, which also mainly consist of phospholipids), and that low surface tension associated with the arrangement of phospholipids in that fluid state avoids formation of a Laplace overpressure on the gas core of the

MB which would typically force the gas core to dissolve. This way, having such low surface tension avoids creating that Laplace pressure on the gas core, allowing it to remain undissolved in solution, and thereby stabilizing the MB. The second phenomenon is the tight packing of the acyl chains resulting in significant hydrophobic attractive forces as well as van der Waals interactions between the chains due to their significant length, which also gives the phospholipid membrane a high degree of stability, and is also not dependent on the formation of chemical bonds such as with the disulfide bridges in protein shells. While the disulfide bridges rely on the presence of generated superoxide radicals during the sonication process, synthesis of phospholipid membranes is not restricted to such a process, allowing for various alternative synthesis methods [52-55].

In all, phospholipid shells are not only cohesive, they are also extremely pliable and weak in the manner of their construction. Therefore, because there is no actual structural covalent entanglement as with proteins or polymers, phospholipid shells are compliant and are capable of undergoing significant amounts of compression and expansion and have minimal damping (friction-like behaviors) and are also self-healing around an extent of fragmentation. These characteristics make phospholipid shells extremely favorable for CEUS imaging. In addition, because lipid species are easily modified in their headgroups or conjugated to other molecules, creation of functionalized MBs for applications such as drug delivery have also been explored, though this is subject to additional steps in synthesis and processing of the MBs themselves [35, 56, 57].

2.3.1.4 Polymer Shells

Polymer shells are much more restrictive than phospholipid shells due to their molecular nature and construction. Typical polymer shells consist of a thick region of cross-linked physically entangled polymer species. As discussed, this makes these shells much less echogenic than protein

or lipid counterparts. In addition, polymer shells may fracture like a cracked egg without complete disintegration during sonication, which results in escape of the gas core while the shell may remain intact.

Various methods of synthesizing polymer MBs have been investigated in previous literature. One method involves spraying both air and an alginate solution into a reservoir of calcium solution, resulting in adsorption of the alginate to the gas-liquid interface and hardening upon exposure to the calcium solution. In a fashion distantly similar to electrospinning, characteristics of the resulting MBs depended on flow rate from the extruding syringes [58]. However, typical diameters resulting from this method were too large for IV administration, being between 30 to 40 microns across. Another method involved emulsification and evaporation steps with ethylidene units [59]. Resulting size and texture characterization with a Coulter counter and through scanning electron microscopy showed that the resulting polymer MBs had a range of size restricted to 1 to 2 microns in diameter, with smooth surface texture and no defects. Biodegradable polymers such as polylactide-co-glycolide (PLGA) have also been explored for MB synthesis through procedures such as multi-phasic emulsification followed by sublimation of a volatile solvent, resulting in a variety of internal morphologies (such as honeycomb-like structures) with a smooth exterior [60]. Gases used for polymer MB applications are similar to the other shell material compositions and include room air and perfluorocarbon species such as perfluoropropane. Animal trials using these PLGA microbubbles showed successful left ventricular opacification (which is an application similar to clinical use in human patients) with increased stability demonstrated by the perfluorocarbon gas-core MBs. Other species of polymers used include poly-vinyl alcohols, which are chemically cross-linked at the gas and fluid material interface using high-speed stirring (8000 rotations per minute) rather than sonification of the material solution, and

rather than varying the mechanical parameters of the agitation to control the resulting MB parameters, temperature was lowered instead to decrease the MB shell thickness. These poly-vinyl alcohol MBs were notable in that they were stable for several months after synthesis and were capable of being functionalized with hydrophobic therapeutic molecules, charged polymer species (with DNA being one such species), and targeted ligands for cell surface molecules. Again, ink-jet printing is a more recent development in polymer MB printing technology, with dispersal of a polylactic acid co-polymer species into an aqueous solution along with an additional non-solvent core species which was later removed to create the hollow MB morphology [61, 62].

2.3.1.5 Polyelectrolyte Multilayer Shells

Polyelectrolyte multilayer shells are a relatively new development of a hybrid class of MB shell coating. This composition involves the deposition of various electrolyte species onto the surface of pre-formed lipid or protein MB shells with the help of an additional substrate coating layer of either charged surfactant molecules or proteins between the electrolyte species and the original MB. Typically, this is achieved through a layer-by-layer technique, with subsequent layers having opposite charges being referred to as polyionic pairs. Shchukin et al. were the first to demonstrate this technique of polyelectrolyte multilayer deposition using the polymers of polyallylamine and polystyrene as a polyionic pair, resulting in a coating that is both uniform and provides the MB with additional stability. Other groups have developed additional material compositions using this technique, including the use of other polyionic pairs for the deposition layers including the cationic trimethylammonium propane and poly(L-lysine) as the other species for the polyionic pair. This technique may also be used to protect various functional molecules which are imbued into the inner layers, such as the coating of a DNA imbued layer with a later

polyallylamine hydrochloride layer, which serves to protect the DNA molecules from enzymatic degradation in the circulating biological environment [63-65].

2.3.2 Molecular Imaging with Microbubble Agents

This application of functionalized MBs will be described briefly here, because while it is an expansive field of research of its own, it is not the particular focus of the work in this dissertation. In essence, molecular imaging with MBs involves surface modification of the MB with a specific ligand prior to injection into subject circulation, resulting in adhesion of the MBs by virtue of their surface modifications to specific molecular or rather cellular targets in the vascular endothelial compartment which express those specific ligand receptors. By leveraging specific ligand-receptor pairs which are upregulated in particular conditions or pathologies, this results in an enhanced, informative, selective contrast methodology which may serve the purpose of quantifying pathological changes in vasculature. Pathologies which are particularly relevant to this type of quantification and which have been well developed for this application of functionalized MBs include angiogenesis, inflammation, and atherosclerosis [35, 66-68].

The technique of imaging molecular targeted MBs typically involves injection of the targeted MBs, a time delay to allow for adhesion and circulation of the MBs, followed by recording and determination of the video intensity of the specific region of interest. This first measured intensity is then recorded. A destructive US pulse (destructive in the sense that it will result in total MB rupture, without damage to the tissue environment) is then applied, and MBs in circulation will then flow back into the field of view for the US, replenishing the depleted region following the destructive pulse. Video intensity for this replenishment is then recorded as well and taken to be the video intensity for freely circulating MBs without significant adhesion due to the lack of a

time delay following the destructive pulse. The subtraction of these two video intensities then becomes a quantification of the 'stuck' MBs, which typically require time to find and adhere to their molecular targets. In this way, the extent of MB adhesion between different pathologic groups of comparison and the difference in video intensities becomes a measure for pathologic severity, which is taken to be represented by the prevalence or concentration of the specific ligand receptor in question, which directly influences the extent and amount of targeted MB binding.

MBs are particularly suited for this type of application in comparison to other types of contrast due to their particular size, which limits their presence to the circulating vascular space, but does not preclude them from smaller vessels of the microcirculation (up to capillary beds), their lifespan in circulation (which is on the order of 10 minutes), which results in sufficient half-life for imaging purposes but does not persist unduly resulting in saturation of the viewing field and allows for a return to normalcy for the patient (and relatively quick imaging sessions on the physician and technician schedule), and also the capacity to apply destructive pulses of US to immediately remove all contrast from the field of view to apply techniques such as the subtraction of the contribution from freely circulating MBs, as previously described. This is again a unique characteristic of MB contrast agents as opposed to fluoroscopy or MR contrast imaging, in which a dye is injected but is not able to have its presence completely removed at the discretion of the imaging practitioner [36].

In addition, physical behaviors of the MB when sonicated by US as we previously described also contribute toward the utility of MBs as molecular imaging agents. In particular, the radiation force, or directional influence of applied US fields targeting circulating MBs, as well as the radial expansion of MBs themselves against the distal boundaries of the vascular compartment, allow for more direct physical interception of the MBs against the endothelial wall. In addition,

oscillation of the MBs during sonication results in expansion of the MB shell, which may also allow for the leveraging of techniques such as the obscuring of the molecular ligands by other components such as a polymer brush layer (through PEGylation of the phospholipid species) and the later reveal of said ligands due to shell expansion and a sort of parting of the brush layer with sonication, which then facilitates binding using the surface ligands. It is these additional details which allows for innovative designs and mechanisms of molecular imaging focused MBs, improving upon the sensitivity and accuracy of these techniques in tracking pathological or physiological changes in the vascular space [69, 70].

2.3.3 Therapeutic Agent Delivery with Microbubbles

Delivery of therapeutic agents using MB vehicles is perhaps the most heavily researched application of modern MBs, including the work of this dissertation. As mentioned before, payload delivery using MBs is intertwined with the technique of ultrasound-targeted microbubble cavitation in that the therapeutic value of the MBs would be incomplete and lacking without the US sonication. Although ultrasound-targeted microbubble cavitation is a therapeutic technique in its own right, with specific benefits, many of the biophysical effects of ultrasound-targeted microbubble cavitation impart significant benefits to delivery of therapeutic agents from the MBs as well. These include the phenomenon of sonoporation, or the poration of the endothelial barrier (cell membranes facing the vessel lumen) by oscillating or rupturing MBs, as well as the fragmentation and impact of the MBs themselves. This phenomenon will be discussed in the later ultrasound-targeted microbubble cavitation chapter [71].

Many of the MB agents used in these therapeutic applications are either commercially available for purposes of contrast enhancement (as previously discussed) or are derivatives thereof.

However, there has been a growing movement toward the development of MB carriers designed specifically to carry and deliver therapeutic agents with greater efficacy and efficiency. The two most common types of therapeutic agents delivered by these MBs include genetic material and drugs.

Delivering genetic material to the human body has been a longstanding challenge in biomedical engineering, with the additional caveat of targeted delivery raising even more barriers. This is mainly because for effective treatment, that is having sufficient exogenous genetic material present for actually producing quantifiably modified expression of said genes, is limited by the large amounts of genetic material needed. In addition, genetic material in the bloodstream is rapidly degraded and cleared with extreme prejudice by the reticuloendothelial system and circulating nucleases. Hence, MB agents are needed to not only protect the genetic material from degradation prior to reaching its target site, but also to deliver adequate amounts of the genetic material to the specific location of interest [72].

Targeted drug delivery holds a similar rationale to delivery of genetic material, although many drugs are much less sensitive to immediate degradation in the bloodstream compared to genetic material. However, they are similar in that ideally the drug will be released into the local circulatory microenvironment after destruction of the bubble through ultrasound-targeted MB cavitation, which is also selective for location based on direction of the beam. One key difference between drugs and genetic material is that drugs are often incorporated within, beneath, or inside liposomes attached to the MB shell, rather than electrostatically bound to the MB surface. Again, the MB agents are used to protect, deliver, and target the drugs, with the additional potential effects of protecting the drug from first pass hepatic metabolism, which often covalently modifies or degrades certain chemical structures.

In a manner similar to previous, well-written reviews on this subject matter, we will organize the delivery of therapeutic agents into specific types of MB shell compositions, similar to the previous sections, namely discussing protein, lipid, and polymer MB shells.

2.3.3.1 Protein Microbubble Shells

As previously discussed, the main manner of structural integrity in protein shells for MBs is in the form of disulfide bridges forming cross-linking bonds between protein molecules. These bridges are formed during the sonication process of MB synthesis. As this is a relatively straightforward and simple process, the incorporation of macromolecules into these structures is also relatively straightforward. The macromolecules are most commonly incorporated into the shell material during the crosslinking phase of the sonication stage of synthesis, with an alternative being simple adsorption, or attaching the macromolecules to the protein surface through electrostatic interactions, which may be more amenable to charged macromolecules such as nucleic acids. As typical MB sizes are on the order of single digit microns in diameter, the presence of these loaded macromolecules does little to disrupt the acoustic behavior of the MB, allowing it to remain contrast enhancing during US imaging.

One example of this in application is the incubation process of a target macromolecule with the protein solution followed by simple agitation with the gaseous core agent. A previous study performed this using a solution of albumin and fructose incubated with adenoviral vectors agitated and mixed with perfluoropropane, resulting in adenovirus loaded MBs, which were then injected into rats with successful delivery and translation of the protein products observed in the animal myocardium. This study, performed by Shohet et al., was one of the earliest studies demonstrating the feasibility of this simple approach [73].

Another similar application using rapamycin loaded albumin MBs performed by Kipshidze et al. emphasized another benefit of using albumin MBs for drug delivery purposes in a disease context in that albumin MBs have adhesive interactions with sites of pathogenic vessel injury, resulting in targeted delivery without specific ligand enhancement of the MBs, and also notably, without MB destruction using ultrasound-targeted MB cavitation techniques [74]. The mechanism of loading the therapeutic agent onto the MBs was not discussed by the authors, although one may hypothesize that their success was the result of electrostatic and hydrophobic intermolecular forces. It is also significant to note that this method has the disadvantage in efficiency of the drug-loading process, in that expensive or scarce drugs/substances may preclude the process of incubation which relies upon sufficient concentration of the therapeutic agent in solution. In addition, the presence of negative ionic charges on both the proteins comprising the shell material itself and on macromolecules (such as other proteins or in the phosphate backbone of nucleic acid chains) may also lower the efficacy of these techniques.

A different approach involves the direct incorporation of the therapeutic agent within the protein shell of the MBs during formulation rather than incubation and subsequent adsorption of the therapeutic agent [75]. Although there have been some studies validating this approach, limitations of evaluating its efficacy include a lack of proper controls in said studies especially of groups consisting of injection of unloaded MBs with a co-injection of free therapeutic agent in solution. Other obstacles include reaching sufficient efficiency of release of the therapeutic agent from the protein shell after MB rupture. Comparisons against commercially available transfection agents revealed that loaded protein MBs had significantly lower efficacy for cell transfection.

As previously mentioned, polyelectrolyte multilayer deposition techniques have introduced new potential for protein MBs to be modified for carrying genetic material. Examples

of intermediate coating compositions (used as a bridge between the protein shell material itself and the genetic material) include negatively charged albumin as well as polyammonium hydrochloride [64, 76-78]. Results of studies investigating polyelectrolyte modified bubbles showed that the MBs themselves experienced greater longevity and circulating half-life of up to 7 hours, and that the MBs remained viable in their response to sonication (and resulting cavitation behavior). In addition, the coated MBs showed that the purpose of protecting the genetic material with the intermediate coatings was indeed achieved, with polyammonium hydrochloride and DNA coated MBs revealing minimal degradation. These new techniques in modifying protein MBs for superior payload protection and delivery continue to be investigated with further goals of improving transfection efficiency and payload capacity.

2.3.3.2 Lipid Microbubble Shells

Lipid MBs are one of the more popular choices for targeted delivery of a therapeutic agent, as previously mentioned, due to their great capacity for chemical modification, favorable intermolecular interactions with many chemically active species of molecules, and resilient acoustic behaviors after modification. Because lipid and protein MBs may share certain types of synthesis procedures as previously discussed, such as simple sonication or agitation, direct incorporation of the therapeutic agent into the lipid shell without additional chemical modification steps is one of the most simple and common methods of modifying the lipid shell. One previous investigation demonstrated this through simple incubation of luciferase in the MB solution prior to formulation, followed by injection into rats with therapeutic ultrasound applied to the thorax [79]. This resulted in significant delivery of the luciferase enzyme and detection of the enzyme activity (thought to be mediated by destruction of the MBs) although loading efficiency, as always, is an ongoing target for improvement.

Another strategy of incorporating therapeutic agents into lipid MB shells involves acoustically active lipospheres, which are essentially lipid MBs with a thick inner coating of oil surrounding the gas core. With this thick coat of oil comes the capacity to incorporate hydrophobic agents without significant disruption to shell integrity, while ensuring their release upon MB destruction. Unger et al. first described this process in 1998, in a study which investigated the loading of paclitaxel (a hydrophobic anti-cancer drug) onto these acoustically active lipospheres [80, 81]. Resulting measurements showed a high efficiency of incorporation with no significant disruption to parameters such as MB size or acoustic behavior. However, it was noted that there were reductions to MB stability. Later studies further investigating and refining this technique have utilized previously described US radiation force and various pulse sequences to mechanically intercept the circulating MBs against the endothelial wall for drug deposition after MB fragmentation, with success both *in vitro* and *in vivo* [82]. Aside from paclitaxel, this concept is applicable to a wide variety of clinical contexts and therapeutic agents.

Both of these techniques, whether incorporation into the lipid shell, or development of a hydrophobic inner layer, involve intrinsic modification of the lipid MB. In contrast to this, a different direction of lipid MB modification is limited to the surface, whether through direct attachment or through an additional carrier system. Advantages of surface modifications only are that the stability and echogenic properties of the MB shell are less likely to be affected.

In some contexts, modification of the lipid shell is favorable to promote surface modification at a later synthesis step. One example of this is the introduction of charged lipid species into the lipid shell, which are by themselves not intrinsically bioactive, for the purpose of using electrostatic charges to later load a charged therapeutic agent onto the surface. One example of this was the use of cationic lipids for the purpose of binding genetic material (plasmid DNA) as

reported by Christiansen et al. in 2003 [83]. Not only has this approach been used with plasmid DNA, it has also been successfully applied to antisense oligodeoxynucleotides in anti-tumor applications both *in vitro* and *in vivo*. Similar to previous *in vivo* loaded-MB studies, the authors concluded that US stimulation of the MBs was a significant driving factor in the success of payload delivery, and interestingly enough even free genetic material was seen to be delivered more successfully in the absence of any MB vehicles.

Again, no discussion of modified lipid MBs would be complete without the mention of polyelectrolyte multilayer membrane assemblies, as their application has again been demonstrated with lipids just as with protein MBs [63]. As with protein MB shells, lipid MB shells were successfully modified to carry plasmid DNA for delivery after sonication. However, it was found that the addition of these layers to the lipid MB shell did have damping effects on the oscillations of MBs during US stimulation which resulted in improvements for MB stability. Therefore, this novel approach toward MB modification holds significant potential in the area of lipid MB modification as well for targeted gene delivery.

As mentioned, various chemical linkers and carrier systems have been developed for surface modification of lipid MBs. One common system is the biotin-avidin linker system, in which biotinylated lipids are incorporated into the MB shell [84]. The avidin molecule, which is capable of binding four different biotin groups, is then incorporated as an intermediate step followed by addition of a biotinylated therapeutic agent. Therefore, this process forms an avidin bridge between the therapeutic agent and the MB surface. Not only may this process be used for therapeutic molecules, but liposomes themselves may also be biotinylated for attachment to the lipid MB surface. Having mean diameters on the order of hundreds of nanometers, these liposomes showed extremely high binding efficiency to the lipid MB surface, allowing for significantly

increased concentrations of the therapeutic agent in modified MBs. Sonication of liposome-linked lipid MBs *in vitro* showed significant deposition of a dummy drug molecule. This approach has also been applied to liposomes containing genetic material, with the resulting structure termed as lipoplexes. These genetic material containing liposomes have been showed to be released from the vehicle lipid MB after MB destruction without significant disruption to the lipoplex structure. Early studies have shown that containment of genetic material in these structures enhances therapeutic efficacy of the material delivery. However, clinical relevance of this approach has yet been limited.

It has generally been a previous pattern that delivery of genetic material using various non-MB vehicles (cationic vehicles) have high efficiencies *in vitro* with a failure to produce quantifiable results of significant transfection *in vivo*, due to what many hypothesize to be immediate clearance in circulation by the reticuloendothelial system. Therefore, attachment to a lipid MB vehicle is thought to reduce this clearance, promote longer time in circulation and therefore increase likelihood of delivery to the proper tissue target, thereby improving efficiency of delivering genetic material to cells.

2.3.3.3 Polymer Microbubble Shells

The development of polymer MBs for drug delivery is less extensive than that of lipid or protein MBs. However, there has been evidence showing that polymer MBs are still a promising option, as one study showed that hard polymer shell MBs resulted in greater transfection rates when loaded with genetic material than an equivalent lipid MB, although polymer MBs often require higher therapeutic US pressures due to their stiffness [85]. These higher pressures and the differences in polymer shell behavior upon fragmentation has been hypothesized to be the cause of this greater efficiency, as their cavitation and rupture may be more violent than equivalent

behavior in lipid MBs, resulting in greater poration of genetic material into cells. In addition, polymer MBs offer the advantage of incorporating both hydrophobic and hydrophilic macromolecules without the need for an additional structural matrix.

Examples of previous investigations of modified polymer MBs for genetic material delivery include a study by Seemann et al. in 2001, where the double emulsion technique was applied to form poly-lactic-co-glycolic acid MBs in the presence of plasmid DNA complexed with polylysine, protamin sulfate, or polyethylenimine cationic polymers, resulting in successfully loaded polymer MBs [86]. However, it was also documented that release kinetics for the genetic material from these polymer MBs was slow, with only 10% of the encapsulated genetic material released after stimulation by US of 10 minutes. These MBs were further evaluated by another group for use with plasmid DNA for delivery to a rodent tumor model. Application with US treatment resulted in successful signal of the genetic material within the tumor, but not surrounding tissue. Later encapsulation of anti-tumor genetic material was also performed, showing that application of the loaded polymer MBs with therapeutic US stimulation resulted in successful slowing of late-stage tumor growth, showing the overall potential of this technique.

More recently, various other applications of polymer MBs have surfaced as well, such as use of poly(lactic-co-glycolic) acid MBs in conjunction with iron oxide nanoparticles resulting in the formation of multifunctional polymer MBs for use in dual-mode US with magnetic resonance imaging [39, 87]. Not only are these MBs dual-purpose in their imaging, but they have also been loaded with doxorubicin, an anti-tumor drug with adverse systemic effects. The investigating group showed that varying concentrations of iron oxide particles incorporated into the polymer MB shell did not significantly affect the capacity for doxorubicin encapsulation nor functional capacity of the polymer MBs during US imaging. These novel agents were used in a model for

treatment of metastatic malignancy in lymph nodes while also assessing various tumor characterization markers including blood vessel density, micro-lymphatic vessel density, and tumor proliferation index.

Furthermore, along these lines, incorporation of various nanoparticle species with polymer MBs for application with other imaging modalities including optical fluorescence, magnetic resonance, and even computerized tomography have been investigated [39]. As stated, iron oxide nanoparticles providing additional contrast for magnetic resonance imaging has been investigated by several groups. In addition, radioactive fluorine-labeled lipids have also been incorporated for use in positron emission tomography. Another recent study showed that gold nanoparticles and quantum dots (which are nanosized semiconductor crystals) may also be incorporated into functionalized polymer MBs successfully, allowing for development of dual mode contrast agents and simultaneous clinical applications of contrast enhanced multi-modal imaging with potential theranostic applications as all of these polymer MB multi-contrast agents may be loaded with various therapeutic agents for targeted drug delivery as well [88, 89]. This is especially useful for pathologies where localization is limited to an imaging modality aside from US, while US imaging is simultaneously required to validate the delivery and MB presence at the local site.

2.3.4 Basic Principles of Microbubble Optimization and Design

This section briefly discusses various topics relevant to the design and optimization of lipid MBs for the purposes of compatibility with novel molecules. The concepts covered represent an intersection of many different disciplines, from biochemistry to physics, considering how MB function entails both acoustic properties in response to US stimulation such as for imaging purposes as well as biomechanical interactions with endothelial physiology. This section is mainly

relevant to the work in this dissertation involving design and fabrication of the novel nitro-fatty acid lipid MB, and much of those processes drew inspiration from the material to be discussed. Each sub-section will discuss a different topic covered in cursory detail to be investigated further at the reader's discretion.

2.3.4.1 Hydrophobic Tail Chain Length

As previously discussed in the general overview of lipid MB structure, many of the phospholipid species commonly used in lipid MB shells are amphiphilic, in that they contain both hydrophilic and hydrophobic structures. The hydrophobic structures are commonly acyl chains, which are long hydrocarbon tail groups that may either be saturated or unsaturated depending on the extent of hydrogen-carbon bonding. Typically, these hydrophobic tail groups face the interior of the lipid MB, and immediately border the gas core.

These tail groups are of immediate relevance when considering MB properties that are significant for performance such as longevity in circulation, half-life in storage, and stability (both when freely circulating and when sonicated by US pulses).This is because the essential mechanism of MB instability is the escape of the gas core from the lipid shell resulting in gas dissolution and disappearance of the MB for all functional purposes, as well as the loss of structural integrity of the lipid shell itself, which also results in an exposed gas core. Therefore, gas permeation through the phospholipid shell, including permeation through these hydrocarbon chains, is a key mechanism contributing to the loss of MB stability [56].

Aside from affecting stability, length of the hydrocarbon tail group also significantly affects the physical properties of the lipid MB itself. Parameters such as yield shear and surface viscosity both increase directly with the length of these hydrocarbon chains, as previously shown. The deformability and flexibility of the lipid shell under physical stimulation not only affects its

echogenic properties which allow it to serve as a contrast agent for US imaging, but also the threshold for MB rupture, which is a key behavior for therapeutic applications of MBs as previously mentioned, including drug delivery. The source of this increased stability in the shells formed by longer hydrocarbon chain group phospholipids is thought to derive from increases in attractive forces and hydrophobic interactions (van der Waals forces) between adjacent phospholipid molecule tails [56, 90, 91].

The concept of hydrophobic chain length affecting permeability of the lipid shell to gas escape into the surrounding aqueous mechanism was confirmed by previous studies investigating a series of various hydrocarbon chain lengths in an empirical setting. It was found that the primary mechanism for MB stabilization are through reduction of surface tension and presenting a physical barrier to gas permeation, although these were thought to not be the only contributing mechanism as discrepancies in MB behavior between theoretical force-modeling approaches and the experimental results existed. Microscopic studies of deforming lipid MBs also showed that lipid MBs composed of hydrophobic chains with length greater than 17 carbon atoms demonstrated significant lipid membrane folding behaviors and development of lipid projections with their own radii of curvatures. These behaviors are consistent with a membrane of negligible surface tension, and that the overall MB was in a constant state of change between various deformations which were significantly smaller than the overall radius of the MB. Carbon chain lengths of up to 24 atoms were investigated, with longer chain lengths resulting in increased stability. Lipids with chain lengths shorter than 17 atoms also demonstrated a behavior of excess lipid shedding, while those with lengths longer than 17 atoms did not demonstrate this shedding, and would deform as described instead, prior to suddenly returning to a more regular sphericity, indicating possible sudden formation of smaller vesicles in the deformation process in a sort of zippering effect due

to the stronger intermolecular forces. This is also because the longer hydrophobic chain phospholipids have stronger interactions with not only resist the typical formation of aggregate leaving structures, but also because the crumpled surface morphology is an energetically unfavorable state [90, 91].

Another study focused on improving the persistence and longevity of circulating lipid MBs *in vivo* again investigated the effect of acyl chain length on these stability measures [91, 92]. Again, various phospholipid species were investigated ranging from chain lengths of 16 carbon atoms to 24 carbon atoms. Similar to the previously mentioned study, stability generally increased with increasing acyl chain length; however, for the longest chain length investigated of 24 carbon atoms, MB stability dropped unexpectedly. In addition, an US phantom imaging model was used to investigate a stimulated circulation environment for the lipid MBs with contrast-mode US used in burst-reperfusion imaging to assess replenishment of the imaging field with new MBs. It was again noted that increase in persistence was associated with increase in acyl chain length, again up to 18 carbons in length. However, imaging persistence did not increase when further increasing the acyl length, including up to 24 carbons in length, suggesting that previous passive dissolution experiments do not quite share the same mechanics of MB dissolution as an actively circulating MB environment. However, when using an *in vivo* rat kidney model of contrast-enhanced US investigation for lipid MB persistence, stability increased with chain length up to 22 carbons in length, while further increase to 24 carbons resulted in decreased persistence.

This study also investigated presence of surfactant molecules in the lipid MB on stability and did indeed verify that presence of surfactant proteins resulted in increased stability in lipid MB shells as well. Notably, this study proposed that significant mismatch in chain length between the main lipid shell component phospholipid and other components such as the emulsifier species

resulted in significant decreases in MB longevity and a less stable MB surface microstructure. The emulsifier investigated was DSPE-PEG, which is the same emulsifier that was later used in the therapeutic MB applications of this dissertation work [93, 94].

Other studies on physicochemical properties of MBs have also raised implications of their efficacy in drug delivery, including the main property of acyl chain length. Specifically, longer chain lengths have been found to result in longer time necessary for re-stabilization following any rupture in the lipid shell and also longer time to full collapse after initial mechanical disruption due to stronger intermolecular forces. Increases in acyl chain length also result in increased in-plane rigidity, which influences factors such as cavitation response and shear stress necessary for MB disruption and rupture. Investigations of lipid MB phospholipid component parameters on *in vivo* performance have also been performed, with the main results that longer acyl chain length MBs resulted in improved tissue delivery and biological basement membrane permeation of large molecular MB payloads, but not for smaller molecular payloads. It was also found that acoustic energy of the stimulating US pulse on the MBs modulated the relationship between lipid shell parameters and delivery efficacy, suggesting that using the proper US regime and acoustic pressure is just as important for effective *in vivo* therapeutic benefits [95].

2.3.4.2 Presence of PEGylated Emulsifier Molecules

Naturally occurring MBs are stabilized by surfactant molecules comprised of lipids and glycoproteins. For example, in many water systems these lipid and glycoprotein molecules are derived from decomposition of multi-cellular organisms. Addition of emulsifier molecules is also a common practice in synthesis of lipid MBs in a laboratory setting. One of the most common types of emulsifiers is the attachment of the hydrophilic polyethylene glycol head group to the phosphate group of phospholipid species. Not only does this head group prevent coalescence of

multiple MBs while in preparation, it also prevents adsorption of various substances including blood plasma proteins onto the surface of the MB while in circulation. Additionally, having this polyethylene glycol form a brush layer around the outside surface of the MB also prevents phagocytosis of the MB to a degree.

Various theories for behavior of these modified emulsified components in lipid shells have previously been presented. These include consideration of the shell as a homogenous structure with relatively even dispersion of the emulsifier molecules, as well as polycrystalline distributions, where clustering and partitioning of different molecular structures occurs, resulting in the formation of specific domains on the surface structure of lipid MBs.

One specific previous study investigated the behavior and miscibility of PEG-40 stearate as an emulsifier in phospholipid shells [94]. This is of particular relevance to the work of this dissertation because PEG-40 stearate is the same emulsifier featured in all therapeutic MBs used in this work. The work of this study further re-affirmed that surface distribution of emulsifier components and other lipid species is not only heterogenous, but that these so-called network domains are increasingly found in MB shells with longer lipid acyl chains. Therefore, inclusion of these emulsifier groups does not result in a uniformly distributed shield of the polymeric brush layer over the entire MB, nor will modifications of these surface lipid species result in uniform distribution or targeting for molecular agents. However, it was noted that emulsifiers still did provide benefits in terms of structural stability and longevity of the MBs over an absence of any emulsifier use.

3.0 Ultrasound-targeted Microbubble Cavitation Principles and Applications

Previously we have discussed US in its imaging and therapeutic modalities, as well as MB contrast agents and their therapeutic modifications. In this chapter, these two topics will be combined into ultrasound targeted microbubble cavitation (UTMC), which is a combination therapeutic-diagnostic (theranostic) technique which serves many purposes. We will begin with an overview of this technique and basic mechanisms which relate to its therapeutic applications, and then discuss several clinical applications of UTMC. The general directions of applying UTMC therapy include cancer therapy, gene and drug delivery, thrombolysis, and cardiovascular disease. Although the last two subjects are often considered together (due to pathologies requiring thrombolysis often being co-morbid with cardiovascular pathologies), various other techniques such as gene and drug delivery may be applied toward cardiovascular disease as well. There will be a specific emphasis placed upon the last two topics, especially thrombolysis, because the context in which the work of this dissertation was initiated was in treatment of microvascular obstruction by micro-emboli, which is relevant to both thrombolysis and cardiovascular disease. Lastly, other applications of UTMC not included in the list above will be discussed briefly at the end of the chapter.

3.1 Ultrasound-targeted Microbubble Cavitation Basic Overview

US targeted MB cavitation (UTMC) has been referred to by a range of different labels, including US targeted microbubble destruction, US-exposed MB therapy, and US-induced

cavitation, among others. All of these names encompass a therapy which, at its essence, consists of two components: therapeutic US and MBs. By directing the external US transducer toward an intended target site which contains circulating MBs, this technique results in MB oscillation and destruction (with stronger US pulses), which lead to biomechanical effects in the local tissue environment. One distinction which has been made lies between destruction and cavitation in nomenclature. As previously discussed regarding the range of possible MB responses as the acoustic pressure of the sonicating US pulse increases, MB destruction does not necessarily occur at relatively lower pressures. Therefore, UTMC is an umbrella term that describes both stable and inertial (destructive) cavitation responses. In addition, although cavitation in the absence of MBs refers to the coalescence of gas into bubbles during the rarefaction phases of US, presence of MBs results in pre-formed nuclei for further cavitation, thereby reducing the necessary pressure, or cavitation threshold, necessary for this process. Along these lines, while US pulses by themselves have an extent of therapeutic capacity, these effects are greatly enhanced by circulating MBs, whose mechanical behavior acts as the immediate effector on biological targets including cells, membranes, and material such as blood clot.

3.2 Basic Mechanisms of Ultrasound-targeted Microbubble Cavitation

The main mechanisms of UTMC to be discussed here are cavitation, radiation force, and sonoporation. These may interact and combine to result in a myriad of other behaviors which contribute to the efficacy of UTMC therapy *in vivo.* Cavitation refers to the oscillation and possible destruction of MBs when targeted by US pulses. Radiation force involves the displacement of MBs along the direction of the US beam. In this way, cavitation and radiation may be leveraged together

to first direct MBs toward their intended target followed by destruction and release of the contained therapeutic payload, resulting in delivery of the therapeutic agent to the tissue site and concentration of the agent in the local vicinity.

Sonoporation refers to the disruption of a cellular membrane by UTMC generated shear-stress. This mechanism functions in conjunction with both radiation and cavitation and is the result of applying the MB oscillatory forces to a biological membrane. Studies using extremely high-speed imaging and incubations of MBs with cells have demonstrated the temporal and spatial co-registration of UTMC application with resulting cellular intravasation with a model drug, followed by re-sealing of the membrane [96-98]. Investigations varying the physical parameters of the US pulse used have shown that there is a lower limit of MB radial expansion necessary for sonoporation to occur; this behavior therefore depends on the characteristics of the stimulating pulse [99]. It has been found that for a fixed pulse frequency, this oscillation threshold increases as pulse duration decreases. Cellular membrane mechanics for sonoporation have been modeled using materials engineering approaches for failure, although this work will not be further discussed here [100, 101]. In essence, it is known that MB oscillation resulting in sonoporation may facilitate delivery of therapeutic agents to the targeted cells, while downstream mechanotransductive events (such as nitric oxide production in the vascular endothelium) may follow [102].

Sonoprinting is another UTMC mediated delivery technique which has subtle distinctions from sonoporation [103, 104]. While sonoporation refers to the formation of pores, or microscopic holes in the cellular membrane, sonoprinting instead entails the surface deposition of therapeutic agents such as nanoparticles onto cell membranes, which are later assumed to be endocytosed by the cell. Sonoprinting has the benefit of avoiding the violent MB behaviors associated with high acoustic pressure US, including phenomenon previously described such as micro-jetting, MB

fragmentation (which has also been referred to as lipid shedding), and sonoporation. Rather, low acoustic pressure US is used, and has actually been found to enhance and favor alternative cellular behaviors such as endocytosis. A disadvantage of sonoprinting is that the therapeutic agent is required to be fixed to the surface of the therapeutic MBs, whereas sonoporation has been shown to result in successful intravasation of therapeutic molecules not fixed on the MB surface, but rather circulating in conjunction with MBs. Sonoprinting also involves direct physical deposition in that surface contact of the MB with the target is assumed and necessary. Target surfaces including cell membranes and cellulose tubes have been successfully deposited with nanoparticles using this technique. Lastly, a major difference between sonoporation and sonoprinting is that sonoporation relies upon fluid movement through the sieve-like holes formed by MB oscillations for delivery of molecules into cells. This may become more difficult and less reliable in the case of larger molecules. However, sonoprinting results in the direct deposition of these molecules onto cellular surfaces, resulting in improved feasibility for larger molecules including polystyrene and mRNA-lipoplexes [103].

Sonoporation and sonoprinting are both mechanisms of UTMC interaction on a cellular level. However, UTMC applications to blood vessels have shown evidence for an additional interaction of increasing vascular permeability by temporarily modulating vascular integrity. Rather than targeting a single cell, this refers to the effects of rarefaction and compression on an entire vascular tissue environment, including the endothelial boundary and the various basement membrane components of blood vessels. High-speed imaging studies have shown that expansion and contraction of MBs in a blood vessel result in circumferential deformation of the vessels, and by definition, increases in strain and potential gaps between adjacent cells [98, 99]. In addition, oscillating MBs have been shown to actually traverse through the endothelial layer after being

attached to the vessel wall, and invaginations of the vessel endothelium have been observed in the absence of the oscillating MB after contraction. This concept of a leaky endothelium is thought to also result from partial delamination of the endothelial layer and contributes to therapeutic efficacy of various drug and gene delivery applications of UTMC therapy.

Stimulation of endocytosis and uptake of material was previously mentioned in the description of sonoprinting and is a veritable means by its own right toward the application of gene or drug delivery by UTMC therapy. This mechanism is the interaction between the mechanical forces of MB oscillation and endocytotic pathways. Previous studies have shown much evidence for this phenomenon, such as the upregulation of clathrin-coated pits, endocytotic vesicles, and endocytotic markers in cells exposed to UTMC with low intensity US, without evidence of concurrent sonoporation or other cellular membrane disruption [102, 103]. This was further supported by work showing the inhibition of cellular uptake of low and high molecular weight dextrans during low intensity UTMC after the administration of clathrin and caveolin inhibitors. ATP depletion, which inhibits endocytosis, was also used to demonstrate the mechanistic significance of endocytotic uptake in molecular delivery of UTMC. However, while mechanistic *in vivo* studies regarding endocytotic uptake are still limited and inconclusive regarding its improved efficacy for material delivery in UTMC, there are potential benefits of using low intensity US in UTMC, including decreased inflammation and potential cellular damage which may occur with sonoporation and high intensity US.

Another mechanism that is hypothesized to be related to various mechanisms of transient cellular and endothelial permeabilization is the formation of extracellular hydrogen peroxide. This has mainly been studied in the context of low intensity US. Previous investigations have shown that low intensity UTMC results in a significant increase in production of hydrogen peroxide [105,

106]. Simultaneous permeabilization of cellular membranes was also measured using influxes of calcium ions. This phenomenon is distinct from the transport of ions across the cell membrane through endogenous ion channels. Other studies on reactive oxide species have also shown increases in macromolecular permeability of cellular membranes in the presence of hydrogen peroxide even without the UTMC stimulus. However, the authors did not explicitly propose any mechanisms for the relationship between hydrogen peroxide and membrane permeabilization.

3.3 Applications of Ultrasound-targeted Microbubble Cavitation

This section will discuss select applications for UTMC, namely toward treatment of Alzheimer's disease (with blood-brain barrier permeabilization), cardiovascular disease, and thrombolysis. Previous sections have discussed various MB modifications for gene and drug delivery. The range of possible applications and contexts for those general uses of UTMC are too many to list here, although the common themes and mechanisms for successful delivery using UTMC have been listed in the previous section. Cardiovascular disease and thrombolysis are subjects of immediate relevance to the work detailed in this dissertation.

3.3.1 Blood-brain Barrier Disruption and Alzheimer's Disease

Interest in using UTMC and focused US in the context of the neurovascular unit has been growing significantly in recent times. Given the versatility of UTMC, these applications have been varied in their goals, from increasing permeability to drug delivery to modification of the local environment in aspects such as gene transcription profile.

3.3.1.1 Blood-brain Barrier Background

The blood brain barrier is a structure common to all organisms which possess a complex central nervous system. It is the boundary between the intravascular compartment and the parenchymal interstitial compartment of both the brain and the spinal cord and is composed primarily of cerebral endothelial cells. Aside from the tight junctions which seal the margins of adjacent endothelial cells, which prevents the occurrence of paracellular transport, the endothelial cells are also in contact and communicate with other neural cell types including microglial cells, astrocytes, and pericytes. The endothelial cells themselves also express a wide range of transport channels and proteins for substances necessary for cellular metabolism including glucose and amino acids. Endocytosis from the endothelial cell surface (and transport across the cell layer, termed transcytosis) is another mechanism for the movement of macromolecules as well. In essence, the blood brain barrier serves the function of regulating the substances which may be transported into the central nervous system, including brain parenchyma, and is also therefore the greatest barrier in delivery of various therapeutic agents to the brain. The reverse is true as well, with the blood brain barrier also serving to actively remove metabolic waste products which are potentially toxic with excessive accumulation. The blood brain barrier also serves to create and stabilize a distinct fluid compartment of the interstitium of the central nervous system which is notably varied from the somatic interstitial fluid in that the central nervous system relies on precise ionic and molecular concentrations for proper synaptic function.

Given its paramount role in regulating brain metabolism, it comes as no surprise that blood brain barrier dysfunction is thought to play a key role in the etiology of several pathological processes. Examples of this include Alzheimer's disease, where transport of the beta-amyloid protein is defective resulting in accumulation of the protein in the brain fluid compartment and

eventual deposition of insoluble protein plaques as well as increases in oxidative stress. Although this is particularly nuanced by the additional role of the brain-cerebrospinal fluid barrier which also participates in clearance of said protein products in the brain, it stands that there are direct connections between impairment of barrier transport function and development of key disease markers. In addition, the integrity of the blood brain barrier is also thought to naturally decline with age, which is also relevant to the development of Alzheimer's disease. Another example is obesity, where blood brain barrier transportation of leptin, a signaling protein, is impaired, resulting in dysfunction of various signaling pathways regulating appetite.

In relation to clinical applications of UTMC, most if not all treatments are not targeted to the blood brain barrier with intent to restore or improve its function [107]. Rather, the blood brain barrier is taken as an obstacle toward delivery of therapeutic agents to the brain parenchyma, given its role in impeding transport of large foreign molecules. The goals of these therapeutic agents may then be varied, whether toward treatment of brain tumors or removal of amyloid plaques. Other applications of general US in treatment of brain pathologies include delivery of neuroprotective agents in ischemia-reperfusion injury, and gene delivery in Huntington's and Parkinson's diseases. As such, the role of the sonicated MB in overcoming the blood brain barrier is achieved through the various physical mechanisms of action including sonoporation, radiation forces, and cavitational forces.

3.3.1.2 Blood-brain Barrier Disruption in Alzheimer's Disease

One of the earliest studies for blood brain barrier disruption using UTMC was performed at an US frequency of 690 kHz, with confirmed results by electron microscopy and negligible damage to brain parenchyma [108]. Since then, various other studies have focused on the investigation of various US frequencies due to the major distortion of the US pulse by the skull.

Given our understanding of the effects of lowering US frequency on phenomenon such as attenuation and distortion, lower frequencies have been found to be distorted less when passing through the skull. An additional benefit of using lower US frequencies is that tissue absorption of US energy is decreased as well, resulting in fewer thermal changes in brain parenchyma (which is obviously favorable), while remaining suitable for blood brain barrier disruption due to the low threshold of energy necessary. A later study sought to apply this type of low frequency US beam (260 kHz) to a rabbit model to demonstrate successful intravasation of injected contrast through the blood brain barrier with minimal adverse effects [109]. Not only would this US regime not necessitate more complex US equipment and transducer arrays, but it would also preclude the need to create a surgical skull window to allow superior access of the beam to brain parenchyma. The results of the study demonstrated successful disruption of the blood brain barrier to the extent of successful delivery of large molecules to the brain. Histologic analysis of brain tissue, including red blood cell extravasation indicative of hemorrhage, and immune cell presence indicative of inflammation, showed minimal aberrative activity. Characterization of the time scale of the disruption and of its temporary nature was also documented. In comparison to other studies using higher frequencies of US for disruption where primary transport was through widening of the blood brain barrier endothelial cell tight junctions, this study demonstrated significant vacuoles in the endothelial cells which were thought to provide transport for the target molecular agents used through transcytosis.

Later studies further elaborated on these advances, as successful blood brain barrier disruption became more consistent, to incorporate therapeutics relevant to Alzheimer's disease. One such example is the delivery of antibodies against the beta-amyloid proteins, which were shown to improve beta-amyloid clearance when previously directly injected into the brain [110].

Given that this process was surgically invasive and essentially infeasible in human patients, disruption of the blood brain barrier presented an alternative mode of delivery. In one study, a focused US beam was applied during simultaneous injection of Definity™ MBs in a transgenic mouse model of Alzheimer's disease during simultaneous magnetic resonance imaging [110]. Because injection of contrast and its subsequent appearance in the brain during magnetic resonance imaging was indicative of successful blood brain barrier disruption, this monitoring allowed for the localization of the US beam for targeted treatment. The authors found that not only was the delivery of the beta-amyloid antibody into the brain successful, but hemispheric pair-wise design of the treatment showed improved clearance of insoluble beta-amyloid plaques from brain parenchyma.

One notable later investigation in the application of UTMC to Alzheimer's disease did not focus on delivery of a therapeutic agent to the brain; rather, it relied upon the UTMC itself and disruption of the blood brain barrier targeted to the hippocampus in an animal model with the aim of modifying disease progression related behaviors indicative of memory impairment. This study continued the use of magnetic resonance imaging guided focused US, and targeted the hippocampus using the rationale that increases in neuronal plasticity were previously demonstrated, albeit in healthy mice that did not display impairment of memory functions [111]. Again, Definity™ MBs were used during sonication at 1.68 MHz US frequency targeting two locations in the hippocampus on one side per animal, followed by gadolinium-based contrast infusion for T1-weighted magnetic resonance imaging to confirm blood brain barrier disruption. This treatment was performed once per week for three weeks, followed by a Y-maze analysis, amyloid plaque analysis, and immunohistological analysis.

The authors' results demonstrated that the magnetic resonance guided UTMC alone resulted in improvement in cognitive task performance, reduced amyloid plaque burden, as well as increased neuronal plasticity without the addition of other therapeutic agents. There were no adverse effects found on the animals' typical behaviors or general health, nor indications of brain parenchymal damage on histological analysis. Potential mechanisms listed by the authors for these positive results included increased transport of endogenous immunoglobulins into the parenchymal compartment as a result of blood brain barrier disruption, leading to increased amyloid clearance, as well as activation of various neural cell species including astrocytes and microglia, which are known to phagocytose beta-amyloid plaques.

In addition to these mechanisms, the authors also tracked the population of immature neurons in the dentate gyrus of the hippocampus, the increase of which is associated with memory functions and general improvement of cognitive behavior in models of Alzheimer's disease. It was shown that UTMC was able to stimulate the proliferation and development of these cells as well, although the mechanisms are not precisely understood. Previous studies without MBs and only focused US stimulation found that such treatment increased production of brain-derived neurotrophic factor, which also serves to mediate hippocampal neuroplasticity, as a potential mechanism for this phenomenon. Other potential explanations include upregulation of Akt signaling in the neurons stimulated by UTMC, which has previously been shown to occur with local blood brain barrier disruption. This results in increased activity in signaling pathways also related to neurotrophic receptors, therefore resulting in improved survival of these immature neurons.

Another study which similarly applied only focused UTMC in the absence of additional therapeutic agents across the entire mouse forebrain in a model of Alzheimer's disease reported

significant cognitive functional improvements after treatment [112]. The US regime used was a 0.7 MPa pressure 10% duty cycle (percent of time the US is active) pulse, with five treatments over a six-week period. Sham controls with only MB infusions were performed as well. All groups received behavioral testing for spatial memory in the Y-maze task, followed by histological analyses of brain tissue for changes in amyloid plaque burden and evidence of cellular damage or inflammation.

This study's results supported the previous study described, as UTMC alone was shown to activate microglial phagocytosis of beta-amyloid protein, resulting in creased plaque burden in treated mice, as well as improvements in spatial memory during the cognitive tasks. The authors also discussed the alternative possibility that enhanced blood brain barrier disruption prevented the deposition of additional insoluble plaques, giving off a similar appearance as improvement. Safety measures and the absence of adverse effects of the UTMC were confirmed again as well. Notably, the authors also address potential barriers in translation of this therapy to human patients in that thickness of the skull and depth of potential targets for UTMC would require significant adjustments to the US parameters. In addition, timing of the UTMC application relative to disease progression would need to be taken into consideration, such as whether to apply UTMC during the prodromal stage of Alzheimer's disease. In addition, to avoid potential excessive immune activation such as with microglial cells, a stepwise approach to covering greater volumes with UTMC may need to be adopted. However, in all, the lack of additional therapeutic agents applied in this animal model study for Alzheimer's disease again demonstrated the significant therapeutic potential of UTMC.

As the significant therapeutic potential and translatability of UTMC became more and more widely recognized after these studies, diversification of the models used and endpoints

evaluated surfaced. One example of an alternative model of Alzheimer's disease related cerebral damage featured the use of aluminum chloride in drinking water given to wild-type rats, which were then treated with a regime of low intensity pulsed US [113]. Cognitive behavioral tasks of the Morris water maze and elevated plus maze were performed in animals following treatment, along with histologic measures of beta-amyloid deposition as well as measures of aluminum related damage. Their results showed that the pulsed US regime resulted in retained memory function over the course of aluminum chloride administration, as well as attenuated accumulation of aluminum as well as beta-amyloid 42 expression in the brain. This study demonstrated that pulsed US (even without MBs) was capable of protecting against an agent known to be associated with increased risk for development of Alzheimer's disease and other types of neurotoxicity.

Aside from measures of plaque burden and immunohistological markers from brain tissue indicative of immune cell activity, recent studies have moved to more sophisticated measures of microvascular changes due to UTMC such as transcriptomic analysis. One such study applied UTMC for blood brain barrier disruption in the dorsal hippocampus and followed changes in transcription up to 24 hours post-treatment [114]. The study found that after UTMC treatment, there was a transient increase in proinflammatory cytokine transcription, potentially promoting the localization and movement of leukocytes across the disrupted blood brain barrier, as well as activating microglial cells and astrocytes. The authors noted that while chronic activation of these inflammatory pathways has been implicated in various disease processes, acute activation has instead been associated with neuroprotection and homeostatic regulation against acute stresses such as ischemia. In all, the authors summarized that these changes result from the oscillation of MBs against the vascular endothelium and may explain for the beneficial effects of UTMC treatment in the context of neurovascular disease models.

These results were noted to be compatible with additional mechanistic studies for UTMC, including upregulated presence of caveolin, a protein involved in transcytosis across the endothelial barrier, which was shown in this study as well [115]. Although this study was not performed with an animal model of Alzheimer's disease, and instead used wild-type Sprague-Dawley rats instead, the implications raised by this type of analysis open avenues for future study specifically in a disease context, given the potential role of inflammatory events in the disease pathogenesis. In addition, the interactions between UTMC therapy and these inflammatory pathways may also reveal different mechanistic implications for the efficacy of UTMC in such disease models as discussed in the previous studies mentioned.

Given the main obstacles of further translation of UTMC for treatment of Alzheimer's disease pathology discussed, such as larger brain size and increased skull thickness in human patients relative to the small rodent models previously investigated, continued investigation of this area transitioned toward work with larger animal models. One such study utilized an aged beagle model, which featured several distinctions from previous transgenic rodent models of Alzheimer's disease [116]. One key difference is that aged beagles (and other species of dogs) naturally develop the amyloid pathology observed in Alzheimer's disease, with corresponding cognitive decline, whereas the transgenic rodent models were engineered to overexpress select proteins. In this way, the canine model represented an aged, pathologic brain rather than merely overexpressing the amyloid protein in an isolated context in the absence of other possible accompaniments to disease etiology associated with the aging process. In addition, the larger brain size of the beagle model presented a more similar physical environment to human patients in that the greater depth of penetration that the US waves would experience prior to reaching their therapeutic destination would allow for the use of the low frequency US waves previously investigated such as in the

rabbit model without development of standing waves, which are essentially stationary waves that oscillate with respect to time but whose peaks do not translate in space. This phenomenon may develop as the result of resonance and wave interference, and due to the accumulation of the US waves effects at the same node locations, adverse biological effects may occur such as the increased development of free radicals and oxidative species. The greater depth of the beagle brain also presents a similar challenge in treatment as human patients, which would facilitate the development of similar US regimes feasible in the similar size scales.

For the blood brain barrier disruption UTMC treatment, a single-element, focused transducer was used. Similar to previous discussion, lead zirconate titanate (PZT) was the material used for the transducer. The US pulse regime was a collection of 10 ms bursts with frequency of 280 kHz (similar to the study of blood brain barrier disruption in the rabbit model, which used a frequency of 260 kHz) with a pulse repetition of 0.33 Hz with a change in position for each second across a millimeter scale grid. The estimated amplitude for the treatment ranged from 0.8 to 1 MPa (in free field, without attenuation from penetration through the skull), starting with the lower estimate and increasing in 0.016 MPa intervals until cavitation signals from injected MBs were detected. For the MB agent, Definity™ MBs were used once again, titrated to a concentration of 0.02 mL per kg of animal bodyweight. This treatment proceeded until an entire hemisphere of the brain was treated, followed by computerized tomography and magnetic resonance imaging with gadolinium-based contrast.

The study results demonstrated consistent safety and efficacy with previous experiments in smaller animal models. All of the blood brain barrier treatments were extremely well tolerated by the animals, and three out of the five animals in each treatment group showed lower beta-amyloid load in the treated hemisphere. However, despite these results, the main takeaway from

this study was the safety rather than efficacy of the focused UTMC treatment, as the authors noted larger sample sizes would be necessary for further comment on statistical significance.

The last study to be discussed in this section represents the final stage in the translational development of this UTMC therapy for blood brain barrier disruption, and also the start of a new area of clinical investigation, that is, application of UTMC for blood brain barrier disruption in human patients in a phase I safety trial [117]. Five patients were enrolled with a mean age of 66 years, and previous positron emission tomography had demonstrated significant amyloid burden past the standardized uptake value ratio cutoff for all patients. A similar treatment protocol as previous studies was performed, with simultaneous UTMC treatment during magnetic resonance imaging with contrast for confirmation of blood brain barrier disruption. T1-weighted gadolinium magnetic resonance images were obtained immediately after sonication and showed a small window of contrast enhancement at the location of the US beam, with disappearance of said window at 24 hours after the treatment, suggesting that the blood brain barrier disruption was indeed transient and had no significant adverse effects that were of immediate notice. The primary US target was white matter in the frontal lobe (more specifically, the dorsolateral prefrontal cortex). All patients were successfully discharged the morning after the US procedure with no significant adverse events including hemorrhages, edema, or death. Again, Definity™ MBs were used in combination with the focused US beam.

While there were no significant functional improvements whether in cognitive performance or in observed amyloid burden before and after the treatment, this did not detract from the study's success or scientific value, as the primary goal of this study was for evaluation of safety and feasibility in human patients, to which end the study was extremely successful. The authors noted that the study had limitations of sample size and target selection, as the blood brain

barrier disruption was limited to a relatively small area in this preliminary study. In addition, more sophisticated targets with additional functional implications in Alzheimer's disease pathology would warrant further investigation in the future. In addition, no therapeutic agents were used in this investigation, which may further enhance the value of UTMC and its role in blood brain barrier disruption.

3.3.2 Toward Treatment of Cardiovascular Disease

Given the wide range of pathologies which fall under the umbrella term of cardiovascular disease, this section will be divided into two main sub-sections of drug and gene delivery for non-acute conditions, and sonothrombolysis using UTMC, which is often directed toward acute conditions, such as acute coronary syndrome. It is noted that both applications may be combined, such as in the work of this dissertation, through the use of therapeutically modified MBs in applications of thrombolysis, as the preserved mechanical performance of the MBs result in their therapeutic cavitational activity simultaneously with the drug delivery resulting from MB rupture after US sonication.

3.3.2.1 Cardiovascular Drug and Gene Delivery

Similar to the difficulties presented by the blood brain barrier, vascular tissue is similarly compartmentalized and highly regulated and restricted in the substances which may traverse this boundary to enact therapeutic effects. Therefore, one of the main goals of UTMC in cardiovascular applications of drug delivery are again disruption and permeabilization of this barrier to allow for enhanced transport of therapeutic agents. In addition, cardiovascular disease may also present various types of pathologic tissue, such as the buildup of atherosclerotic plaque, which is

composed of lipids, cholesterol, cellular debris, and calcified tissue, in the walls and lumen of affected vessels. In this context, and in the context of diseases such as cardiomyopathies, peripheral vascular diseases, and rheumatic heart diseases, the therapeutic target often presents beyond the vascular endothelium. Aside from the physical barrier that this cell layer presents, other characteristics of the physical microenvironment that limit therapeutic delivery include blood flow itself, which may reduce lumen concentration of the therapeutic agent. Many larger blood vessels such as the aorta and coronary arteries also possess elastic lamina which present significant resistance to permeabilization, and their endothelial linings are highly resistant to shear stresses due to the high-pressure, high-flow conditions of the immediate environment. In addition, compliance and muscular activity of these vessels are highly coordinated with endogenous homeostatic systems such as the nitric oxide pathway and adrenergic pathways, disruption of which may result in significant adverse effects upon cardiac function and local tissue perfusion.

Early applications of targeted delivery to cardiovascular tissue using UTMC involved cellular studies with targeted MBs to adhesive proteins expressed by said vascular cells. One example was ICAM-targeted liposomes conjugated with vascular stem cells delivered to *ex vivo* murine aortas in the presence of continuous US, which demonstrated successful extravasation past the vascular endothelium and subsequent stem cell deposition confirmed in the intimal layer. Although no US associated damage to the tissue was reported, there was also extremely limited delivery of the stem cells beyond the first elastic laminae. Increase of the peak US pressure from the 0.15 MPa used to 0.23 MPa with actin-targeted liposomes labeled with fluorescent calcein resulted in strong signal from the intima to the adventitia, as well as within the smooth muscle layer, which suggests greatly enhanced transendothelial delivery [118].

Further success with UTMC for drug delivery to the myocardium was experienced by many studies targeting a wide range of both molecular growth factors and genetic material as payloads for therapeutically modified MBs. This resulted in therapeutic outcomes ranging from enhanced revascularization and angiogenesis through transmyocardial delivery of vascular endothelial growth factor (VEGF), as well as plasmid DNA delivery with loaded MBs to rat myocardium resulting in significantly increased target gene expression relative to untreated samples [119].

From these early studies emerged predominant strategies toward the targeting of MBs to major pathologic and inflammatory molecular markers. Both ICAM-1 and VCAM-1 (vascular cell adhesion protein) have been popularly targeted by conjugation of their respective antibodies on the surface of MBs, resulting in localization of circulating MBs to specifically activated vascular endothelial cells. In addition, P-selectin, another cellular adhesion protein upregulated in conditions of endothelial inflammation, has been successfully targeted by modified MBs, with the adhesion characterized by increased shear stress necessary to dislodge the successfully adhered MBs. Combinations of these antibodies have also been applied to MBs for even greater efficiency in localization compared to MBs selective for single species of molecular targets [120, 121].

In addition to endothelial targets, intraluminal thrombi have also been the subject for localization of modified MBs. As a surrogate marker for thrombi, platelets with their surface glycoproteins, have been the subject of thrombolytic drug delivery applications with modified MBs, such as against GP IIb/IIIa targeted MBs. Fibrin itself has also been the target of modified therapeutic MBs. Conjugation of drugs such as plasminogen activator to these MBs has resulted in significantly enhanced thrombolysis *in vitro* [121]. In contrast to drug delivery, gene delivery to cardiovascular targets faces additional barriers such as degradation of the genetic material by the immune system or blood enzymes, electrostatic repulsion by cellular membranes, degradation

by intracellular compartments such as lysosomes, and penetration of the nuclear membrane for successful transcription. Current advances in gene therapy toward treatment of cardiovascular disease have distinguished two main categories for delivery vectors for genetic material: viral vectors and non-viral vectors. As the names suggest, viral vectors encompass many different families of viruses including adenoviruses, retroviruses, and lentiviruses [122-125]. Examples of viral vector applications include the delivery of calcium channel genes to coronary arteries resulting in the prevention of ventricular arrhythmias, silencing of phospholamban gene expression (a calcium channel regulator in cardiomyocytes) resulting in treatment and slowed deterioration in heart failure, although viral vector approaches in gene therapy in general have been subject to criticism due to their potentially unpredictable nature and the capacity to develop mutations in the genetic material and during the gene insertion process, potentially resulting in devastating adverse effects [126, 127]. On the other hand, non-viral vector gene therapy involves the use of macromolecules and molecular constructs including the liposomes, particles, and polymers that have been partially discussed in the previous section on therapeutic modifications of MBs for gene delivery [128, 129]. Although naked DNA may also be used directly, this is unpopular due to the high rates of deterioration and low targeting efficiency after circulation in the subject vasculature. Therefore, many of the conjugated constructs also serve the purpose of protecting the genetic material from exposure to destructive mediators such as enzymes and phagocytic immune cells.

Other strategies for enhancing delivery efficacy of genetic material include conjugation of constructs to antibodies targeting specific molecular components of cardiac tissue, such as cardiac myosin, which resulted in successful enhancement of *in vitro* transfection [130]. However, these generally biologically inert non-viral constructs are tasked with the main obstacle of penetrating

the physical barrier of the cellular membrane, something which viral vectors are innately equipped to handle [131].

Therefore, in this context UTMC provides an efficient solution to the delivery of genetic material through overcoming the physical barrier of cellular membranes through the many mechanisms previously discussed, including sonoporation, radiative forces, inertial cavitation, and increased endothelial permeability. Indeed, studies have shown that use of UTMC successfully increases transfection efficacy of both plasmids and short hairpin RNA both *in vitro* and *in vivo* [132-134]. Use of UTMC to enhance gene therapy also confer advantages of low toxicity (as the material components of most MBs are biocompatible and the gas core species will diffuse to be exhaled by the subject), low immunogenicity (compared to viral vectors, which may trigger a host immune response after delivery), decreased invasiveness (due to external US application and injections of MBs being extremely non-invasive to the subject), and improved targeting (due to external manipulation of the US beam for selection of a location for MB cavitation and subsequent release of genetic material). Due to all these reasons, UTMC is highly favored as a recent development and tool for enhanced gene therapy. One such example is the TFPI-2 gene, which is involved in the processes of atherosclerosis, thrombosis, and re-stenosis following intervention. Previous investigation has demonstrated the successful delivery of the gene with SonoVue as the MB agent, with increased efficacy even compared against an adenoviral vector [135]. Other gene targets include the TB4 gene, which stimulates differentiation of immature cardiac progenitor cells, naked plasmids which have been incubated with liposome formulations as previously described, fibroblast growth factor for stimulation of myocardial angiogenesis, and tissue plasminogen activator gene plasmids for treatment of thrombotic disease [136].

Viral vectors have also been successfully shown to be enhanced with adjuvant UTMC therapy. Although viruses have the innate ability and machinery to penetrate through the cellular membrane, their efficacy may still be improved through the mechanisms of UTMC such as sonoporation in a synergistic manner [137, 138]. Moreover, UTMC may enhance the specificity of viral targeting due to increased concentration of viral activity to cavitation regions, as well as increased spread of the viral vectors through increased permeability of the endothelial barrier. This increase in transduction efficiency has been demonstrated with retroviral vectors to over 5-fold increases in transduction for various types of cells [139]. Further experiments on transgene expression *in vivo* showed similar results with infusion of therapeutically modified MBs into the myocardial microvascular beds followed by rupture with high intensity US pulses at 1.3 MHz [140]. Therapeutically modified MBs have also been shown to confer a cloaking effect on the immunogenicity of injected viral vectors, as systemic administration of viral vectors has previously triggered host innate immune responses that were potentially concerning. In addition, certain types of viruses (such as retroviruses) require their own viral envelope membrane to successfully integrate and penetrate the cellular membrane for payload delivery [141]. However, previous studies of envelope-deficient retroviruses which were loaded into MBs still resulted in successful delivery and transfection using UTMC, suggesting that MB lipid shells may possibly perform similar roles, or are enhancing cellular mechanisms of material incorporation such as endocytosis [142]. In further mechanistic studies regarding the delivery of partially inactivated viral vectors with UTMC, one group developed pegylated adenoviruses which were essentially prevented from interacting directly with the cellular membrane based on steric hindrance from the polymer brush layer [143]. Use of these modified viruses with UTMC still resulted in successful delivery into the

cytosol of cells, hence suggesting that mechanisms of sonoporation alone are highly capable of mediating viral particle delivery.

3.3.2.2 Thrombolysis

Thrombolysis, or the destruction of blood clot, is relevant to many pathologies including acute coronary syndromes, stroke, pulmonary embolism, and peripheral vascular disorders. Although there exist endogenous mechanisms for prevention and resolution of thrombosis, including signaling from endothelial cells and hematologic systems such as the tissue plasminogen activator pathway, development of thrombi that overwhelm these defenses often require medical intervention to prevent potentially irreversible damage. Use of US to dissolve thrombus has been a long-sought after solution to this issue, which has more recently become refined with the development of UTMC and various elaborations on this minimally invasive technique. The mechanisms of efficacy of UTMC in performing thrombolysis have their foundations in the same physical mechanisms previously described that are attributed to the efficacy of UTMC in other applications as well; these cavitational and radiative forces may leverage the explosive nature of MB destruction to instead cause maximal impact on the surface and penetration into the depths of thrombus material to not only cause disruption of the thrombus mechanical integrity but also to increase the available surface area for activity of both endogenous and exogenous molecular thrombolytic therapies. In this section, the application of UTMC for thrombolysis in various pertinent clinical applications will be discussed. (It is noted that the context of microvascular obstruction, because of its central nature to the work in this dissertation, will be reserved for discussion in a later chapter.)

It is first to be noted that US alone has been shown to have thrombolytic effects. Low frequency US has been delivered both transcutaneously and intravascularly (via a catheter-based

system) to destroy arterial thrombotic obstructions and has been demonstrated to be successful in a number of previous studies in coronary arteries and vein grafts [144-146]. The US frequencies used have ranged from 20 kHz to 2 MHz, both in continuous and pulsed regimes of delivery. In addition, many of these studies have sought to use therapeutic US alone to enhance the efficacy of a simultaneously delivered thrombolytic agent to significant effect. In one example, 26 kHz US at an output of 18 watts per square centimeter was applied to thrombotic rabbit femoral arteries as an adjuvant therapy to streptokinase administration [147]. The study's results showed that use of both therapeutic US and streptokinase together resulted in over a 50% increase in the number of rabbits successfully recanalized compared to streptokinase alone. Improved results using the same model showed even greater increases at over 90% recanalization rate for the animals when frequency of the US was further increased to 37 kHz.

UTMC has also shown highly positive results for thrombolysis, of course. However, the mechanism of UTMC in thrombolysis has been strongly suggested to be mechanical, not biological in nature. One previous study showed that UTMC resulted in increased thrombolysis than US alone with urokinase infusion [148]. However, measured D-dimer levels, which are molecular markers of enzymatic thrombolysis, were non-elevated with UTMC. While the residual particle size was indeed smaller, similar to sizes seen in biological thrombolysis, the lack of D-dimer elevation suggested that the UTMC merely mechanically reduced the thrombi to smaller sizes.

One area in which UTMC has demonstrated significant clinical utility is in the treatment of stroke. Stroke, or ischemic stroke, is the event of neuronal cell death due to obstructed blood flow through the cerebral vessel supplying the local region, commonly due to a thrombotic event. This may lead to death, or sustained neurological damage, leading to potential disability. The current prevailing treatment for stroke is infusion of recombinant tissue plasminogen activator, which is a biological

thrombolytic agent unfortunately accompanied by increased risk for subsequent hemorrhage. With developing medical technology, thrombectomy, or the intravascular procedure of non-invasive surgical thrombus removal, has become an alternative to recombinant tissue plasminogen activator (rtPA) therapy. However, this technique is limited to specific treatment centers and also by vessel size, as vessels with diameters smaller than 2 mm are generally inaccessible to the equipment. Therefore, UTMC based thrombolysis has been explored as an additional minimally invasive therapy toward treating stroke. Because the injected MBs themselves have no innate biological function or adverse effect, there is no increase of hemorrhage as in the case with rtPA therapy, nor is there a size limitation for access as in the case of thrombectomy because the size of the MBs (on the order of single digit microns) is much less than most vessels of the major cerebral vascular system. A meta-analysis of randomized controlled trials and case-control studies as well as a recent clinical trial have both concluded that thrombolysis with UTMC, termed sonothrombolysis, is a viable therapeutic strategy for treatment of stroke and demonstrates no significant adverse effects in the patient [149].

In one most recent meta-analysis of pre-clinical animal studies, a number of successful aspects of sonothrombolytic therapy were emphasized [149-151]. General trends included the favor toward intra-arterial administration of treatment MBs over intravenous administration, targeted MBs over non-targeted MBs for patency and recanalization rates, and adjuvant rtPA therapy with concurrent sonothrombolysis over sonothrombolysis alone. Outcomes of sonothrombolysis with UTMC included lower infarct volumes, better TIBI scores, patency rates, and vascular volumes of treated versus untreated hemispheres. However, there were some negative results reported as well suggesting that sonothrombolysis with rtPA treatment was ineffective in certain scenarios of thrombi with high platelet concentrations. With the main adverse effect of

stroke intervention being hemorrhage, sonothrombolysis has been shown to not increase cerebral hemorrhages relative to control; however, the meta-analysis notes that the other treatment groups, including rtPA (which is known to be accompanied by an increased risk of hemorrhage), also did not show increased cerebral hemorrhage. The meta-analysis proposes several potential reasons for this, with one being the lack of an ischemic phase prior to treatment in animal studies. With the development of multimodal imaging techniques, as well as combination theranostic (therapeutic and diagnostic) interventions, the combination of magnetic resonance imaging with therapeutic US continues to be a strong source of innovation for treatment of stroke just as it has been for treatment of Alzheimer's disease and in disruption of the blood brain barrier. Specifically, magnetic resonance guided high frequency US (HIFU, as previously described), has become a targeted, minimally invasive method for thermal heating and ablation. Both the size and extent of ablation depend on the delivered thermal dose, which is determined by the characteristics of the US wave used due to the mechanical principles of attenuation and absorption as previously described [152]. Although several human clinical trials for unfocused US alone with rtPA for treatment of stroke have been either unsuccessful or prematurely terminated due to an unacceptable rate of adverse events, there are those who feel that the use of rtPA and the use of unfocused beams (which may generate standing waves, a phenomenon of stationary nodes and antinodes due to waveform interference) resulted in such adverse events which would be addressed through the use of HIFU. Preliminary *in vivo* studies have shown viability for this technique in thrombolysis in animal models such as a carotid rabbit model [153]. In addition, HIFU with injected MBs, an additional factor not studied in the clinical trials previously mentioned, further reduced the US energy required for successful recanalization of the occluded vessel. One further advantage of HIFU with magnetic resonance guidance is the treatment of hemorrhagic stroke, which may be

caused by trauma to the head, cerebral aneurysm rupture, and hypertension, among other factors. This results in a need for thrombolysis as well, as otherwise the resultant clots from the hemorrhage often require craniotomy and aspiration for surgical removal. Catheter based magnetic resonance guided HIFU has also been shown to enhance thrombolysis in such cases, while also potentially augmenting CSF circulation and improve hydrocephalus.

One other clinical area to mention for the use of US for thrombolysis is in acute pulmonary embolism [154]. Pulmonary embolism, which has generally been limited to systemic anticoagulation for treatment, may result in hemodynamic instability, severe hypoxia, right cardiac ventricular failure, and death. Although use of systemic anticoagulation therapy results in an improvement in overall mortality, again, as in the case with stroke, increased risk for major hemorrhage is a significant factor in weighing the risks for its application. Again, in parallel with interventions for stroke previously discussed, catheter-based techniques for treatment of pulmonary embolism have also been developed. The goal being to remove the obstructing thrombi from the pulmonary circulation, this involves mechanical disruption of the thrombus using fragmentation, suction, and torsion. Additionally, delivery of thrombolytic agents in the immediate vicinity of the catheter device is also possible, resulting in a direct distribution of the agent to the thrombus surface. However, peri-procedural complications and procedural-related deaths have still occurred, and the therapeutic contribution of the catheter intervention alone (versus thrombolytic agent administration with the catheter intervention) is still not fully understood. One device designed specifically for this need is the EkoSonic® Endovascular System, which is a combination of a multi-sidehole drug infusion catheter outside of a core wire consisting of several US elements [155]. This device was approved by the FDA in 2008 for intravascular applications. One clinical trial for US thrombolysis in acute pulmonary embolism is the ultrasound accelerated

thrombolysis of pulmonary embolism (ULTIMA), hypothesized that use of US thrombolysis would result in improvement in right to left ventricular ratio compared to systemic anticoagulation alone [156]. The treatment arm of the trial consisted of an US thrombolysis combination therapy with rtPA administration, and resulted in a highly significant improvement in right ventricle to left ventricular ratio at 24 hours after therapy (therapy lasting 15 hours), while the control group receiving systemic thrombolytic therapy showed no such improvement at that time, only managing a later catch-up effect. Ventricular ratio at 90 days after therapy and systolic function of the right ventricle were both assessed to be in favor of the US thrombolysis group, and only minor adverse events of some hemorrhaging were observed. A later meta-analysis noted that the previous study, as well as an aggregate of other clinical studies on patients with acute pulmonary embolism treated with US thrombolysis, demonstrated significantly lower rates of major bleeding events than seen in systemic thrombolytic therapy by almost five times [157]. It was noted that the newest catheter devices are capable of delivering the high frequency US (2.2 MHz) needed for successful disruption of thrombus and delivery of the concurrently administered thrombolytic agent. Additionally, one of the most recent US thrombolysis trials showed no incidences of intracranial hemorrhage, with significant improvement of hemodynamic status. Overall, US thrombolysis with local thrombolytic agent delivery has been shown to have significantly improved prospects for patients with acute pulmonary embolism [158, 159].

3.4 Summary

This chapter was an introduction to the concept of UTMC, with several examples of notable clinical applications for the technique. While the work in this dissertation remains at a pre-clinical

animal model stage, the further refinement of UTMC itself still warrants investigation and innovation with novel therapeutic agents and biological applications. Now that much of the relevant concepts and techniques involving US, both imaging and therapeutic have been discussed, the next few chapters will mainly detail the biological contexts in which UTMC operates, which will also be relevant to the disease and animal model context of the work in this dissertation.

4.0 Microvascular Obstruction Background and Clinical Implications

In this chapter we will discuss the concept of microvascular obstruction as a pathological condition as well as a therapeutic target for UTMC. Although microvascular obstruction is not directly addressed in the work of this dissertation (an ischemia-reperfusion injury model is instead used), it has been the target for the previous work in the author's laboratory. However, many of the pathological changes which occur in MVO are sought to be captured in the ischemia-reperfusion disease model, including processes such as inflammation and oxidative stress. In addition, for further translation of this work, including transitioning to larger animal models and even human patients, MVO and the no-reflow phenomenon remain to be the target pathologies. Therefore, this chapter will consist of the pathophysiology of microvascular obstruction, its underlying mechanisms, its occurrence in human patients, current treatments for microvascular obstruction (including with UTMC), and its implications on patient outcomes.

4.1 Microvascular Obstruction Pathophysiology

Coronary artery disease is the pathological deterioration of the capacity for the coronary arteries to supply blood to myocardial tissue. One specific form of coronary artery disease is when there is an acute, sudden obstruction of an epicardial vessel, due to a combination of thrombosis, embolization, plaque disruption, and vascular spasm, and is called acute myocardial infarction. The resulting myocardial ischemia may result in permanent damage to the heart if left untreated, although modern medicine has developed percutaneous coronary interventions to prevent such

occurrences [160]. Percutaneous coronary intervention involves patient catheterization and the deployment of various wire, catheter, balloon, and sheathe type devices to the heart to store blood flow to the occluded artery. However, despite these advances, there is a phenomenon in which ischemic myocardial tissue fails to reperfuse (or reflow) after successful recanalization of the epicardial artery, termed no-reflow. Another source defines no-reflow as inadequate perfusion of myocardial tissue without evidence of a mechanical obstruction to perfusion for that specific region. This term for the phenomenon described was first coined in 1967 in the setting of cerebral ischemia and has persisted since [161]. The occurrence of no-reflow has also been accompanied by terms such as the no-reflow region, which refers to the area in which no-reflow occurs, and microvascular obstruction, which is essentially synonymous with no-reflow but places emphasis on the contribution of deranged microvasculature conditions to the phenomenon [162]. Nowadays, no-reflow has been used to refer to the physiological state of absent myocardial perfusion following successful epicardial recanalization, while microvascular obstruction is referred to as the underlying mechanism resulting in the no-reflow condition [162]. Microvascular obstruction refers to the obstruction of vessels fewer than 200 microns in diameter. In addition, pathophysiology of microvascular obstruction in relation to epicardial vessel atherosclerotic disease and obstruction has been well documented, with plaque erosion from epicardial vessels shown to have strong implications in development of microvascular obstruction in patients [163, 164].

There has been a distinction of two overall types of microvascular obstruction resulting in no-reflow: myocardial infarction reperfusion no-reflow and interventional no-reflow. In the myocardial infarction reperfusion type, the underlying source of injury results from ischemia-reperfusion and endothelial injury due to ischemia [161]. Briefly, endothelial injury is caused by

a wide range of factors including oxidative damage from reactive oxygen species, inflammation, excessive intracellular calcium influx, and a loss of mitochondrial membrane integrity. The resulting damage causes endothelial swelling and protrusion, as well as myocardial edema, which result in bulging of tissue into the vascular compartment and thereby causing microvascular obstruction. Of course, vasospasm and distal embolization from the epicardial event site may also exacerbate the damage described above. The second type of microvascular obstruction described as interventional refers to the scenario in which percutaneous coronary intervention and deployment of stents and balloons results in fragmentation and distal embolization of the main thrombus, as well as the release of atherosclerotic debris, which is highly inflammatory [161]. This deployment of debris results in significant activation of platelets and inflammatory cells, which further contribute to the obstructions which develop in the downstream microvasculature in a combination of mechanical plugging and biological aggravation of endothelial health. These various processes will be described in further detail in following sections.

Another type of classification for microvascular obstruction separates cases into structural and functional obstruction [165]. Structural obstruction is due to factors such as endothelial swelling and myocardial edema causing vascular compression and obstruction, or damage to capillary integrity which renders them unfunctional after prolonged ischemia (and development of an ischemia lesion). Functional microvascular obstruction, on the other hand, refers to transient factors such as vascular spasm, ischemia-reperfusion injury resulting in a build-up of neutrophils and platelets, and distal microembolization [165]. Structural obstruction is generally irreversible, whereas functional obstruction is reversible to an extent. In human patients, there have been four main components of microvascular obstruction, described as distal embolization, ischemic myocardial injury, ischemia-reperfusion injury after successful percutaneous coronary

intervention, and previous individual vulnerability for microvascular injury [165]. Distal embolization may occur both from an epicardial thrombus as well as an atherosclerotic plaque and is the downstream circulation of various atherothrombotic particles ranging from tens to hundreds of microns in size. Such emboli are thought to range from 20 to 200 microns in size, although microemboli greater than 200 microns may result in severe obstruction [165]. Ischemic myocardial injury commonly consists of cellular swelling and bulging, including the development of luminal endothelial protrusions. In addition, erythrocyte extravasation is extremely common due to the loss of structural integrity in cellular junctions and widening endothelial gaps, which further contributes to myocardial swelling and edema, further compressing the microvasculature.

Reperfusion-ischemia injury will be described again in a later chapter, but in the context of microvascular obstruction, occurs after successful epicardial recanalization. Sudden return of blood flow also results in a massive influx of inflammatory cells, neutrophils, and platelets to the previously ischemia area [166]. Due to the buildup of toxic metabolites and waste products during the period of ischemia, activation of these cells typically occurs, which only results in the feedback loop of further production of various antagonistic products by neutrophils, such as reactive oxygen species, free radicals, proteolytic enzymes, and pro-inflammatory signaling mediators which may cause not only endothelial damage, but also further amplify this signal and pattern of activity to other immune cells in the body after circulation [167]. Damaged endothelial cells may then release various vasoconstrictive mediators, which may result in vascular spasm and exacerbation of microvascular obstruction [167]. Specifically, some of these molecular mediators include interleukin-1 beta, tumor necrosis factor-alpha, selectin, and superoxide radicals [167]. Interleukin-1 beta has been shown to be associated with ischemia-reperfusion injury and inflammation. Tumor necrosis factor-alpha has been shown to be associated with decreased

coronary flow reserve (which increases vulnerability to microvascular obstruction as there is less capacity for additional recruitment and vasodilation of the coronary vessels) [167]. Selectin is a cellular adhesion molecule expressed on endothelial surfaces and is relevant to mechanical obstruction. Superoxide radicals, which are formed by the enzyme xanthine oxidase of neutrophils, also contributes toward inflammation through damage of cellular proteins and genetic material. Another mediator of endothelial injury is vascular endothelial growth factor (VEGF) when produced in a metabolically deranged context. VEGF may be produced in response to hypoxia during myocardial infarctions, and while it typically complexes with cadherin to stabilize endothelial cellular junctions, during ischemia, this signaling molecule dissociates its own receptor molecule from the cadherin junction complex, resulting in increased endothelial permeability [167].

Other aspects of reperfusion injury aside from cells and molecular mediators is the change in electrolyte concentrations of the extracellular fluid compartment during and after ischemia [167]. During ischemia, there is an accumulation of sodium ions due to an increase in hydrogen ions produced by anaerobic metabolism, an accumulation of calcium ions due to a sodium calcium exchanger's overactivity, and extrusion of accumulated sodium ions through the sodium potassium ATP dependent transporter is impaired, again due to lack of ATP and anaerobic metabolism. In all, this leads to cardiomyocyte swelling and mitochondrial permeability, which results in sudden rupture when there is a drastic and sudden change in extracellular osmolality during reperfusion and influx of typical extracellular fluid to the region [167]. For predisposing factors and vulnerability to microvascular injury, vascular disease factors such as diabetes, hypercholesterolemia, and other genetic conditions involving oxidative stress are implicated due to the role of oxidative stress and inflammation in the development of microvascular obstruction

pathology [167]. In addition to these factors, microvascular obstruction continues to present additional adverse effects which continue on to affect patient prognosis. These are thought to include hemodynamic obstruction of the delivery of various molecular mediators involved in the recovery process and remodeling of the ischemic lesion into a myocardial scar, as well as limiting of circulation and localization of various cellular participants in post-infarct remodeling such as macrophages, which phagocytose cellular debris and promote infarct healing [161, 162, 166, 168, 169].

4.2 Diagnosis of Microvascular Obstruction

Microvascular obstruction, as we previously defined, is a deficiency in perfusion of myocardial tissue despite patency in the proximal epicardial vasculature. It may be caused by a wide range of contributing factors, including ischemic damage promoting the release of toxic and vasoconstrictive factors, myocardial edema, endothelial swelling, distal microembolization from the epicardial atherothrombotic event site, and neutrophil and platelet activation and aggregation. Typically, microvascular obstruction occurs at the core of the ischemic region, although its pathology may spread to surrounding myocardial tissues within the first 48 hours. The prevalence of microvascular obstruction is different depending on the study population referenced. For the population of all patients receiving a catheter procedure, microvascular obstruction may be as low as 8-10%. However, for the population of only patients experiencing an acute myocardial infarction with ST elevation, previously investigated incidence of microvascular obstruction has been as high as 60% [166].

The diagnosis of microvascular obstruction most commonly requires the use of an imaging modality, of which there is a wide range of options available. These include angiography, US echocardiography, cardiac magnetic resonance imaging, and nuclear scintigraphy. As previously mentioned, the Thrombolysis in Myocardial Infarction (TIMI) flow grading system is used to assess microvascular blood flow on angiography. For contrast echocardiography, use of MB agents is included, with the rate of myocardial MB uptake being the quantitative measure [170]. However, this is a less consistent measurement due to greater dependence on consistency in MB contrast infusion, operator skill, and acquisition of an optimal acoustic imaging window. Another method used is through electrocardiography, especially changes in ST segment elevation after percutaneous coronary intervention. Studies have shown that with successful myocardial reperfusion following intervention, there should be a rapid decrease of ST elevation (assuming myocardial infarction with ST elevation) [161, 166]. A drop of ST elevation less than 70% after one-hour post-intervention is therefore taken to be a sign of microvascular obstruction and has been shown to be highly specific (91%) as well as sensitive (77%). Intracoronary guidewires and catheters have also been used to measure coronary blood flow rate, flow reserve, and also therefore microvascular function and possible obstruction. Microvascular obstruction is associated with alterations in observed flow characteristics, specifically reversal in systolic flow, reduced anterograde flow during systole, and rapidly decelerating diastolic forward flow. Because microvascular obstruction is at its essence a derangement of hemodynamics and capillary damage on the microvascular level, these velocity patterns are associated with such hemodynamic changes. Intracoronary pressure measurement using double lumen catheters has also been performed with two measurement points. A significant pressure gradient may also be investigated as potential microvascular obstruction.

Cardiac magnetic resonance imaging remains the most comprehensive method of diagnosing and assessing microvascular obstruction [171]. Cardiac magnetic resonance imaging utilizes infusion of gadolinium-based contrast agents to delineate the infracted region, and the appearance of microvascular obstruction to this contrast imaging may change depending on the timing of the magnetic resonance image acquisition with the instance of contrast administration. In early stages, microvascular obstruction is identified as a defect in perfusion in the core of the infarcted region, essentially a hypointensity on T1-weighted imaging typically 2 to 5 min after contrast administration [171]. If the microvascular obstruction is particularly severe, this hypointensity and absence of contrast enhancement may persist up to greater than 10 minutes after contrast administration, which is then referred to as late microvascular obstruction. Compared to early microvascular obstruction imaging, late microvascular obstruction has much greater spatial and contrast-enhancement resolution, and also fully encompasses the left ventricle [171]. As such, the filling in, or washing in of the gadolinium contrast into the microvascular obstruction region at the core of the infarct zone varies based on each individual case, and the prognostic significance of this timing is yet undetermined [171].

Another development of severe microvascular obstruction is described as intramyocardial hemorrhage and occurs after the development of microvascular obstruction in the infarct zone core and may expand even after successful percutaneous coronary intervention [171]. The cause of intramyocardial hemorrhage is the accumulation of vascular endothelial damage and loss of intercellular junction integrity, resulting in extravasation of red blood cells into the interstitial myocardial space. Due to this lack of compartmentalization between the bloodstream and tissue interstitium, this inundation is accompanied by severe ischemia reperfusion injury, and is also highly correlated with the overall infarct size [171]. Other factors contributing to intramyocardial

hemorrhage and possibly exacerbating its severity include presence of collateral flow (to mitigate ischemic damage by having supplementary pathways for blood to reach the infarct zone), extent of necrotic damage (also related to timing of percutaneous coronary intervention), extent of distal microembolization, and individualized risk factors including lifestyle factors such as hypercholesterolemia, smoking, and diabetes, among others [171].

Diagnosis and assessment of intramyocardial hemorrhage is once again achieved through cardiac magnetic resonance imaging, and intramyocardial hemorrhage is typically observed as a hypointensity within the infarct zone in T2-weighted imaging [171]. This is because the paramagnetic characteristics associated with the hemoglobin molecule and its various metabolic decomposition products shortens the T2 relaxation time after sequences. In addition, T2*-weighted imaging may also be used to identify intramyocardial hemorrhaging due to the sequence marking hemorrhages as hypointense [171]. However, T2* images are slightly noisier than T2-weighted images, and the T2* signal gradually normalizes to the surrounding tissue due to tissue remodeling associated processes such as collagen deposition and removal of interstitial iron deposition. Further comparison between T2 and T2*-weighted imaging is needed in study, however, as microvascular obstruction without significant hemorrhage may also appear as hypointense on T2-weighted images [171].

4.3 Clinical Outcomes Following Microvascular Obstruction

One major study pooling data from 7 randomized trials studying microvascular obstruction after percutaneous coronary intervention showed strong associations between microvascular obstruction and mortality and development of heart failure in patients after 1 year [172]. MVO

itself was also quantitatively analyzed using gadolinium-based contrast and cardiac magnetic resonance imaging. Briefly, with gadolinium contrast after myocardial infarction, there is a hyperintense infarct area, and then a dark region within the hyperintensity which represents microvascular obstruction. In the study, 1688 patients with cardiac magnetic resonance imaging performed after percutaneous coronary intervention for acute myocardial infarction were analyzed with clinical follow-ups at 6 months and 1 year after the event [172]. There were significant associations found between microvascular obstruction and all-cause mortality as well as subsequent hospitalization for development of heart failure, including a graded response when microvascular obstruction was separated into three categories based on severity [172]. In addition, it was found that MVO itself was a strong independent predictor of all-cause mortality, and that patients who experienced microvascular obstruction had greater infarct sizes [172]. However, even while adjusting for infarct size, microvascular obstruction remained significant for the mortality and heart failure rehospitalization previously described. In addition, area of microvascular obstruction also was significant in modeling, with a 1% increase in the absolute extent of microvascular obstruction being associated with a 14% increase in 1-year mortality and an 8% increase in re-hospitalization due to heart failure [172].

In a separate meta-analysis, presence of early or late microvascular obstruction was correlated against clinical outcomes including major adverse cardiac events, cardiac death, congestive heart failure-related re-hospitalization, and recurrence of acute myocardial infarction [173]. In addition, for studies in the meta-analysis which analyzed both early and late microvascular obstruction, a comparison between the two was also investigated for intra-study correlation. In addition, functional measures such as left ventricular function and volume and infarct size were correlated against presence of early and late microvascular obstruction [173]. The

results showed that early microvascular obstruction was independently associated with both left ventricular remodeling and incidence of major adverse cardiac events [173]. In addition, there were significant difference in ejection fraction and left ventricular volumes at later follow-up examinations for patients who presented with and without early microvascular obstruction. In addition, there were trends of early microvascular obstruction increasing cardiac mortality, incidence of future acute myocardial infarction, and congestive heart failure re-hospitalization, although the results were not statistically significant.

For effects of late microvascular obstruction, which was investigated as a potential alternative marker to early microvascular obstruction for prognostic purposes, similar outcome measures were analyzed [173]. Similar to early microvascular obstruction, late microvascular obstruction was significantly associated with both left ventricular remodeling and incidence of major adverse cardiac events using multivariate analysis, with presence of late microvascular obstruction predicting greater declines in ejection fraction at both baseline measurement and longitudinally during follow-up examinations. However, most studies did not report any significant additional benefit of assessing presence of late microvascular obstruction to predict the previously mentioned functional outcome measures. The few studies which did, though, reported significant correlation between size of the late microvascular obstruction with incidence of major adverse cardiac events, and the ratio of the microvascular obstruction to infarct size was found to be the strongest predictor of major adverse cardiac events by one study, possibly suggesting that late microvascular obstruction holds stronger predictive capacity with future major adverse cardiac events experienced by the patient [173].

Another study investigating the prognostic implications of microvascular obstruction found that presence of microvascular obstruction was significantly associated with an increased

mortality at 30 days post-event (relative risk ratio of 2.1), and that 5-year re-hospitalization is also more frequent in microvascular obstruction patients [174]. In addition, evaluation of infarct regions using positron emission tomography showed that microvascular obstruction patients typically had larger infarcts and almost twice as many deaths at the 5-year survival mark.

In all, microvascular obstruction has been characterized as a pathologic phenomenon which is extremely common and identifiable, with significant impact on patient outcomes. The following section will discuss current attempts at intervention for microvascular obstruction [165, 171, 174-177].

4.4 Current Treatments for Microvascular Obstruction

There have been numerous trials investigating treatments for microvascular obstruction, from pharmacological agents to medical devices. General consensus in the field is that there is currently no standardized treatment for this phenomenon, although results from various meta-analyses and reviews have been mixed in opinion regarding suggestions for treatment [161, 178]. One class of drugs that have seen consistent use in applications of cardiovascular disease are calcium channel blockers such as verapamil, diltiazem, and nicardipine. Recent meta-analyses have shown significant benefits of intracoronary calcium channel blocker therapy compared to standard of care [179]. However, many of these studies claiming benefits were also performed in different clinical contexts such as atherectomy, which involves removal of atherosclerotic plaque, and percutaneous interventions for venous grafts rather than native coronary vessels [179]. While positive, and certainly demonstrating the value of these drugs, the results from these trials suggest

the need for a larger standardized trial investigating calcium channel blocker therapy in acute myocardial infarction and specific treatment to microvascular obstruction [179].

Nitroprusside is another pharmacological agent which has been investigated for treatment of microvascular obstruction. Nitroprusside chemically dissociates to release a nitric oxide molecule (more on which will be later discussed) which leads to relaxation of vascular smooth muscles and vasodilation. Some studies propose that intracoronary nitroprusside infusion is clinically effective in treating microvascular obstruction, although application of this drug has varied between the various supporting studies [179]. In one case, it was documented that patients receiving nitroprusside experienced more rapid resolution of ST elevation, although the various outcome measures of flow were not significantly different between treatment groups. Another study investigating nitroprusside treatment in microvascular obstruction showed significant improvement in TIMI frame counting compared to nicorandil, another drug, although the sample size in this study was admittedly limited to 49 patients. However, two meta-analyses conducted on nitroprusside therapy for microvascular obstruction during percutaneous coronary intervention have suggested significant benefits. Therefore, as pharmacologic agents go, nitroprusside has garnered significant attention as a potential treatment for microvascular obstruction [179].

However, use of these pharmacologic agents was associated with improved clinical outcomes after resolution of microvascular obstruction. One example of this is the use of the purine nucleoside adenosine, which has effects on smooth muscle relaxation in the coronary blood vessels. One study found that while adenosine administration following thrombectomy was not significantly associated with clinical benefits as observed up to 30 days follow-up, at the 1-year timepoint, there was significantly increased beneficial remodeling of the left ventricle in the group receiving adenosine compared to nitroprusside or the control group [179]. In addition, this group

with favorable remodeling showed lower incidences of future acute myocardial infarctions and development of congestive heart failure [179].

An alternative strategy of placing a downstream device to protect against distal microembolization in the patient coronary arteries also failed to show any improvements in perfusion or reduction in infarct size. Another technique called thrombectomy, which involves aspiration of the main obstructing thrombus, applied before percutaneous coronary intervention, was investigated in a clinical trial and has resulted in positive results overall for acute myocardial infarction with ST elevation. However, despite being associated with a decrease in microvascular obstruction, long-term benefits of this additional intervention were not found in a later meta-analysis [161, 166, 170, 178-181].

4.5 Treatment of Cardiovascular Pathology with UTMC

Previously, various applications of UTMC were discussed, including its use in treatment of thrombotic conditions such as stroke and pulmonary embolism. Myocardial infarction with ST elevation is one of the main manifestations of cardiovascular disease which requires immediate treatment. Contemporary standards of care for acute myocardial infarction is percutaneous coronary intervention, as previously discussed [160]. However, as with the development of microvascular obstruction, as well as due to geographic limitations, treatment with percutaneous coronary intervention is not perfect. Other therapies include thrombolysis with pharmacologic agents, although such interventions are accompanied by an elevated risk of hemorrhage and poorer recanalization rates [179]. Therefore, UTMC, with the portable nature of US therapy and its relatively non-invasive nature, holds great potential in treatment of acute myocardial infarction

with ST elevation. As with other conditions, treatment of myocardial infarction essentially simplifies to an issue of UTMC thrombolysis. Many previous groups have investigated the ideal US regime for use in these scenarios, given the difference in clot size, accompanying thrombolytic agent, and treatment contexts (whether *in vivo* or *in vitro*).

One camp of thought involved the use of low-frequency, high-intensity US, which demonstrated significant success in thrombolysis, even showing significant decreases in vessel obstruction in an *in vivo* canine model without signs of injury to the surrounding tissue and vessel walls [182, 183]. However, while other follow-up studies showed good safety and efficacy based on TIMI flow, the lack of improvement in recanalization rates over PCI slowed further development of this methodology. An alternative US regime that has been investigated is with low intensity but high frequency US [184, 185]. Although this type of US was unable to significantly cause thrombolysis by itself, since approximately 50% of the material found in MVO autopsy specimens is comprised of thrombus, addition of a thrombolytic agent such as tPA resulted in significance enhancement of thrombolysis compared to tPA alone [163, 164, 183]. Given our previous discussions on the mechanisms behind different regimes and intensities of US, it is possible that these two types of US functioned through different mechanisms. It is likely that the high intensity US involved destructive inertial cavitational mechanisms, while the low intensity US involved more stable rather than inertial cavitation, with mechanisms such as microstreaming causing enhancement of thrombolysis.

These studies, performed with US alone, were soon followed by the use of contrast MB agents, which lowered the cavitational threshold as previously described [183]. As expected, addition of MB agents significantly increased the amount of thrombolysis achieved, especially with an additional thrombolytic adjuvant therapy on top of the UTMC.

Another parameter of the US pulse investigated for efficacy was pulse duration. Several groups demonstrated that a longer pulse length was more favorable for thrombolysis because such pulse resulted in increased sustained MB activity, resulting in increased amounts of cavitation experienced by the clot [184, 186]. This was also later confirmed in an *in vivo* rat study and *in vitro* microvascular obstruction model, where simulated myocardial infarction treated with a longer pulse resulted in improved rates of recanalization versus a shorter pulse [184, 187]. However, despite these positive results, pulse length faces a ceiling of limitation due to the presence of adverse effects such as vessel damage or hemolysis with excessive length. In all, there is still no single value for any of these parameters which has been determined to be optimal to this day.

There have been several clinical trials for UTMC treatment of acute myocardial infarction with ST elevation. One trial by Cohen and colleagues applied low frequency US for 60 minutes to patients after pre-treatment with thrombolytic therapy [188]. Their results were generally positive with 64% of patients demonstrating TIMI III class flow. However, a different trial of 360 patients was pre-emptively halted due to a lack of efficacy of low frequency US added to thrombolytic agents, although no MB agents nor image-guided approach were used in this trial [189]. Subsequent studies which did feature the use of MB agents with US (true UTMC) found that there was a significant improvement in recanalization rate for patients receiving high intensity US pulses guided by imaging prior to percutaneous coronary intervention [185]. In addition, even patients receiving short pulses with high intensity showed improvements in recanalization, suggesting that a long pulse approach may not be necessary.

Treatment of microvascular obstruction is slightly different than that of acute myocardial infarction with ST elevation. Namely, with microvascular obstruction, there is no epicardial

thrombus target, and several other pathologic processes are involved including ischemia-reperfusion injury, inflammation, and oxidative stress, on top of distal microembolization as a result of percutaneous coronary intervention. UTMC applied toward treatment of MVO may have the aim of improving any or all of these measures, as well as taking a preventative approach in reducing the frequency of MVO occurrence after percutaneous coronary intervention.

In multiple studies involving animal models, high intensity long pulse UTMC was found to significantly improve microvascular perfusion in models of microvascular obstruction [190-192]. In addition, adjuvant thrombolytic therapy further enhanced the results of restoring perfusion, with further augmentation of microvascular blood flow sustaining for far longer than the treatment duration itself, up to 24 hours. To explain for these results, mechanistic studies *in vitro* have also been performed, including implication of nitric oxide (NO) metabolism and signaling [190, 191]. This will be discussed in a later chapter. For now, previous studies have found that UTMC-associated vascular shear stress (due to MB cavitational activity) may result in production of nitric oxide, which serves as a vasodilatory signaling molecule associated with improvements in microvascular perfusion, especially given various studies antagonizing nitric oxide activity to see an ablation of this effect.

In terms of clinical trials, a first-in-human phase II trial was abridged due to occurrence of coronary vascular spasm in 3 out of 6 enrolled patients [193]. This trial applied a long pulse UTMC at 15 minutes before and 30 minutes after percutaneous coronary intervention. Although the precise source of the spasm was undetermined, the results were confirmed in a follow-up pig study involving UTMC treatment of balloon injury and thrombus injection in simulation of acute myocardial infarction [193]. Therefore, long pulse UTMC has been associated with potential local vasoconstriction and continues to be a subject of investigation given its promising pre-clinical

results for thrombolysis. However, using a similar US pulse configuration, a different trial reported on over 100 patients and did not report on any occurrence of US-induced adverse effects including epicardial coronary artery spasm [186].

For all of these experiments, safety in application of UTMC remains at the forefront of consideration, especially in the context of potential future clinical trials. Normal concentrations of MBs have been found to have minimal hematological disturbances (such as platelet activation and hemolysis) when used in UTMC. In addition, vessel damage has been found to be minimal in UTMC with the exception of some extremely high intensity experiments on *in vitro* tissue samples that were not replicated *in vivo*. Coronary spasm that was found in the trial of UTMC in treatment of MVO was unfortunate; however, utilization of the short duration, high intensity pulse in the previous trial for acute myocardial infarction which demonstrated significant recanalization may be applied to avoid this issue given that the spasm seems to be associated with an US regime with longer pulse length.

5.0 Nitric Oxide and Nitrite Physiology and Applications

As it is applied to a biological environment, UTMC and its mechanical forces may produce significant effects on mechanotransductive systems of the vascular endothelium. One such system is that of nitric oxide, a potent signaling molecule which pleiotropically mediates a wide range of downstream effects. One key effect is vasodilation, as endogenous nitric oxide is a key regulator of hemodynamic status and smooth muscle tone in blood vessels. This, along with many other effects of nitric oxide, will be discussed in this chapter due to the relevance of nitric oxide to both cardiovascular disease as well as the bioeffects of UTMC therapy.

Furthermore, nitrite, a chemical species closely related to nitric oxide, which is involved in nitric oxide metabolism in circulation, will also be discussed both in terms of its physiology as well as clinical applications and relevance to cardiovascular disease. One of the main portions of work in this dissertation involves the combination of nitrite and UTMC therapies, and the background established in this section will be referred back upon in the subsequent chapter detailing said work.

5.1 Nitric Oxide Physiology

The earliest sources investigating what would later be known to be nitric oxide detailed a so-called labile and humoral endothelium-derived relaxing factor which resulted in significant vascular relaxation along with other properties of inhibition of platelet aggregation and adhesion. Its actions were known to be mediated by the guanylate cyclase enzyme, and it was only later

chemically identified as nitric oxide. Nitric oxide is synthesized from the terminal nitrogen of the amino acid L-arginine by the enzyme nitric oxide synthase and is stereo-specific to the L isoform of arginine given the biological inactivity of its D-enantiomer. N-monomethyl-L-arginine and the methyl esterified form of L-arginine (N-LMMA and L-NAME) are known inhibitors of this synthesis step. The result of this synthesis is one molecule of nitric oxide and L-citrulline, the metabolic byproduct from the rest of the L-arginine molecule. The nitric oxide synthase molecule (NOS) is known to be dependent on NADPH and calcium/calmodulin [194].

The earliest studies of nitric oxide function in animals involved indirect study through application of its inhibitors such as L-NMMA. Administration of L-NMMA was found to result in dose-dependent, prolonged increases in blood pressure reversible by administration of L-Arginine in multiple vascular beds including the renal, mesenteric, carotid, and coronary vascular beds. The release of nitric oxide, on the other hand, was found to be dependent on both the pulsatile nature of flow through a specific vessel, as well as shear stress induced upon the vessel lining. Given the immediate increases in blood pressure after specific inhibition of nitric oxide activity, it was established that nitric oxide is one of the main endogenous vasodilatory systems. Other roles of nitric oxide have since been identified, including the presence of various other isoforms of nitric oxide synthase, namely neuronal nitric oxide synthase and inducible nitric oxide synthase. Neuronal nitric oxide synthase, as the name suggests, is mainly present on neuronal cells while inducible nitric oxide synthase is found in various immune cells such as macrophages and neutrophils and is induced by presence of bacterial endotoxins or inflammatory cytokines such as IL-1 or interferon-gamma. These two other forms of nitric oxide synthase are not as involved in management of vascular hemodynamics and will not be discussed in further detail in this dissertation [194, 195].

The mechanism of nitric oxide in activating the enzyme guanylyl cyclase was only later elucidated through a complex series of biochemical experiments which led the investigators to hypothesize that the nitric oxide molecule binds to the heme group of guanylyl cyclase to form a nitrosyl-heme product resulting in molecular conformational changes of the porphyrin site though to modify the structure of a neighboring catalytic site which served to bind GTP (for its subsequent cleavage). Subsequent cleavage of GTP and production of cyclic GMP resulted in vascular smooth muscle relaxation (and vascular vasodilation) through several pathways. One pathway involves phosphorylation of myosin light chain kinase, an enzyme which phosphorylates myosin light chains and therefore activates actin-myosin cross-bridge cycling and muscular contraction. Phosphorylation of myosin light chain kinase by a cyclic GMP dependent protein kinase results in its diminished affinity for the calmodulin and calcium ion complex, which ultimately results in the stabilization of an inactive form of myosin and decreased muscular contraction [194, 196].

Therefore, the inhibitory effect of myoglobin and hemoglobin on nitric oxide activity (by diluting the presence of reactive heme groups) supported these mechanistic assertions. Furthermore, addition of superoxide dismutase prolonged the half-life of nitric oxide while addition of superoxide anions decreased said half-life, which is now understood to derive from the reaction between nitric oxide and the superoxide anion to form peroxynitrite, a biologically harmful reactive oxygen species.

Nitric oxide itself is an extremely small and lipophilic molecule. These properties allow it to rapidly diffuse through cellular membranes, acting as a local regulator of blood flow. As such, nitric oxide diffuses from the endothelial cells in which it is produced to neighboring target cells such as vascular smooth muscle cells. Nitric oxide is also rapidly scavenged in the extracellular, intravascular environment by molecules such as hemoglobin, and as such is extremely short-lived

and limited in its vasodilatory signaling effects to the local environment. Additionally, nitric oxide itself may act as a feedback regulator of nitric oxide synthase activity due to interaction between nitric oxide and the heme group of nitric oxide synthase.

As discussed, one of the main roles of nitric oxide is to regulate vascular smooth muscle tone through its metabolism in the vascular endothelium. As such, endothelial nitric oxide is almost continuously produced, as shown by experiments involving constant bioassay experiments on effluents from perfused vascular preparations. Production of nitric oxide was also found to be concentrated in vessels with smaller overall diameter but possessing large amounts of smooth muscle (and smooth muscle associated cyclic GMP). In addition, production of nitric oxide by endothelial cells was shown to be dependent on shear stress of flowing blood on the endothelial surface, later determined to be mediated through the opening of mechanosensitive calcium channels and calmodulin-related signaling. Currently, it is understood that nitric oxide synthesis and nitric oxide synthase activation may occur through both calcium dependent and independent pathways, although both pathways involve tyrosine phosphorylation and other enzymatic cascade events. More specifically, endothelial agonists of nitric oxide production such as acetylcholine or bradykinin stimulate the production of inositol triphosphate, which then binds to receptors on the surface of the endoplasmic reticulum, causing calcium ion release from intracellular sources. These calcium ions then bind to calmodulin, creating a complex which activated nitric oxide synthase until the level of intracellular calcium decreases [196-198].

In a longer timescale, nitric oxide regulation of vasodilatory status also involves the regulation of genes involved in vasoconstricting agents and growth factors. Nitric oxide has been found to suppress expression of endothelin-1 and platelet derived growth factor B, both

vasoconstrictors, in environments of hypoxia. This is one mechanism involved in the response of vasoconstriction to hypoxia such as seen in pulmonary arteries [199].

Given its role in regulation of hemodynamic status, it is unsurprising, therefore, that the dysfunction of nitric oxide metabolism or impairment of its production is a key role in the pathogenesis of several disorders of the cardiovascular system, including hypertension, ischemia-reperfusion injury, and atherosclerosis [197, 200]. However, the functions of nitric oxide extend beyond mere vasodilation. Interactions between the vascular endothelium and circulating platelets are also thought to be mediated by endothelial nitric oxide production. Nitric oxide has been found to inhibit ADP-induced platelet aggregation, while also actively dis-aggregating platelets, in processes mediated by cyclic GMP. Additionally, platelets themselves contain nitric oxide synthase and have the capacity to synthesize nitric oxide during platelet activation. This mechanism may serve as a natural feedback inhibition of the cascading behavior of platelet aggregation and thrombus formation, and this behavior is also seen in neutrophils as well. Nitric oxide may also work in tandem with other vasodilating agents and inhibitors of platelet activation such as prostacyclin, which is mediated by cyclic AMP rather than cyclic GMP [197, 200]. In addition, the anti-platelet properties of nitric oxide also provide an additional safeguard measure against unwanted thromboembolic events in the occurrence of prostacyclin blockade by common pharmacologic agents such as aspirin [197, 200].

In addition to mediating the interactions between the vascular endothelium and platelets, nitric oxide also has inhibitory effects on leukocyte aggregation. Not only has direct evidence been shown for this both *in vitro* and *in vivo*, inhibition of nitric oxide signaling also results in the opposite effects, including leukocyte localization, adhesion, and emigration, as well as increases in microvascular permeability [201, 202]. The underlying mechanism between nitric oxide and

inhibition of leukocyte adhesion has been shown to be dependent on the chemical reactions between nitric oxide and the superoxide anion, as presence of the superoxide anion activates other inflammatory mediators such as mast cells, which degranulate to produce signaling molecules which promote leukocyte adhesion. Therefore, the capacity of nitric oxide to scavenge and remove superoxide anions from the cellular compartment has been proposed to be one mechanism of its anti-inflammatory properties [203].

Given the various properties of nitric oxide in cell signaling as well as the role of its absence in the development of many disease states, modulation of endothelial nitric oxide synthase activity through artificial means has been a topic of much interest in cardiovascular disease research. There are many directions to approach the concept of enhancing endothelial nitric oxide synthase activity, whether through enhancing its genetic expression or through increasing the activity levels of existing enzymes. In terms of targeting nitric oxide production, additional molecular substrates of endothelial nitric oxide synthase may be administered to enhance activity. These include L-arginine and tetrahydrobiopterin, an enzymatic co-factor. Studies have shown that administration of L-arginine, while theoretically intracellular levels of L-arginine should generally be saturated due to its concentration being significantly above the rate-limiting concentration based on enzyme kinematics of endothelial nitric oxide synthase, has been shown to produce significant reductions in blood pressure, improvements in vasodilation, and decreased endothelial damage as quantified by platelet and leukocyte adhesion. These benefits were especially apparent in patients with pre-existing cardiovascular disease such as congestive heart failure, where administration of L-arginine resulted in improvements in cardiovascular and renal function. However, despite these positive results, other studies have also reported that supplementation of L-arginine resulted in no

effects on endothelial dysfunction, suggesting that its potential benefits and therefore intracellular shortages have differences in etiology from endothelial dysfunction [197, 198, 200, 204].

Simulating these effects through direct addition of nitric oxide donating molecules such as molsidomine, glyceryl trinitrate, and sodium nitroprusside, is another strategy for increasing nitric oxide bioavailability. Not only does the exogenous source of nitric oxide function essentially the same as endogenously produced nitric oxide, but additional pharmacokinetic details of the drugs themselves may actually prolong nitric oxide release for therapeutic effect. Examples of these types of drugs in clinical use (or previously in clinical use) include nitroglycerin, nitroprusside, and nitrate. Clinical studies have shown that inhibition of endothelial nitric oxide synthase, and therefore of endogenous nitric oxide production, may be overcome through administration of exogenous nitric oxide donors, resulting in not only reduction of blood pressure through vasodilation, but also the other various bioeffects of nitric oxide including decreased leukocyte infiltration and extravasation, reduced atherosclerotic lesion sizes, and reduced endothelial dysfunction [196, 198].

Aside from administration of enzymatic substrates, co-factors, or direct exogenous nitric oxide molecular donation, another method of enhancing endothelial nitric oxide synthase activity is through upregulating or artificially increasing its expression such as through genetic modification [205]. As previously discussed, genetic modification may occur through both viral and non-viral means of transferring the endothelial nitric oxide synthase gene to a target location, although use of the adenovirus vector is very common, and has been successfully applied to various *in vitro* tissue types including vascular tissue and smooth muscle. Other studies have shown that successful gene transfer of endothelial nitric oxide synthase results in improved outcomes in disease models such as of hypertension, ischemia reperfusion injury, and atherosclerosis [198, 200,

205]. Additionally, lifestyle factors may also affect endothelial nitric oxide synthase activity, such as the lowering of low-density lipoproteins, which have been found to affect nitric oxide synthase activity. Other medications such as statins, which also serve to reduce levels of low-density lipoproteins, may also be utilized along with estrogens, which have been found to phosphorylate the enzyme itself [198, 200, 205].

5.2 Pathways Governing Endothelial Nitric Oxide Synthase Activity

Given the various roles of nitric oxide in maintaining a homeostatic environment for the vascular endothelium, the molecule itself plays several roles in affecting cell proliferation, as previously discussed. Not only does nitric oxide inhibit expression of leukocyte adhesion molecules and platelet aggregation, it also inhibits the proliferation of smooth muscle cells while also enhancing the proliferation of vascular endothelial cells. These bioeffects, along with the inhibition of matrix metalloproteinases (which affects atherosclerotic plaque stability and remodeling), are at essence anti-atherosclerotic properties of nitric oxide. With connections between atherosclerosis and derangement of hemodynamic conditions becoming more apparent, and as our understanding of mechanotransductive pathways improves, the role of nitric oxide, and the sensitivity of endothelial nitric oxide synthase to shear stress, become more central in these processes.

Previously, we discussed that shear stress results in an increase in intracellular calcium, which complexes with calmodulin, binding to endothelial nitric oxide synthase and enhancing its activity. However, studies have shown that levels of nitric oxide production far exceed the expected values explained only by increases in intracellular calcium, and that the production of

nitric oxide is sustained despite a return of intracellular calcium to normal concentrations, suggesting that there are alternative, calcium-independent mechanisms affecting nitric oxide synthase activity (and phosphorylation). Previous experiments have shown that shear stress itself mediates phosphorylation of endothelial nitric oxide synthase through protein kinase A at various sites, while also up-regulating nitric oxide synthase transcription, which involves a MAP kinase pathway. In addition, certain regions of the endothelial nitric oxide synthase promotor (a non-expressing gene sequence which up-regulates transcription of a particular gene), have been shown to be shear sensitive, along with several protein kinases including protein sub-units of the NF-kappa B protein, which typically leads to increased expression of pro-inflammatory genes with its activation.

In addition to regulation of gene expression, post-translational modification of endothelial nitric oxide synthase, especially phosphorylation at key sites such as Ser1177, affects its activity in nitric oxide production [206, 207]. Shear stress has also been found to affect several enzymatic pathways leading to this phosphorylation, including Akt and protein kinase A, as previously mentioned [208, 209]. In addition to these pathways, AMP-activated protein kinase (AMPK) has recently been implicated in phosphorylation of endothelial nitric oxide synthase [209]. This is significant, as not only is AMPK sensitive to physiological stresses including exercise and hypoxia, any increase in cellular metabolism which drives the conversion of ATP to AMP results in its activation [204, 210]. Therefore, implication of AMPK in the regulation of nitric oxide synthase also raises questions regarding the role of energy balance and nitric oxide metabolism. In addition, AMPK itself was shown to be sensitive to shear stress, including changes in shear stress of magnitude and pulsatile characteristics [208, 209]. In terms of the connection between energy metabolism of ATP and shear stress, no explicit connections have been made, although shear stress

exposure of endothelial cells has been associated with some ATP release as well, resulting in a shift in the equilibrium toward AMP (and leading to AMPK activation). In addition, exercise training of both animals and humans, which typically leads to increased cardiac output and improved capacity for vascular dilation, have been associated with increased levels of AMPK activation (and therefore endothelial nitric oxide synthase phosphorylation), suggesting that exercise and shear stress are all intrinsically related to nitric oxide metabolism and vascular health [209, 211].

In elaboration of this work, other groups have investigated the more precise mechanistic steps in the enzymatic pathway from AMPK to endothelial nitric oxide synthase phosphorylation, and have identified a novel pathway of AMPK, Rac1, and Akt (which was also previously mentioned) to culminate in nitric oxide synthase regulation [212]. Previous studies have also shown conclusively that AMPK is a mediator for vascular endothelial growth factor-mediated activation of endothelial nitric oxide synthase [213]. In addition, S1P, a regulator of endothelial function through its interaction with G protein-coupled receptors, was also found to be a significant mediator of AMPK activation, resulting in the advent of multiple AMP-independent pathways for AMPK activation [212]. This suggests that the role of AMPK is more complex than previously envisioned given its impression as a sort of metabolic regulator with dependence on the presence of AMP, and instead the AMPK pathways are significantly affected by extracellular signaling and stimuli which may be present in pathophysiologic states, as well as during endothelial cell migration and angiogenesis. In addition, another study found that nitric oxide itself serves as an activator of AMPK in vascular endothelial cells [214]. This positive feedback mechanism also results in increased phosphorylation of the Ser1177 site on endothelial nitric oxide synthase, as was found in isolated aorta preparations. The implications raised by these results are relevant not

only to physiologic production of nitric oxide, but also potentially therapeutic applications of nitric oxide donors given the identical natures of the molecule despite the different sources. Although these experiments were carried out *in vitro*, the results were replicated in an inverse manner with inhibition of nitric oxide resulting in decreased phosphorylation of AMPK [214]. However, the study did find that this feedback cycle was also partially dependent on intracellular calcium levels, as down-regulation of intracellular calcium resulted in some suppression of AMPK activity. Another study which focused on skeletal muscle biopsies from human participants replicated these results in that not only did nitric oxide increase AMPK activity, it also increased cyclic GMP levels and glucose transport [215]. These study results confirmed many previous investigations which were limited to rodent muscle samples. In addition, the source of nitric oxide in this experiment was from spermine NONOate, a nitric oxide donor, showing that exogenous nitric oxide sources participate significantly in these endogenous regulatory pathways of endothelial nitric oxide synthase [215]. Similar results using sodium nitroprusside have also been reported as well [198, 200, 205, 214].

Lastly, and as segue to the next sub-section, a recent investigation demonstrated that nitrite, a biological reservoir and metabolic byproduct of various reactions of nitric oxide, also participates in the AMPK signaling pathway. The study demonstrated that nitrite resulted in significant endothelial nitric oxide synthase activation as mediated through the AMPK pathway, which may be a mechanism for the various protective effects of nitrites. The mechanism and clinical applications of nitrite will be discussed, and this concept of interaction with endogenous endothelial nitric oxide synthase pathways will be re-visited in a proposed mechanism of synergy between nitric oxide synthase activation and administration of exogenous nitrite [210].

5.3 Nitrite Basic Physiology and Metabolism

Historically, nitrite (and nitrates) have been known as byproducts of various preservation and flavoring applications in the food industry. However, this molecule also has a wide range of applications and natural functions as a participant in nitric oxide metabolism and physiology. Nitrite has a wide range of pathways for its chemical modifications in the human body, including reactions with hemoglobin, myoglobin, xanthine oxidoreductase, and various other biological components, and its chemical equilibrium is affected by various physiological parameters such as oxygenation and acidosis.

As an overview of the nitric oxide pathways previously discussed, nitric oxide is synthesized by nitric oxide synthase, which uses substrates of L-arginine, an amino acid, and molecular oxygen. The mechanisms of nitric oxide are involved in vascular status (for vasodilation), immune signaling, and endothelial homeostasis. Nitric oxide may also be converted through oxidation into nitrite and nitrate, which are stable in blood and tissue compartments, and may be later reverted back to nitric oxide under different environmental conditions. Therefore, nitrite may be thought of as a biological reservoir of nitric oxide, which will be further expounded on later in this subsection. Nitric oxide synthesis through the endogenous pathway as described, however, is an oxygen dependent process. In conditions of hypoxia, where oxygen is deficient, this pathway becomes less and less favorable, whereas different pathways in nitric oxide metabolism and conversion gradually dominate. More specifically, the nitrite to nitric oxide reactions become more favorable in hypoxic conditions and may serve as a natural regulatory mechanism to maintain nitric oxide bioavailability in conditions where synthesis through nitric oxide synthase are less feasible. The importance of nitric oxide bioavailability in conditions of

hypoxia is emphasized in physiological processes such as hypoxic vasodilation and protection in settings of ischemia reperfusion [216].

For the general endogenous sources of nitrite in the human body, the greatest contributions come from endogenous synthesis of nitric oxide which becomes oxidized in blood, and from diet (including natural dietary supplements such as beetroot juice) [217]. For endogenously synthesized nitric oxide, chemical reactions converting it to nitrite include oxidation by ceruloplasmin, oxidation by oxyhemoglobin to produce nitrate and methemoglobin, and subsequent conversion of nitrate to nitrite through enzymes such as nitrate reductase, are all extremely common and occur regularly. Previous animal studies involving genetic knockout techniques against endogenous nitric oxide synthase resulted in reductions of endogenous nitrite by up to 70% [217]. Other factors affecting endogenous circulating levels of nitrite include exercise conditioning (which also increases endothelial nitric oxide synthase activity), systemic inflammation and inflammatory conditions (which results in increased inducible nitric oxide synthase induction and therefore synthesis and conversion of nitric oxide), and cardiovascular diseases such as atherosclerosis (which result in endothelial dysfunction and diminished activity of endothelial nitric oxide synthase, and therefore reduced levels of nitrite from lack of chemical conversion) [217]. Dietary consumption is the other major source of endogenously found nitrite in circulation. As mentioned, certain vegetables, such as beetroots, lettuce, or spinach, contain significantly higher amounts of nitrate than endogenous production in the human body. Preserved foods, such as cured meats and bacon, also contain significant amounts of nitrite depending on the method of production [217]. After dietary consumption, various processes independent of nitric oxide synthase act to render the consumed nitrate and nitrites biologically available in the bloodstream. As evidence of this, dietary nitrite and nitrate products are rapidly absorbed from the upper GI tract and become

detectable in plasma with significant elevation for a prolonged half-life of up to 6 hours after consumption [217]. Excretion through kidney filtration does apply for circulating nitrites and nitrates, although nitrate is also actively absorbed and concentrated in the salivary glands, after which it is secreted into the oral cavity. In the oral cavity, various species of facultative anaerobic bacteria use nitrate in their respiratory processes as a destination for electron transport alternative to oxygen (hence facultative anaerobic metabolism), and in doing so, reduce secreted nitrate to nitrite through nitrate reductase (as previously mentioned) [217]. Thus, this newly formed salivary nitrite is then swallowed into the stomach's acidic environment, where it is then further reduced to various byproducts, and eventually nitric oxide. Various studies have also demonstrated that this process of nitrite formation occurs not only in the oral cavity, but also on the surface of the skin and in the lower GI tract. Production of nitric oxide in the gastric compartments has been shown to have significant cyclic GMP-dependent increases in blood flow through vasodilation [217].

However, aside from its involvement in the GI system, nitrite has been shown to have a wide range of other physiologic roles, including peripheral vasodilation. Specifically, nitrite has been shown to serve as a sort of vasodilatory mediator similar to nitric oxide in that infusion of nitrite into human participants resulted in significant increases in blood flow even at concentrations of nitrite below 1 micromolar [217]. This vasodilation and decrease in blood pressure have also been observed in oral consumption of nitrate (and subsequent increases in plasma nitrite). While in the periphery, nitric oxide is typically scavenged extremely quickly by hemoglobin-containing red blood cells, resulting in limitation of the range of its efficacy, nitrite is able to maintain its vasodilatory effects even in the presence of such conditions, although said effects still do derive from its conversion into nitric oxide [216]. The key factor for nitrite's bioeffects derives from a

shift toward favor of its chemical equilibrium resulting in nitric oxide production correlating with an increase in deoxyhemoglobin, which has been shown to have nitrite reductase type activity [216]. This chemical reaction involves deoxyhemoglobin as well as a proton, and accordingly is therefore favored in conditions of hypoxia as well as acidosis (which accompanies environments of either poor perfusion, increased metabolic activity, or pathologic processes). Other interconversions between nitrite, nitric oxide, and other metabolic byproducts also occur, but will not be discussed within the scope of this dissertation.

Other enzymatic sources of this nitrite reductase activity to nitric oxide also include myoglobin and xanthine oxidoreductase [218]. Myoglobin, or rather deoxymyoglobin, is an even stronger catalyst of nitric oxide production through nitrite reduction than hemoglobin and is heavily present in muscular compartments (of course) such as skeletal muscle or the heart [219]. Therefore, when muscle is active in exercise and metabolic depletion of local oxygen occurs, myoglobin may therefore convert nitrite into nitric oxide as described and induce effects including vasodilation and decreased oxygen utilization (which is physiologically favorable in conditions of hypoxia) [216]. Dietary supplementation with nitrate supported these results as investigated in healthy human participants, as oxygen consumption was significantly reduced due to metabolic nitrite to nitric oxide conversion in skeletal muscle, as associated with plasma nitrite metabolism. Xanthine oxidoreductase, on the other hand, is a part of the mitochondrial electron transport chain, which will not be heavily elaborated in this dissertation. However, in essence, xanthine oxidoreductase is a facultative oxygen reducer (to the superoxide anion) which may also utilize nitrite (reducing it to nitric oxide) in environments of low oxygen availability [220]. It is significant to note that the alternative to nitrite reduction results in production of superoxide anions, which are aggressive reactive oxygen species, which may result in local damage from oxidative stress,

while also greatly scavenging nitric oxide and reducing nitric oxide bioavailability. Therefore, in reducing nitrite to nitric oxide, not only does this metabolic pathway result in the formation of nitric oxide, it also competes against the production of superoxide, which results in a reduction of nitric oxide scavenging [220]. This ultimately results in increases in nitric oxide bioavailability on multiple levels and protection against scavenging of nitric oxide. Other effects of nitrite include modification of proteins have also been documented and are the subject of current investigations [221].

Specifically, mechanistic studies involving nitrite and its protective properties in ischemia-reperfusion injury have identified correlations between nitrite-induced cytoprotection and increases in mitochondrial oxidative phosphorylation [222]. Specifically, nitrite causes a concentration and dosage dependent modification and inhibition of complex I, a component of the electron transfer chain. This modification of S-nitrosation results in significant inhibition of electron transfer, and therefore also inhibits formation of reactive oxygen species generation and mitochondrial permeabilization, which would typically lead to release of cytochrome c, a signaling mediator for apoptosis [222]. Although ischemia-reperfusion injury and oxidative stress will be further discussed in a later chapter, here we will emphasize the role of nitrite in protecting cellular mitochondria from damage, which ultimately results in protection against the endpoints of ischemia-reperfusion injury and oxidative damage including inflammation and tissue necrosis [203].

Extrapolation of this efficacy suggests there is strong potential for relevance of therapeutic nitrite to other disease settings heavily featuring ischemia-reperfusion injury, including sickle cell disease, myocardial infarction, microvascular obstruction, and stroke. Other more recent studies of therapeutic nitrite include cardiac arrest (which involves ischemia reperfusion injury in the brain

as well as myocardial dysfunction), where nitrite infusion resulted in significant improvements in hippocampal CA1 neuron preservation after simulated cardiac arrest (where control conditions resulted in significant neuronal death) [223]. Mechanistically, these improvements were associated with nitrite concentration in the hippocampus as well as nitrosothiol involved modifications of macromolecules in the local region, but not cyclic GMP. Development of a phase 1 clinical trial for nitrite therapy in these patients demonstrated safety and a lack of adverse effects such as hypotension or methemoglobinemia, suggesting that nitrite may be a safe candidate for further investigation in settings of brain injury and cardiac arrest [223].

5.4 Therapeutic Applications of Nitrite

There are many applications of nitrite in various forms for many different pathologies. Many of these involve the effect of nitrite on vasodilation, either to restore perfusion to vessel beds or to combat vascular spasm. One example of this is in patients with subarachnoid arterial aneurysms, which may result in spontaneous hemorrhages eliciting delayed cerebral vasospasms. Non-human primate models of this condition showed successful prevention of these vasospasms with systemic nitrite administration, while the condition was also associated with low levels of cerebrospinal fluid nitrite concentration [224]. Another example of nitrite applied to a clinical pathology is in pulmonary hypertension, which is associated with abnormally increased pulmonary vascular resistance and poor oxygenation as a result. Inhaled nitrite (which is then converted to nitric oxide) administered to a sheep model of this disease resulted in successful vasodilation of only the pulmonary vasculature (due to the inhaled nature of the therapy) for treatment of the condition [225].

However, more relevant to the work of this dissertation and our main clinical context of interest are the roles of nitrite in settings of ischemia-reperfusion injury and cardiovascular disease. Endogenously, nitrite has been shown to have strong involvement in cardiac models of ischemia reperfusion injury, concurrent with other mechanistic work suggesting its predominance in conditions of hypoxia. Specifically, both endogenous and exogenous levels of nitrite (natural and therapeutically induced) have been shown to have protective effects in the face of ischemia reperfusion injury in various tissue settings including the heart, liver, brain, and kidney [203, 221, 226-229].

One previously mentioned application of nitrite is in treatment of acute myocardial infarction. One previous study investigated this in a canine model of myocardial infarction using low dose intravenous nitrite given over the course of myocardial infarction development [227]. The study outcome of the ratio for infarct size normalized against area at risk ratio showed that both a 60 minute infusion of nitrite as well as a 5 minute infusion of nitrite both significantly reduced infarct size despite the 5 minute infusion having significantly lower overall dosage of nitrite as well as peak concentration, suggesting that the efficacy of nitrite in protecting against ischemic damage spans a wide range of concentrations [227]. Additional TUNEL analysis staining for cardiomyocyte apoptosis as another outcome measure for severity of damage resulting from the myocardial infarction showed a significantly lower number of apoptotic nuclei for both infusion treatment groups of nitrite [227].

However, despite showing significant effects in cardioprotection and prevention of apoptosis, the effects of nitrite (which are typically thought of as being centered on vasodilation after conversion to nitric oxide) were not significantly associated with hemodynamic changes during administration as measured by changes in preload, afterload, or the pressure-rate product

[227]. This suggests that the protective effects of nitrite were mediated by biological pathways rather than by merely providing increased perfusion to surrounding areas during focal ischemia. Notably, functional outcomes such as ejection fraction were significantly improved by nitrite therapy, and presence of microvascular obstruction as qualitatively observed on magnetic resonance imaging as well as through measurement of endocardial blood flow using microspheres showed that nitrite reduced the cross-sectional area of microvascular obstruction after reperfusion had been achieved in the canine model. As described before, microvascular obstruction was characterized on serial magnetic resonance perfusion imaging as a hypointense residual region remaining after reperfusion of the heart.

There were many significant implications raised by this study that directly motivated subsequent work in this dissertation with regards to therapeutic nitrite administration, most notably the time course of therapeutic effect of nitrite observed in the study as well as its effectiveness in treating microvascular obstruction after ischemia-reperfusion of the heart. In consideration with the timescale of emergent intervention for myocardial infarction, sufficiency of a 5-minute infusion of nitrite for significant therapeutic effect is a strongly favorable attribute for its relevance and potential for future application and translation. Given the emphasis on door-to-balloon time and emergent time dependence of the extent of ischemic damage and deteriorating patient outcomes, minimizing therapeutic duration for both nitrite administration and UTMC treatment while maintaining therapeutic efficacy is a definite priority. In line with this, other characteristics to prioritize for translational therapy involving nitrite and potential use with UTMC include low expense, rapid onset of action, short half-life, minimal systemic side effects, and biological efficacy not dependent solely on hemodynamic changes.

Another previous study investigated nitrite efficacy in protection against ischemia-reperfusion injury through both a focal cardiac ischemia rat model as well as an *ex vivo* cardiac perfusion model [221]. For *in vivo* cardioprotection evaluation, a wide range of doses from 0 to 10 mg of nitrite per kg of animal body weight was tested with the main outcome of infarct size normalized against area at risk. The results showed that a dosage of 4 mg per kg body weight resulted in the lowest normalized infarct size [221]. Additionally, timing of nitrite administration was evaluated both 15 minutes prior to onset of cardiac ischemia as well as 10 seconds after onset of reperfusion using the 4 mg per kg bodyweight dose of nitrite previously identified. The most optimal timings evaluated were either 15 minutes prior to ischemia or 15 minutes after ischemia, while the treatment group receiving nitrite 10 seconds after reperfusion showed no significant decreases in normalized infarct size relative to the drug-free control group. Most notably, results from this study showed a biphasic relationship of nitrite dose against effectiveness in reducing infarct size, in that both low as well as high doses of nitrite showed diminished efficacy [221]. The dosage of 10 mg per kg bodyweight of nitrite showed no significant differences compared to the control group in infarct size reduction.

Other mechanistic investigations of this previous study also explored roles of other involved mediators in nitrite metabolism and their roles in the cardioprotective properties of nitrite. The role of hemoglobin was investigated through the use of an isolated *ex vivo* cardiac model of focal ischemia [221]. Nitrite perfusion was used similar to the *in vivo* model at various dosages, showing again similar results to the *in vivo* model where nitrite dosage followed a biphasic relationship for infarct size reduction, with recovery of left ventricular diastolic pressure following an inverse pattern of said relationship [221]. These results also suggest that hemoglobin acting as a nitrite reductase is not required for enabling the cardioprotective effects of nitrite. Another

enzyme target of investigation was xanthine oxidoreductase, which has also been shown to have nitrite reducing activity. Administration of oxypurinol, a xanthine oxidoreductase inhibitor, resulted in significant ablation of the protective effects of nitrite on reducing infarct size, thereby significantly implicating xanthine oxidoreductase as a mediator of nitrite cardioprotection. Nitric oxide synthase and nitric oxide itself were also investigated in inhibitory test group designs using L-NMA and C-PTIO respectively (a general nitric oxide synthase inhibitor and a nitric oxide scavenger) to demonstrate that neither nitric oxide synthase nor presence of nitric oxide itself were necessary for the cardioprotective effects of nitrite [221].

Significant findings of this study included the dose-dependent effect of nitrite on cardioprotection with specific titration to rodent models, optimized timing for nitrite administration relative to an ischemia-reperfusion model, and several mechanistic findings regarding nitrite efficacy. As previously discussed, xanthine oxidoreductase plays key roles both in nitrite metabolism as well as in the formation of reactive oxygen species, specifically the superoxide anion. In hypoxic and acidic conditions, activity of xanthine oxidoreductase in reducing nitrite is significantly increased, conditions which are found in focal tissue ischemia. These results support previous mechanistic findings as well. Interestingly, efficacy of nitrite was shown to be independent of both endogenous nitric oxide generation through nitric oxide synthase as well as converted nitric oxide itself. While it has been noted that nitric oxide synthase itself may function in a nitrite reducing capacity, inhibition of the nitric oxide synthase in this investigation using L-NMA without significant detraction from nitrite efficacy suggests alternative signaling pathways.

6.0 Nitro-alkenes (Nitro-fatty Acids) Physiology and Applications

Nitro-fatty acids, or fatty acids with a nitro group modification, are a relatively new class of therapeutic molecules. As will be discussed in this chapter, the functional mechanisms of these molecules are diverse and range beyond simple nitric oxide donation, spanning into modification of key transcriptional factors to elicit anti-inflammatory and protective effects against ischemia-reperfusion injury. In addition, their molecular structure, in being amphiphilic with a long acyl chain group, is extremely similar to traditional components of MB agents such as phospholipids as we previously discussed. Their application in a functionalized MB design will be discussed in a later chapter of this dissertation. This chapter will cover what we currently understand with regards to their physiology and therapeutic application, including in treatment of a variety of cardiovascular disease contexts as represented by animal models. Although the applications of nitro-fatty acids, including the settings of various clinical trials such as kidney disease or cancer therapy, may range beyond solely cardiovascular disease, these applications are beyond the scope of this dissertation and will not be discussed.

6.1 Basic Mechanisms for Formation of Nitro-Alkenes (Nitro-Fatty Acids)

To first understand the functions of nitro-fatty acids which arise from their specific chemical structure, we will first discuss basic mechanisms for the formation of these species. At its essence, the formation of nitro-fatty acids involves a reaction between nitric oxide and nitric oxide-derived oxidative species such as peroxynitrite, reactive oxygen species (which are

inflammatory mediators) such as superoxide or hydrogen peroxide, and unsaturated fatty acids. Endogenous formation of nitro-fatty acids therefore involves environmental factors previously discussed including nitric oxide bioavailability, tissue inflammation and oxidative stress, as well as presence of oxygen (or hypoxia, the lack thereof) [230-232]. Common unsaturated fatty acids available in biological systems include linoleic acid and oleic acid. These species are also especially suitable for nitration due to the presence of double bonds in their hydrocarbon chains, which are available targets for attack from the various nitric oxide associated species such as nitrogen dioxide. The result of these nitration reactions are mostly nitroalkenes or nitrohydroxy-related molecules. The work in this dissertation pertinent to nitro-fatty acids uses only nitroalkene species. The reaction of fatty acid nitration itself involves multiple steps. First, the nitrogen dioxide molecule (or other related species) adds to the double bond of the unsaturated fatty acid, resulting in a beta-nitroalkyl radical. This is a fast process which may be elaborated by further modification and nitration if the environment is hydrophobic and has a relatively high presence of nitric oxide or other nitrogen oxides. A second attack from another nitrogen dioxide molecule results information of a nitronitrite ester, which may lose a nitrous acid molecule resulting in a nitroalkene with the double bond in its original position. Alternatively, hydrolysis of the nitronitrite ester may result in a nitrohydroxy-type molecule, which may lose a molecule of water to also result in a nitroalkene [230-232].

6.2 Basic Chemical Reactions of Nitro-fatty Acids

As mentioned, the chemical structure and reactivity of nitroalkenes, which will be referred to as nitro-fatty acids for simplicity, determines the pluripotency of their impact on cellular

signaling and gene expression. Some of these reactions may involve an intermediate species such as previously described with the reaction between nitroalkenes and water to result in a nitrohydroxy-type molecule. Another type of reaction that nitro-fatty acids undergo involves release of a nitric oxide molecule. These reactions typically involve conversion to intermediate species such as a nitronate anion (in which the nitrated carbon gains a negative charge) and is then reduced to yield a nitric oxide molecule. Given that nitro-fatty acids have been observed to induce vasorelaxation in animal experiments is further evidence for the significance of this nitric oxide release, although the true biological significance of this effect outside of isolated experiments is still a subject of investigation [230].

Nitro-fatty acids are stabilized by hydrophobic environments, in which equilibrium shifts further away from nitric oxide release. Stabilizing agents, including those used in the delivery of nitro-fatty acids in the work of this investigation, are organic solvents such as polyethylene glycol and various alcohols. Formation of micelles or liposomes with surfactant molecules such as phosphatidylcholine and cholesterol has also been noted to further stabilize nitro-fatty acids from decomposition (which includes nitric oxide release). Partitioning of nitro-fatty acids into organic membranes such as cell membranes or with lipoproteins follows suit with these mechanisms for stabilization and may promote downstream signaling mechanisms of nitro-fatty acids after subsequent activation by biological enzymatic mediators such as esterases or phospholipases [230]. Many protein modification reactions involving nitro-fatty acids are mediated through electrophilic adduction reactions of thiol groups and histidine residues.

6.3 Signaling Mechanisms of Nitro-fatty Acids

The various mechanisms of nitro-fatty acids in signaling to modify downstream cellular events including gene expression and post-translational modification of proteins will be discussed in brief detail. Although each mechanism has been characterized through many studies, this section will offer a brief overview of the mechanism and implications on macro-scale cellular and tissue environments.

6.3.1 Vascular Relaxation

As extensively discussed in the previous chapter, vasorelaxation of vascular smooth muscle involves nitric oxide and nitric oxide donors for regulation. As mentioned, nitro-fatty acids and release of nitric oxide molecules do have an effect on cyclic GMP-dependent signaling. This was demonstrated by an *ex vivo* experiment involving perfusion of pre-constricted rat aortic tissue. Nitrohydroxy-type molecules derived from arachidonic acid have also been implicated in vasorelaxation. However, there are several factors which discourage this effect, mainly acting to stabilize nitro-fatty acid molecules either through intercalation into micelles and liposomes or in biological membranes. The potential for nitro-fatty acids to act as a nitric oxide donor has not been fully characterized given the potential for involvement of other actors including enzymes or activation of signaling pathways relevant to nitric oxide bioavailability and will be further discussed in a later subsection [233-235].

6.3.2 Anti-inflammatory Mechanisms

Nitro-fatty acids interact with several key inflammatory mediators to inhibit development of an inflammatory milieu, namely neutrophils and platelets. In activated neutrophils, nitro-fatty acids inhibit reactive oxygen species production, degranulation, and CD11b production. In platelets, nitro-fatty acids inhibit thrombin-mediated aggregation through increasing intracellular cyclic AMP levels likely through upregulation of adenylate cyclase activity. Macrophages are affected by nitro-fatty acids as well, both through inhibition of nitric oxide synthase isoform 2 and through inhibition of endothelial expression and surface migration of cellular adhesion molecules, including VCAM-1, E-selectin, and P-selectin. These adhesion molecules mediate the rolling, adhesion, and extravasation stages of monocyte localization and infiltration in the setting of inflammation and are key to further downstream signaling for activation of other immune cell types [236-239].

6.3.2.1 Heme Oxygenase-1 Induction

Another mechanism by which nitro-fatty acids decrease inflammatory signaling is through upregulation of various mechanisms which protect against inflammatory damage. One such mechanism is through the upregulation of heme oxygenase-1 (HO-1). HO-1 is a key enzyme involved in heme catabolism, or the breakdown of heme into various metabolic byproducts such as biliverdin, ferrous iron, and carbon monoxide. HO-1 expression is also regulated by Nrf2, which will be further discussed. Carbon monoxide has been implicated as an anti-inflammatory mediator, as well as HO-1 itself in not only prevention of excessive nitric oxide scavenging, but also in inhibition against oxidative stress, cellular apoptosis, and other sub-processes of inflammation including edema, leukocyte adhesion and extravasation, and production of inflammatory signaling

mediators. Mechanisms underlying HO-1's anti-inflammatory functions include removal of heme, which has been identified as a mediator of oxidative stress when not bound to a protein, production of bilirubin (as a metabolic byproduct), which has been associated with antioxidant and anti-inflammatory effects, and prevention of iron toxicity through coordination of ferritin synthesis and storage [240, 241].

6.3.2.2 Nuclear factor-κB inhibition

Inhibition of nuclear factor kappa B (NF-κB) is key anti-inflammatory mechanism of nitro-fatty acids. NF-κB is a transcription factor comprised of many different subunits with their respective governing domains. Certain NF-κB subunits (p50 and p65) have critical roles in governing cellular survival as well as development of inflammation and are surpressed by nitro-fatty acids. More specifically, nitro-fatty acids alkylate the p65 unit of NF-κB and prevent it from successfully promoting inflammatory genes, resulting in downstream effects of tumor necrosis factor-α inhibition and abrogation of lipopolysaccharide-stimulated inflammatory responses. Inhibition of lipopolysaccharide-based inflammatory responses also include inhibition of inflammatory cytokines including interleukin 6, tumor necrosis factor alpha, monocyte chemoattractant protein 1, as well as down-regulation of inducible nitric oxide synthase expression. It is noted here that these signaling mediators are selected as endpoint outcome measures for gene expression analysis of tissue samples taken from the ischemia-reperfusion animal model studied for these reasons [235, 236, 238].

In addition, the regulation of NF-κB by nitro-fatty acids occurs at multiple levels in its signaling pathway beyond alkylation of the p65 subunit. Upstream events such as surface membrane expression of toll-like receptor 4 as well as tumor necrosis factor receptor associated

factor 6 recruitment are inhibited as well as inhibition of inhibitor of kappa B (IκB) phosphorylation (which would result in its dissociation from NF-κB, allowing the NF-κB protein to translocate to the nucleus and activate the aforementioned gene expression).

6.3.2.3 Peroxisome Proliferator-Activated Receptor Agonism

Another mechanism by which nitro-fatty acids inhibit inflammation that is also involved in metabolic regulation is through activation of peroxisome proliferator-activated receptors. These receptors are involved in mediating fat metabolism, adipogenesis, regulation of glucose metabolism and storage, as well as inflammation. These peroxisome proliferator-activated receptors are expressed by a wide range of cell types, including endothelial cells, vascular smooth muscle cells, white blood cells, and adipocytes. Previous studies have shown that nitro-fatty acid agonism of these receptors rivals that of rosiglitazone, a thiazolidinedione which is a class of drugs used in treatment of type 2 diabetes. The resulting effects of nitro-fatty acid agonism of peroxisome proliferator-activated receptors is similar to that of thiazolidinedione agonism and include increased glucose uptake but also a diminished capacity to affect adipogenesis. Notably, this also suggests the relevance of nitro-fatty acids to treatment of type 2 diabetes given their capacity to potentially improve insulin sensitivity without significant weight gain (adipogenesis). Many other thiazolidinedione associated adverse effects including edema and increased risk for cardiovascular events may be avoided in utilizing nitro-fatty acids over thiazolidinediones as well. Aside from regulation of glucose metabolism and insulin sensitivity, nitro-fatty acid agonism of peroxisome proliferator-activated receptor gamma also mediates lipid metabolism as it has been associated with decreased plasma triglyceride levels, reductions in lipoprotein biomarkers for cardiovascular risk, and prevention of triglyceride accumulation in macrophages through increased expression of

key metabolic enzymes including hormone-sensitive lipase and adipose triglyceride lipase. Along these lines, nitro-fatty acids themselves may also be incorporated directly into mono-, di-, and triglycerides, suggesting that there may be mechanistic implications of the affinity that nitro-fatty acids have for these molecules. Peroxisome proliferator-activated receptors also interact with the NF-κB transcription factor previously mentioned in that peroxisome proliferator-activated receptor gamma may directly interact with subunits p50 as well as p65 of NF-κB to inhibit subsequent inflammatory signaling (which is upregulated by nitro-fatty acid agonism of peroxisome proliferator-activated receptors). In addition, the sumoylation (process of adding small ubiquitin-like modifiers) of peroxisome proliferator-activated receptor gamma results in transcriptional repression of inflammatory mediators such as inducible nitric oxide synthase [230, 233, 237].

6.3.2.4 Nuclear Factor Erythroid 2-related Factor 2 Activation

Nuclear factor erythroid 2-related factor 2 (Nrf2) is a mediator of cellular responses to oxidative damage and presence of oxidants. As a transcription factor it regulates the expression of a variety of antioxidant factors as a cytoprotective measure. These include NADPH quinone oxidoreductase 1, heme oxygenase-1, glutathione s-transferase, UDP-glucuronosyltransferase, and multidrug resistance-associated proteins. These proteins are involved in reduction or prevention of oxidative stress, detoxification of oxidative stress mediators such as hydrogen peroxide and peroxynitrite, conjugation of potentially harmful compounds to glutathione or glucuronic acid moieties to facilitate their excretion (through increasing water solubility), and increasing efflux of toxic compounds into bile, leading to their excretion.

Nrf2 is maintained in an inactive form complexed for proteosomal degradation in the cytosol by the activity of Kelch-like ECH-associated protein 1 (Keap1). Keap1 is the target of nitro-fatty acids (being lipid electrophiles), allowing dissociation of Nrf2 from its ubiquitin complex and migration to the nucleus, where Nrf2 may affect downstream gene transcription. Nrf2, similar to NF-κB, is expressed in and protects many cell types from oxidative stress including vascular smooth muscle cells and endothelial cells [236, 242].

6.3.2.5 PGHS and NADPH Oxidase Modulation

Two other mechanisms of nitro-fatty acid mediation of anti-inflammatory effects involve prostaglandin endoperoxide H synthase (PGHS) and NADPH oxidase (NOX). PGHS is involved in the formation of prostaglandins, and various isoforms of these enzymes are the target of nonsteroidal anti-inflammatory drugs. Prostaglandins themselves are paracrine or autocrine signaling molecules which have a wide variety of effects which include regulation of inflammation and platelet aggregation. Nitro-fatty acids have been shown to inhibit synthesis of prostaglandins at two separate steps in the enzymatic pathway. Activity of PGHS in platelets was also significantly attenuated with nitro-fatty acid administration (along with decreases in thromboxane formation, resulting in a decrease in platelet aggregation), giving nitro-fatty acids antiplatelet aggregation effects. Previous studies have also shown that these effects are not dependent on cyclic GMP or intracellular calcium store mobilization (which are mechanisms for nitric oxide mediated anti-platelet aggregation effects), suggesting that nitro-fatty acids may operate through distinct mechanisms.

NOX isoforms may be involved in the production and regulation of superoxide anions and are present in a wide variety of inflammatory cells including macrophages. Previous studies have shown that administration of nitro-fatty acids results in inhibition of NOX isoform 2 formation of

superoxide anions in activated macrophages, with potential mechanisms including prevention of NOX subunit migration to the cellular membrane and assembly of the final enzyme. Although this nitro-fatty acid mechanism is still early in a full characterization, it is also though to attenuate inflammation [230, 240].

6.4 Nitro-fatty Acids and Nitric Oxide Metabolism

As previously discussed, nitro-fatty acids have a wide range of protein modification mechanisms which result in downstream effects on gene expression which make up a significant portion of its total therapeutic benefits. Nitric oxide donation is thought to be a less prevalent or significant therapeutic mechanism due to various conditions which go against the equilibrium of nitric oxide donation (and therefore toward nitro-fatty acid stabilization) such as incorporation into various hydrophobic compartments or cellular membranes. However, recent studies have shown that despite these factors, nitro-fatty acids may have significant ramifications on nitric oxide metabolism and bioavailability through other alternative means.

One such study evaluating the effect of nitro-fatty acids on nitric oxide bioavailability involved its administration via osmotic pumps with outcome measures of gene expression for HO-1 and endothelial nitric oxide synthase in a mouse model as well as *in vitro* for endothelial cell cultures [243]. The study found that there were increases in gene expression for both of the mentioned targets (3-fold increase for endothelial nitric oxide synthase and 1.9-fold for HO-1) in mouse aortic tissue [243]. Quantification of nitro-fatty acid concentration in plasma was performed (to ensure successful delivery and validation of results as correlated against increases in nitro-fatty acid concentration) and showed that administration of nitro-fatty acid at 3 mg/kg bodyweight per

day for 3 days resulted in approximately 28.3 nanomolar serum concentration of the nitro-fatty acid species. This further suggests that a nanomolar concentration in plasma is sufficient for significant therapeutic effects including gene transcriptional changes. These results were supported by gene expression results for *in vitro* culture of endothelial cells as well [243].

Additionally, *in vitro* studies showed that endothelial cells treated with nitro-fatty acids showed a significant increase in endothelial nitric oxide synthase phosphorylation at the Ser1177 site [244]. As previously discussed, this is a critical site for up-regulation of endothelial nitric oxide synthase activity and is a key step in other mechanistic pathways for endothelial nitric oxide synthase activation and subsequent nitric oxide production. Further mechanistic investigation showed that administration of nitro-fatty acid increased phosphorylation of Akt and p38, which are upstream enzyme cascade participants for nitric oxide synthase activation [244]. Time-course investigations showed significant phosphorylation at 7.5 minutes after treatment administration, which fits the timescale for the treatment later administered in the work for this dissertation. Later production of nitric oxide in cellular cultures was quantified as well to support the observed increase in nitric oxide synthase activation and demonstrated significantly increased production of nitric oxide with only 2.5 micromolar concentration of nitro-fatty acid administered in the culture medium for up to 120 minutes [244].

The results of this study hold significant implications for the involvement of nitro-fatty acid therapy in nitric oxide metabolism on multiple levels. Increased expression of HO-1 has been previously discussed to increase nitric oxide bioavailability due to the role of hemoglobin and free heme (which are degraded by HO-1) as nitric oxide scavengers [226]. Additionally, nitro-fatty acid has been shown to not only increase expression of nitric oxide synthase but also increase post-translational modification of the protein directly resulting in increased activity and production of

nitric oxide itself. Although applications of nitro-fatty acid therapy in cardiovascular disease will be discussed shortly, the implications on vascular pathology are already visible, with HO-1 having a significant role in protection against atherosclerosis and vascular disease as well as nitric oxide having an anti-inflammatory effect.

Another similar study corroborated these results in an analysis of nitro-fatty acid administration on gene expression and phosphorylation of key targets in nitric oxide metabolism [245]. Similar to the previously discussed study, *in vitro* cultures of endothelial cells were used with the addition of serial measurements of various outcomes including nitric oxide production (measured by the Griess method, which quantifies nitrite concentration as a byproduct of nitric oxide production) and mRNA expression of endothelial nitric oxide synthase, heat shock protein 90 (Hsp90), and caveolin-1 (Cav-1). Phosphorylation of key enzymes including endothelial nitric oxide synthase, Akt, and ERK1/2 protein kinases was also quantified [245].

Results for the study showed that nitro-fatty acid stimulated the production of nitric oxide in endothelial cells in a time-dependent manner, increasing significantly above baseline levels of nitric oxide in as soon as 2 hours and reaching 50% increased production of nitric oxide above baseline at 8 hours [245]. Controls featuring administration of the un-modified fatty acid showed no significant increase in nitric oxide production. Results of gene expression analysis showed that nitro-fatty acid treatment significantly increased expression of peroxisome proliferator-activated receptor gamma at early intervals (2 to 8 hours post-treatment) as well as Hsp90. Interestingly, results from the study showed significantly decreased endothelial nitric oxide synthase and Cav-1 expression, which in theory contradicts previous results showing upregulation of both endothelial nitric oxide synthase and HO-1 expression by nitro-fatty acid administration. However, analysis of enzyme phosphorylation showed significantly increased phosphorylation of endothelial nitric

oxide synthase at the Ser1177 site (as previously discussed) as well as the Ser633 site. However, nitro-fatty acid administration conversely decreased phosphorylation of endothelial nitric oxide synthase at the Ser113 and Thr495 sites, suggesting that these sites may have additional significance in regulating enzymatic activity. Phosphorylation of signaling protein kinases including Akt at the Ser473 site and ERK1/2 at the P44-Thr202 and P42-Tyr204 sites was significantly increased with nitro-fatty acid administration.

These results hold significant mechanistic implications on the effects of nitro-fatty acids on post-translational modification and cellular transport of endothelial nitric oxide synthase, especially Hsp90 and Cav-1, which are significantly involved in cellular membrane structure and transport. Hsp90 is a chaperone protein for endothelial nitric oxide synthase and enhances the effect of calmodulin binding on activation of nitric oxide synthase. This association and enhancement of activation has previously been demonstrated with Hsp90 and is also associated with other stimuli of endothelial nitric oxide synthase activity including fluid shear forces, vascular endothelial growth factor, and estradiol. On the other hand, Cav-1 is a structural inhibitor of the calmodulin complex binding site of endothelial nitric oxide synthase, and also inhibits production of nitric oxide. Previous studies have shown significant increases in nitric oxide synthase activity with gene knockout of Cav-1 in animal models. The results of altered gene expression of both Hsp90 and Cav-1 show that administration of nitro-fatty acids also regulates endothelial nitric oxide synthase activity at the level of these two additional regulators which are involved in protein transportation as well as calmodulin association with the enzyme, in addition to increased gene expression and phosphorylation of nitric oxide synthase previously demonstrated.

For the results of endothelial nitric oxide synthase phosphorylation in this study, the various sites of phosphorylation and de-phosphorylation identified are all corroborative with

increased activity of the enzyme, although the precise functional effects of each site are still not clear. However, this study demonstrated that involvement of the nitro-fatty acid in altering nitric oxide synthase phosphorylation is more involved than previously identified. This along with the functional assay supporting these results with time-dependent increases in nitric oxide production of the *in vitro* cellular culture support the authors conclusion that multisite coordination of phosphorylation is indeed legitimate. The authors also provided additional commentary on the specific hypothesized mechanisms of each site individually and their interaction effects in the context of the enzymatic subunits of nitric oxide synthase which will not be discussed here. However, the reduction in mRNA expression of endothelial nitric oxide synthase itself in response to nitro-fatty acid stimulation is not fully characterized by the authors. The results demonstrated an approximately 50% reduction in endothelial nitric oxide synthase expression at 4 and 8 hours post-treatment, although this magnitude is significantly lower than the increases seen in other gene targets such as Hsp90 and peroxisome proliferator-activated receptor gamma which saw increases in expression up to 100% relative to control samples.

6.5 Previous Cardiovascular Applications of Nitro-fatty Acids

Given the previously discussed downstream functions of nitro-fatty acids relevant to oxidative stress, nitric oxide bioavailability, and endothelial function, there are many potential therapeutic applications of nitro-fatty acids to cardiovascular disease. Previous studies have administered nitro-fatty acids to animal disease models of several pertinent varieties which will be discussed in this sub-section.

One such study investigated the therapeutic effects of nitro-fatty acids in a mouse model of atherosclerosis [246]. The disease model was characterized by apolipoprotein E deficiency in transgenic mice, leading to the development of atherosclerotic lesions in blood vessel walls. Natural atherosclerosis is mediated by a variety of inflammatory mediators, and its pathogenesis typically involves endothelial expression of inflammatory cell adhesion markers, derangement of lipid metabolism, and immune cell accumulation of said lipids and forming vascular deposits which develop into atherosclerotic lesions or plaques. Given the role of nitro-fatty acids in reducing inflammation through modification of gene expression, therapeutic potential was identified in this study. Results from the study showed successful reduction in atherosclerotic lesion formation for the disease model mice compared to untreated disease mice by 32%. However, nitro-fatty acid administration did not affect overall metabolism of lipids as characterized by plasma concentrations of various lipid species including total cholesterol concentration and plasma triglyceride levels, as well as glucose. Use of immunofluorescent imaging showed that for the vascular lesions which did develop in the nitro-fatty acid treated disease mice, there was a significantly decreased extent of infiltration and recruitment of monocytes and neutrophils to the lesion site. These cells are recruited and localized by expression of VCAM-1, MCP-1, and ICAM-1 on endothelial surfaces. Given that expression of these markers falls under the governance affected by nitro-fatty acids (as previously discussed), this diminished immune cell localization is supported by previous investigations. The effects of nitro-fatty acid on production and accumulation of various mediators of oxidative stress were investigated as well, characterized by levels of superoxide anion and peroxynitrite, with successful reduction of these measures in nitro-fatty acid treated disease animals. Lastly, conversion of macrophages to lipid-laden foam cells is a key step in the formation and maturation of atherosclerotic lesions with disease progression. To

characterize this, the study investigated the extent of lipid accumulation as well as STAT-1 phosphorylation (a key factor in this conversion of cell phenotype), showing that both these factors are reduced in nitro-fatty acid treated disease animals.

Particularly relevant to the work involving nitro-fatty acids in this dissertation, another previous study evaluated the therapeutic efficacy of nitro-fatty acids in a mouse model of focal cardiac ischemia and reperfusion injury [235]. Not only did this study demonstrate that administration of NFA at several different time points relative to ischemia-reperfusion injury result in significantly improved outcomes in terms of infarct size to area-at-risk ratios as well as morphological analysis, gene expression measurement of several key factors in inflammation and oxidative stress revealed protective effects of NFA as well.

Aside from these two applications, other cardiovascular applications of NFAs in animal pre-clinical models include effects of NFA on neointimal formation after vascular injury, ischemic preconditioning, inflammatory insult from exogenous stimuli such as LPS, fibrosis and fibrotic remodeling after vascular injury, and hypertension [234, 247-249].

7.0 Nitrite Co-therapy with Ultrasound-targeted Microbubble Cavitation

This chapter is derived from a published manuscript as follows:

Gary, Z. Y., Istvanic, F., Chen, X., Nouraie, M., Shiva, S., Straub, A. C., & Pacella, J. J. (2020). Ultrasound-Targeted Microbubble Cavitation with Sodium Nitrite Synergistically Enhances Nitric Oxide Production and Microvascular Perfusion. *Ultrasound in Medicine & Biology*, *46*(3), 667-678.

7.1 Introduction

Cardiovascular disease (CVD) is the leading cause of death in the United States. With coronary artery disease (CAD) accounting for over 40% of all cases, it is estimated that an acute myocardial infarction (AMI) occurs every 40 seconds [160]. Contemporary treatment for AMI is percutaneous coronary intervention (PCI), which focuses on restoring patency of the infarcted artery to reestablish perfusion to the ischemic bed [250]. However, a major obstacle to myocardial reperfusion post-PCI is microvascular obstruction (MVO). MVO is a combination of distal obstruction by microthrombotic debris, oxidative stress, and inflammation which occurs in up to 60% of AMI cases and is associated with worsened patient outcomes independent of age, infarct size, and ejection fraction [162, 165, 166, 168, 169, 172, 177]. MVO also directly correlates with decreased post-AMI ejection fraction and is the leading independent contributor to post-AMI congestive heart failure and major adverse cardiovascular events [171, 175, 251].

Recently we have demonstrated that ultrasound-targeted microbubble cavitation (UTMC) may be used to relieve MVO [184]. UTMC utilizes imaging-guided ultrasound sonication of

intravenously injected lipid microbubbles (MBs) which causes MB expansion and contraction. This results in mechanical disruption of microthrombi, relief of MVO, and restoration of microvascular blood volume (MBV). In addition to these physical mechanisms of microthrombi disruption, MB oscillation also results in generation of intravascular shear stress stimulating release of endothelial derived nitric oxide (NO); our group has shown that UTMC increases endogenous NO bioavailability, which was shown to be a key contributor to its therapeutic efficacy [96, 190, 252].

Decreased NO bioavailability is a known major contributor to the development of MVO due to vascular vulnerability to ischemic injury, increased propensity for platelet and neutrophil aggregation, and decreased protection against reactive oxygen species [167, 253]. AMI patients with coronary artery disease are especially vulnerable due to pre-existing endothelial dysfunction and a milieu of oxidative stress [254, 255]. NO holds a crucial role in numerous pathways that may protect against MVO and its sequelae: decreasing tissue reactive oxygen species (ROS), platelet aggregation and adhesion, inflammatory cell adhesion, and increasing endogenous endothelial tPA release [203].

NO bioavailability may be increased through administration of nitrite (NO_2^-), an exogenous NO donor with increased activity during hypoxia and acidosis, conditions found in MVO. Numerous preclinical and clinical studies have demonstrated the cardioprotective role of nitrite in AMI, where it consistently reduced infarct size, myocardial dysfunction, and occurrence of major adverse cardiovascular events when administered during PCI for AMI [222, 226, 227]. Previous studies have also shown that nitrite may further enhance endogenous NO production, which may potentially lead to synergistic interactions with UTMC therapy [210].

Therefore, in this study, we sought to investigate the potential for therapeutic enhancement of UTMC with co-administration of intravenous nitrite. We hypothesized that, compared to UTMC alone, their combination would result in further increases in NO bioavailability and microvascular blood volume (MBV) and accompanying decreases in ROS activity. This was tested in a series of experiments during UTMC and nitrite combination therapy in normal rat hindlimb microcirculation. Blockade of endogenous NO production with N-Nitro-L-Arginine methyl ester (LNAME) was also used to parcel dependence on endothelial nitric oxide synthase (eNOS). During these studies, NO concentration was measured, and ROS activity was evaluated using H_2O_2 concentration and protein carbonylation. To determine whether the specific source of exogenous NO had an effect on the above measures, the experiments were repeated with sodium nitroprusside (SNP), a direct NO donor.

7.2 Methods

7.2.1 Lipid Microbubble Agents

The therapeutic phospholipid MBs used for UTMC therapy were synthesized in-house and measured as described by our previous work [190]. For contrast perfusion imaging, DEFINITY® MBs (Lantheus Medical Imaging, North Billerica, MA) were prepared at full concentration with mean diameter of 1.1-3.3 μm and approximate concentration of 1.2×10^{10} microbubbles/mL for infusion at 2 mL/hr.

7.2.2 Animal Preparation

All animal studies in this investigation received prior approval by the Institutional Animal Care and Use Committee at the University of Pittsburgh. The rat hindlimb model, previously developed in our laboratory, was used for modeling of healthy microvasculature of the gastrocnemius muscle [190]. In rats weighing 275±20 g, anesthesia was induced by inhalation of isoflurane (2.5%). An arterial cannula (PE-10, Becton Dickinson, Franklin Lakes, NJ) was placed into the right femoral and advanced into the abdominal aorta for infusion of therapeutic MBs directly into the left hindlimb for first pass delivery. The femoral arterial cannulation site was also used for infusion of sodium nitrite (4 mg/kg, Sigma-Aldrich, St. Louis, MO) and/or LNAME (10 mg/kg, Sigma-Aldrich, St. Louis, MO). The right internal jugular vein was cannulated (24G, 0.75 inches long) to deliver DEFINITY® MBs (Lantheus Medical Imaging, Inc., North Billerica, MA) at 2 mL/hr for contrast imaging.

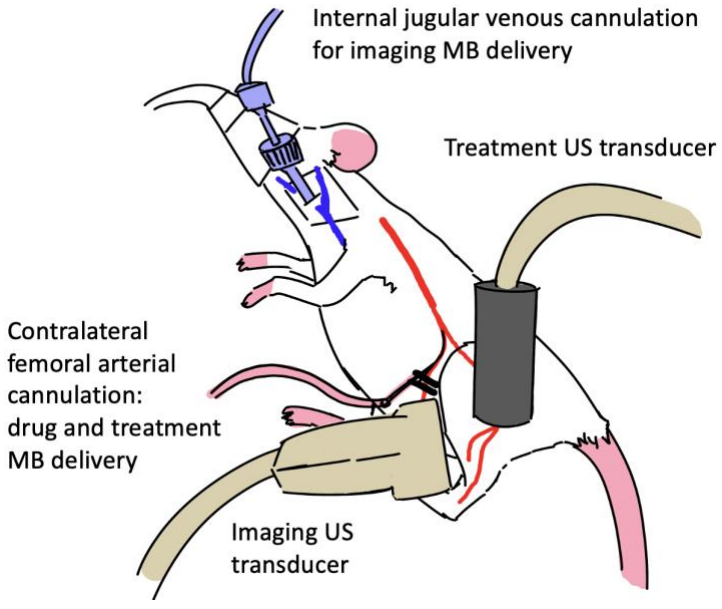

Figure 1: Experimental diagram for rat hindlimb model

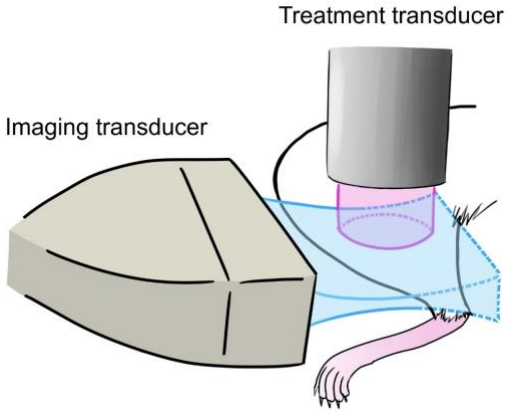

Figure 2: Specific arrangement of US transducers in hindlimb model

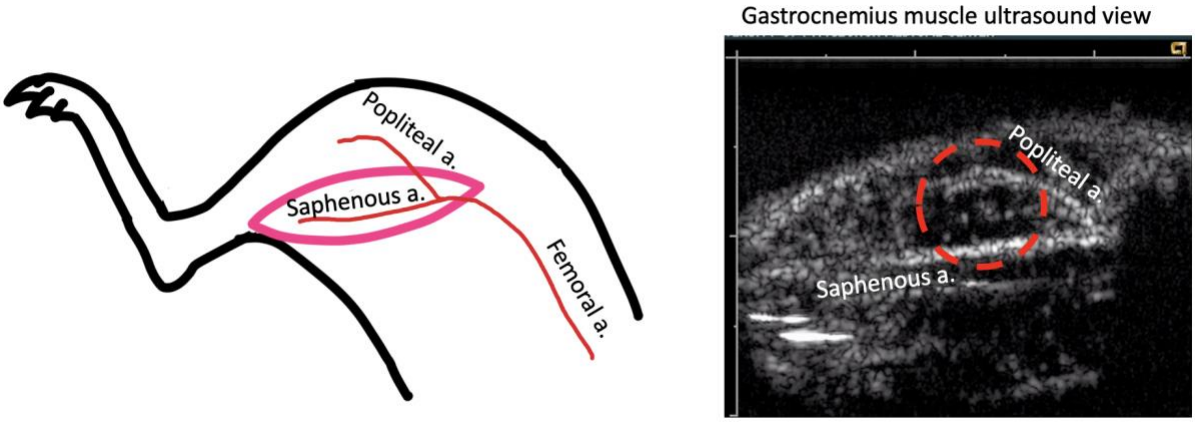

Figure 3: Anatomic landmarks and US view of gastrocnemius muscle

A simplified diagram (left) of the local major feeding vessels (red lines) and gastrocnemius muscle (rough pink outline) is shown with the corresponding contrast US image (right) with labeled vessels and treatment US beam approximate location shown in a red dashed circle.

7.2.3 Ultrasound Therapy and Perfusion Imaging

All therapeutic ultrasound (US) was delivered using a 1 MHz single-element transducer 12.7 mm in diameter (A303S, 0.5 inch, Olympus NDT, Waltham, MA) with calibration performed in free field. The transducer was driven by an arbitrary function generator (AFG3252, Tektronix, Beaverton, OR) connected to a radio frequency power amplifier (800A3B, Amplifier Research, Souderton, PA). The therapy transducer was placed vertically with the rat hindlimb and coupled to depilated skin using acoustic gel (transducer orientations shown in Figure 2). The therapeutic pulse consisted of a long tone 5,000 cycle duration with a pulse interval of 3 seconds at a peak negative acoustic pressure of 1.5 MPa. Ultrasound perfusion imaging was performed using a clinical scanner (Siemens, Sequoia, 15L8 probe) during infusion of DEFINITY®. The syringes holding the MBs were rotated gently throughout delivery to maintain uniform MB suspension.

Burst-replenishment imaging was performed in contrast pulse sequence (CPS) mode at 7 MHz with mechanical index of 0.2 and framerate of 5 Hz, and a 5-frame burst pulse at an MI of 1.9 was used to completely clear MBs from the field of view. The dynamic range (60 dB), gain (0 dB), and linear compression curve were fixed throughout the study. Replenishment of DEFINITY® MBs to the target microvasculature was recorded in cine-loops for processing of perfusion kinetics.

7.2.4 Image Acquisition and Processing

Positioning of the imaging transducer was perpendicular to the treatment transducer such that the junction of the saphenous and popliteal arteries was clearly visible on the right side of the image with blood flow through these major vessels proceeding from right to left. White line

artifacts visualized in the hindlimb at this imaging position represent strong reflection by bone or cartilage and were excluded from the region of interest for perfusion analysis.

Image analysis was performed using recorded cine-loops in MATLAB following a previously described approach to obtain a measure of peak microvascular blood volume (MBV) as a correlate of vasodilatory status and microvascular perfusion [190]. The justification and derivation of this method of using a mono-exponential regression for quantification of microvascular blood volume has previously been documented [256, 257]. For each animal, MBV measurements at post-treatment time points were normalized against the pre-treatment baseline measurement.

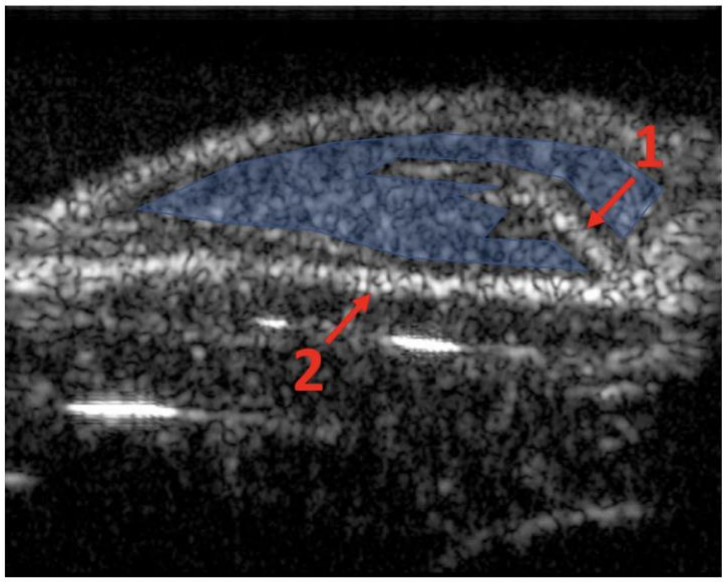

Figure 4: Contrast US image of gastroc. with microvascular ROI

The contrast US image of the gastrocnemius muscle is shown (with major feeding vessels labeled in red numbers) and the selected region-of-interest for microvascular analysis shown in blue with major feeding vessels excluded.

7.2.5 Measurement of Hindlimb Nitric Oxide and Hydrogen Peroxide

For real-time measurement of intramuscular NO, a calibrated porphyrinic membrane catheter probe (amiNO-IV, Innovative Instruments Inc., Tampa, FL) was inserted into the left gastrocnemius muscle in the treatment area of the therapeutic US beam. The probe signal was allowed to equilibrate for 30 min prior to drug infusion and treatment. NO concentration was recorded up to 30 min post-UTMC therapy, followed by background subtraction and normalization against the start of the observation interval. Due to a lack of absolute NO quantification for *in vivo* probe calibration, all measurements are presented as relative changes in concentration as represented by change in current (in pA) detected by the probe. Additionally, a similar probe sensitive to tissue H_2O_2 was calibrated and placed in a separate cohort (HP250, Innovative Instruments Inc.). H_2O_2 concentration was recorded for 7 min post-UTMC therapy.

7.2.6 Measurement of Protein Carbonylation

Protein carbonylation was measured as an indicator of damage from oxidative stress and production of ROS. To avoid tissue damage from catheter probe placement, tissue samples were collected from animals receiving the experimental protocol previously described without NO nor H_2O_2 probe placement. 5 animals received combination nitrite and UTMC therapy, while 5 animals received UTMC therapy only. For each animal, tissue from the gastrocnemius muscle of the treated hindlimb in the region directly beneath the therapeutic US transducer and tissue from the ipsilateral biceps femoris muscle (not directly treated by UTMC) were excised 7 minutes after UTMC therapy and snap frozen in liquid nitrogen.

The tissue samples were then homogenized and prepared for quantification of protein carbonylation using a standard 2,4-dinitrophenylhydrazine assay (Sigma-Aldrich). Total protein content was evaluated using a BCA assay (Sigma-Aldrich) on the tissue homogenates used. The resulting protein carbonylation per unit mass protein measurements were normalized against the control group receiving no treatment. Each animal served as its own control as tissue samples taken from UTMC treated and untreated regions of the same hindlimb were compared in a carbonylation ratio.

7.2.7 Measurement of Nitrite in Blood and Muscle Tissue

To verify the successful infusion and delivery of nitrite to the rats receiving combination therapy, nitrite concentration in blood samples were measured using ozone-based chemiluminescence. Prior to euthanasia, a catheter was inserted into the rat carotid artery for collection of blood into a tube with EDTA for anticoagulation. Blood samples were spun down in a centrifuge and the plasma layer was isolated for assay use, as previously described [258, 259]. For muscle tissue samples, specimens were collected from the treated gastrocnemius muscle and ipsilateral biceps femoris muscle in animals receiving combinations of UTMC and nitrite therapy 7 minutes after treatment. All tissue samples were snap frozen in liquid nitrogen and homogenized in a nitrite preservation solution prior to analysis with ozone chemiluminescence. Tissue nitrite measurements were normalized against protein concentration measured by a BCA assay (Sigma-Aldrich) while intravascular nitrite was normalized against sample volume.

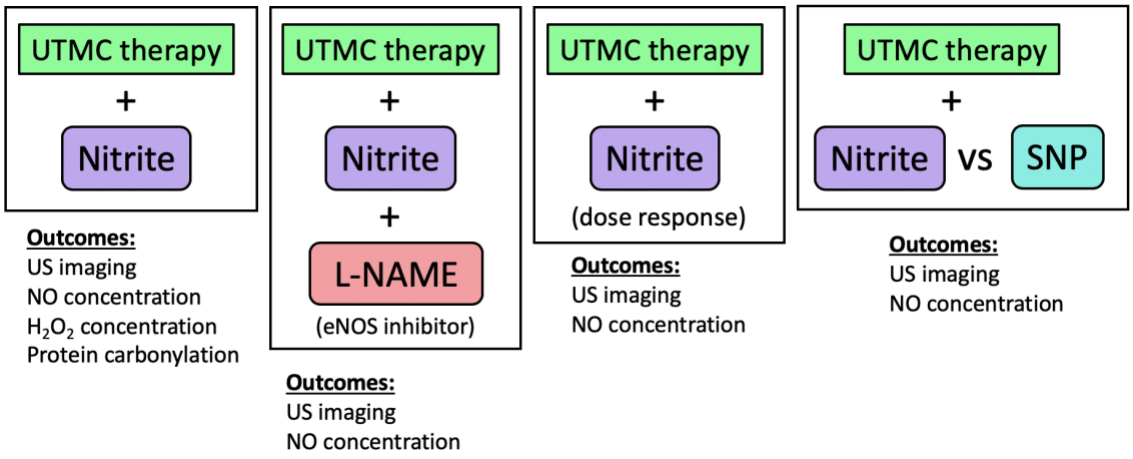

Figure 5: Simplified schematic of experimental groups

7.2.8 Experimental Protocol

Nitrite (4 mg/kg iv, ~ 0.25 mL volume) was delivered as a slow bolus in saline into the femoral site over 15 seconds, 5 min prior to UTMC. LNAME was delivered with the nitrite in the same saline bolus (10 mg/kg iv) in the appropriate groups to inhibit the activity of eNOS. For UTMC therapy, treatment US was delivered during the infusion of treatment MBs at the femoral site (2×10^8 treatment microbubbles/mL, 1.5 mL/hr) via syringe pump for 2 min. Placement of the therapeutic US transducer was confirmed by visualization of MB destruction by the therapeutic pulses in the perfusion image during treatment. Microvascular tissue perfusion was then measured by bust-replenishment imaging cine-loops during DEFINITY® infusion at baseline (prior to drug administration and UTMC), 3, 6, 10, and 30 min post-UTMC. Heart rate, respiratory rate, and O_2 saturation were continuously monitored. After the 30-minute observation interval, the animals were euthanized by isoflurane overdose followed by heart excision.

To observe the effects of peak negative US pressure and MB concentration on microvascular perfusion and NO perfusion, three different conditions of each parameter were used

in the combination therapy of UTMC and sodium nitrite. For the effect of US peak negative pressure, therapeutic MB delivery concentration was kept constant at 1×10^9 microbubbles/mL infused at a rate of 3 mL/hr. Peak acoustic pressures of 1.5 MPa, 0.75 MPa, and 0.33 MPa were used. For the effect of MB concentration, therapeutic US peak negative pressure was maintained at 1.5 MPa. MB concentrations of 1×10^9 and 5×10^8 microbubbles/mL at 3 mL/hr, and 2×10^8 microbubbles/mL at 1.5 mL/hr were used.

Similar to the experimental protocol for nitrite co-therapy with UTMC, sodium nitroprusside (SNP) was given in the pre-treatment bolus at a dosage of 8 μg/kg in saline, followed by a 5 min waiting period and 2 min of UTMC therapy. A MB concentration of 1×10^9 microbubbles/mL given at 3 mL/hr was used for UTMC. Burst-replenishment cine-loops were obtained at baseline, 3, 6, 10, and 30 minutes post-treatment and processed for total MBV. Changes in local NO concentration were also measured over 30 minutes post-treatment.

7.2.9 Statistical Analyses

For the factorial design between UTMC, nitrite, and LNAME administration, effects on MBV and change in NO concentration were analyzed using a mixed effects model (with random intercept for each animal and restricted maximum likelihood) using Stata 14.2 (StataCorp., College Station, TX). Remaining data were analyzed using one-way and two-way repeated measures ANOVA followed by Tukey's HSD post-hoc test and both paired and unpaired t-tests performed using GraphPad Prism (GraphPad Software, La Jolla, California) with significance considered at $p < 0.05$. All data are presented as mean ± SD.

7.3 Results

7.3.1 Effects of UTMC and Nitrite on NO and Microvascular Blood Volume

Figure 6 shows still frame contrast images for peak plateau video intensities obtained 30 s post-UTMC for experimental groups without LNAME at baseline and 3, 6, 10, and 30 min after treatment. MBV for all treatment groups are shown in **Figure 7**.

There was a significant three-way interaction effect between UTMC, nitrite, and L-NAME on change in MBV over the 30 min observation interval ($p < 0.0001$) (**Figs 7A, C**). At the 3 min time point specifically, the UTMC only group showed a transient decrease in MBV below baseline, likely indicating a post-UTMC microvascular spasm ($p < 0.0001$) previously observed by our group [190].

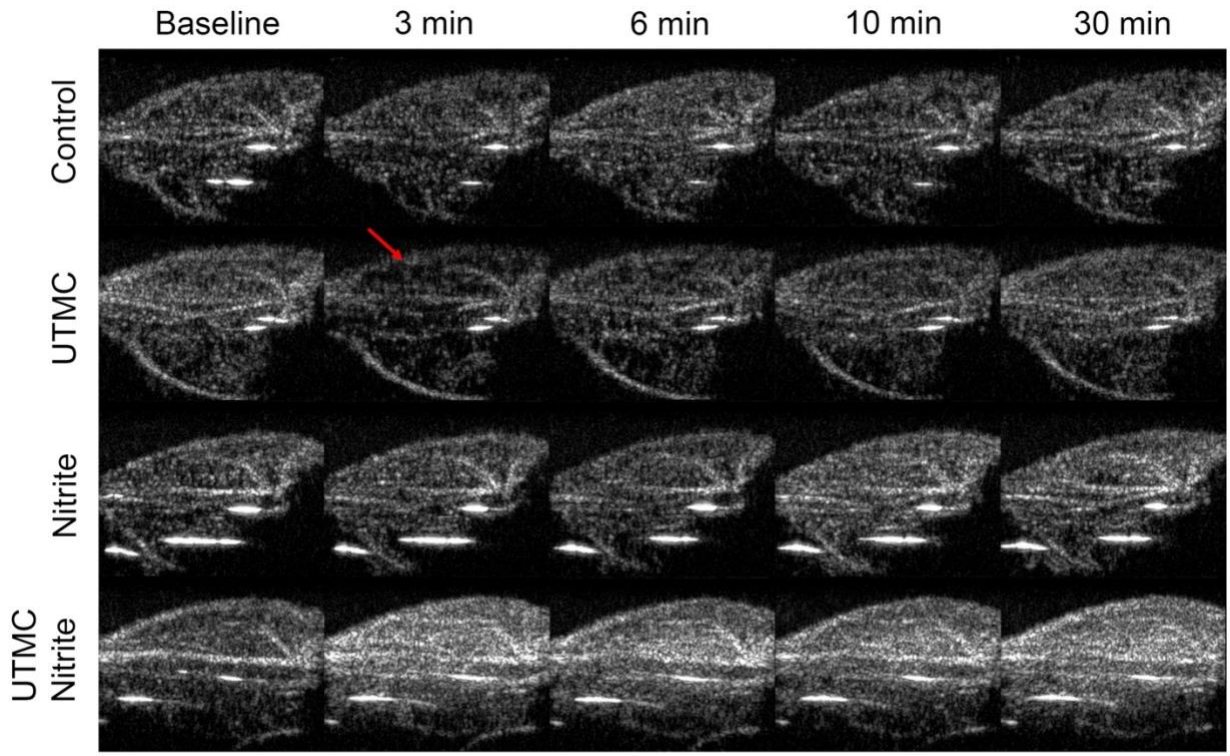

Figure 6: Effect of UTMC nitrite combination therapy on microvascular blood volume

Contrast-enhanced still-frame ultrasound images of the treated hindlimb gastrocnemius region are shown for all groups after UTMC (2×108 MB/mL at 1.5 mL/hr for 2 min) at 1.5 MPa negative peak acoustic pressure. Images were taken 30 sec after burst in the reperfusion sequence at baseline, 3, 6, 10, and 30 min after the 2 min treatment period. Note the transient decrease in image intensity at 3 min for the UTMC group (red arrow). For the UTMC nitrite group, large increases in image intensity are seen at all time points after baseline.

However, addition of nitrite to UTMC eliminated this event and instead resulted in significantly increased MBV ($p < 0.0001$). With the addition of LNAME (**Fig 7C, D**), which removes eNOS dependent NO, both UTMC LNAME and UTMC LNAME nitrite showed significant decreases in MBV ($p < 0.0001$ for both), suggesting eNOS dependence of the UTMC-nitrite interaction effect.

Change in concentrations of intramuscular NO versus time are presented in **Figure 2B and D**. There was a significant three-way interaction effect between UTMC, nitrite, and L-NAME on changes in NO concentration over 30 min ($p < 0.0001$). No change in NO concentration was seen in the control group. In both UTMC alone and nitrite alone, there was a mild increase in NO above baseline. However, when UTMC was combined with nitrite, there was a marked, synergistic increase in intramuscular NO (**Fig. 7B**). In congruence with the MBV data, LNAME reversed these NO enhancing effects. Specifically, UTMC combined with LNAME caused a marked reduction in NO and the addition of nitrite decreased the magnitude of this reduction.

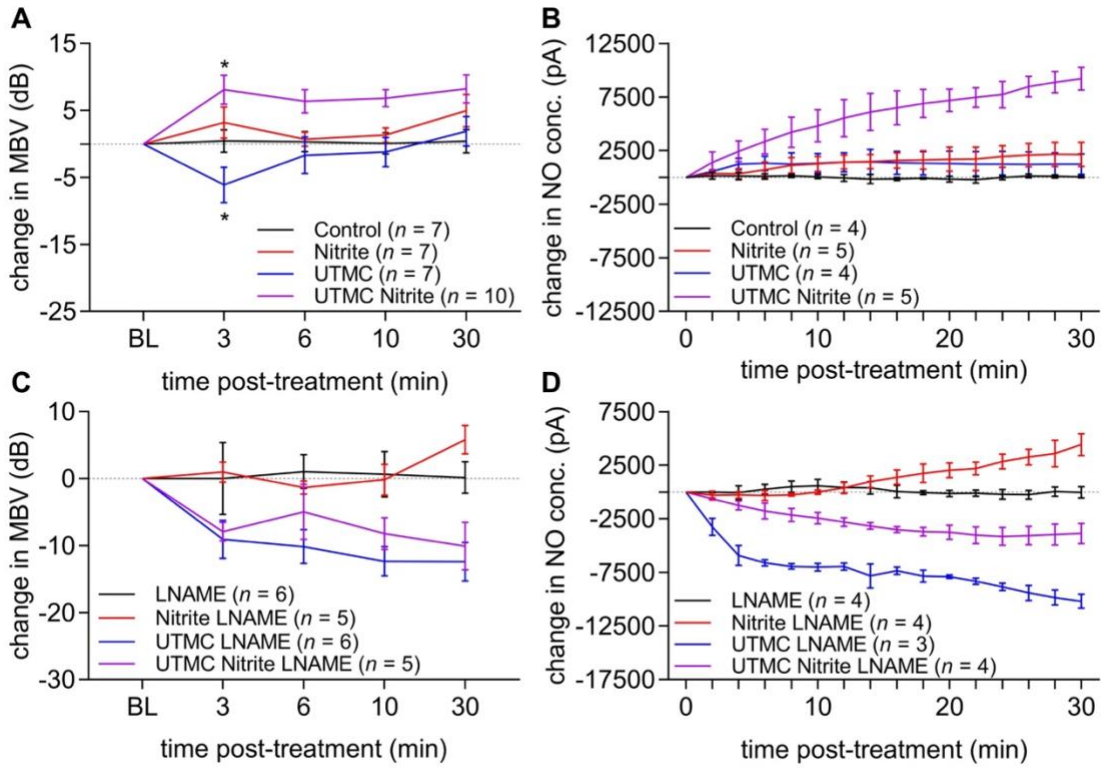

Figure 7: Changes in MBV and NO concentration after UTMC nitrite therapy

Changes in MBV (A and C) and NO concentration (B and D) are shown. Asterisk indicates $p < 0.0001$ compared to control. The transient decrease in MBV in the UTMC group at 3 min was reversed with the addition of nitrite, while addition of N-Nitro-L-Arginine methyl ester (LNAME) resulted in persistent and exacerbated decrease. UTMC with nitrite resulted in greatly increased NO over individual treatments. Addition of LNAME to UTMC resulted in decreased NO which was partially rescued by addition of nitrite. There was a significant three-way interaction effect between factors of UTMC, nitrite, and LNAME ($p < 0.0001$) for both change in MBV and NO concentration. All error bars indicate standard deviation.

7.3.2 Effect of US Pressure and MB Dose on UTMC Nitrite Co-therapy

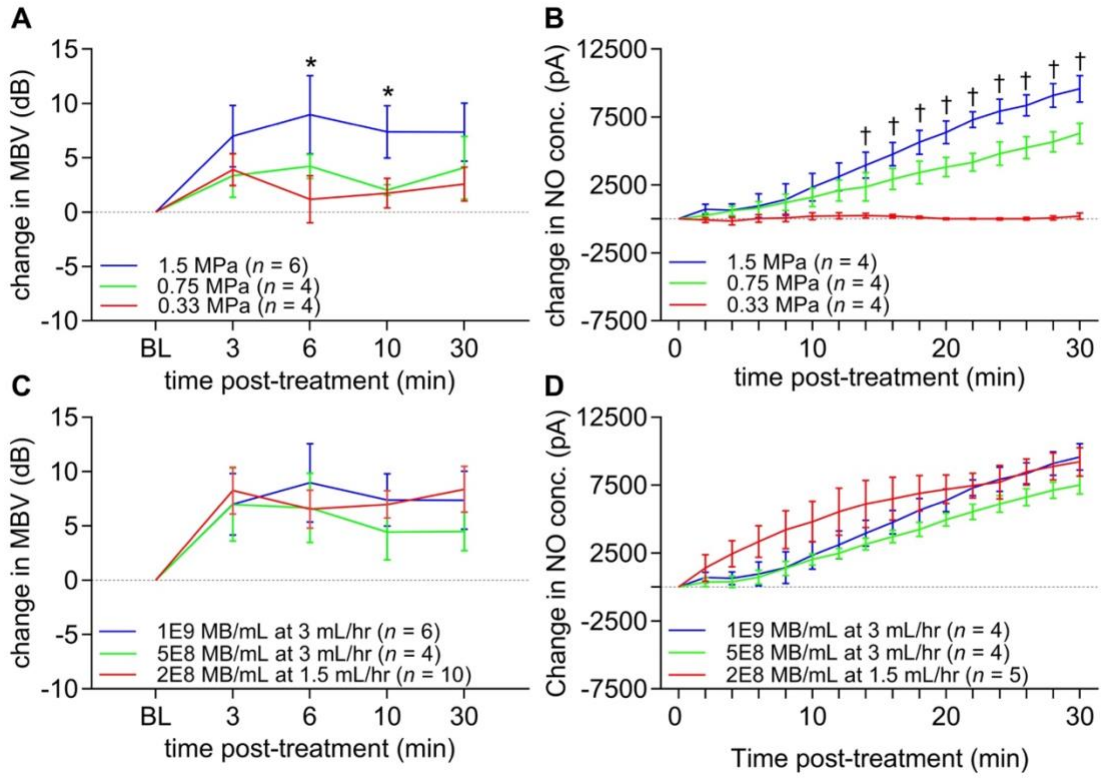

Figure 8: Effect of US pressure and MB dosage

For animals receiving UTMC nitrite therapy, changes in MBV and NO concentration for varied US pressures with constant MB dosage of $1\times10_9$ MB/mL, 3 mL/hr for 3 min (A and B) and varied MB doses at a constant 1.5 MPa peak negative US pressure (C and D) are shown. While there was a significant effect of varying US pressure on MBV and NO concentration, the effect of MB dosage for the levels shown was not significant. Asterisk (*) indicates $p < 0.05$ compared to other groups. Dagger (†) indicates all groups are significantly different from each other ($p < 0.0005$). Error bars indicate standard deviation.

7.3.2.1 Effect of US Dose

As shown in **Figure 8A**, there was a significant effect of varying US pressure on MBV for the tested levels of 1.5, 0.75, and 0.33 MPa ($p < 0.0005$). In post-hoc testing, the 1.5 MPa group had significantly higher MBV than both other groups at 6 and 10 min ($p < 0.05$). Only the 1.5 MPa group had significantly higher MBV than baseline at all subsequent time points ($p < 0.001$).

For the 0.33 MPa group NO concentration was significantly lower than both the 1.5 and 0.75 MPa groups from 12 min onward ($p < 0.0005$, **Figure 8B**). While NO concentration in the 1.5 MPa group exceeded the 0.75 MPa group at 14 min onward ($p < 0.0005$). The 0.75 MPa group increased significantly above baseline at 10 min while the 1.5 MPa did so at 8 min ($p < 0.0001$).

7.3.2.2 Effect of MB Dose

There was no significant effect of varying MB dosage on MBV for the groups investigated (**Figure 8C**). All groups increased in MBV significantly above BL at 3 and 6 min post-treatment ($p < 0.005$), while only the 1×10^9 microbubbles/mL at 3 mL/hr and the 2×10^8 microbubbles/mL at 1.5 mL/hr increased significantly above BL at 10 and 30 min ($p < 0.0001$).

For NO concentration, there was a significant MB effect on NO concentration as the group receiving 1×10^7 MBs briefly rose above the other two groups from 8 to 12 min post-treatment ($p < 0.0001$, **Figure 8D**). Both the 1×10^8 and the 5×10^7 MBs groups increased significantly above baseline after 10 min ($p < 0.0001$) while the 1×10^7 MBs increased above baseline at 2 min post-treatment ($p < 0.0001$).

7.3.3 Effect of UTMC Nitrite Therapy on Oxidative Stress

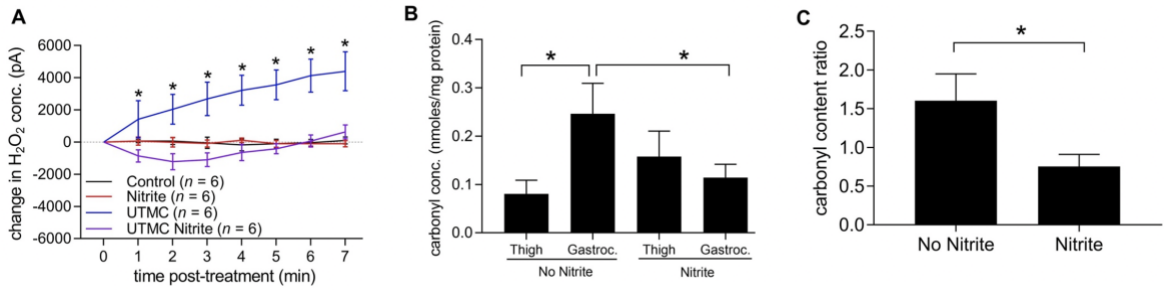

Figure 9: Protective effects of nitrite with UTMC therapy on oxidative stress

Change in hydrogen peroxide concentration (A) show that addition of nitrite to UTMC prevented early increases in hydrogen peroxide seen in UTMC alone in the first seven minutes after treatment. Extent of protein carbonylation is presented as a concentration for each group (B), and as a carbonyl content ratio (C). The carbonyl content ratio was obtained by taking the ratio of carbonyl concentration of a muscle tissue sample within the US treatment region (gastrocnemius) to one outside the US treatment region in the same rat hindlimb (thigh). For each group in (B) and (C), n = 5 animals. Addition of nitrite with UTMC therapy resulted in no increase in carbonylation seen in UTMC without nitrite. Asterisk (*) signifies $p < 0.005$ against all other groups (left) or compared group (middle, right). Error bars indicate standard deviation. (Gastroc. = gastrocnemius)

7.3.3.1 Hydrogen Peroxide Concentration

There was a significant interaction effect between nitrite and UTMC on H_2O_2 concentration ($p < 0.0001$) with results shown in **Figure 9A**. Nitrite alone did not result in significant increase in H_2O_2 concentration. UTMC alone resulted in significant increases in H_2O_2 concentration from 1 min onward compared against control, nitrite alone, and UTMC with nitrite ($p < 0.0005$ for all). Addition of nitrite to UTMC resulted in significantly decreased H_2O_2 concentration compared to all other groups up to 3 min post-treatment ($p < 0.05$), with no significant difference up to 7 min.

Relative to each group's own baseline value, UTMC alone increased H_2O_2 concentration significantly at all later time points ($p < 0.005$) while UTMC with nitrite reduced H_2O_2 concentration at 2 and 3 min ($p < 0.005$).

7.3.3.2 Protein Carbonylation

Carbonyl concentration (nanomolar amount per gram protein) for groups receiving combinations of UTMC and nitrite therapy were normalized against the mean control group value (**Figure 9B**). Significance differences in carbonyl concentration were seen between groups ($p < 0.0005$) using one-way ANOVA. The group receiving UTMC without nitrite had significantly higher normalized carbonyl concentration than the control group and the UTMC nitrite combination group ($p < 0.005$). There was no significant change in normalized carbonyl concentration between the UTMC nitrite group or either the nitrite only or the control group.

When normalizing each animal's UTMC treated region against its UTMC untreated region as a paired control, carbonylation ratios were obtained for the groups with and without nitrite **(Figure 9C)**. Animals which did not receive nitrite had significantly higher carbonylation ratios (UTMC treated over untreated) than those which did receive nitrite ($p < 0.005$).

7.3.4 Comparison of Nitrite with SNP during UTMC Therapy

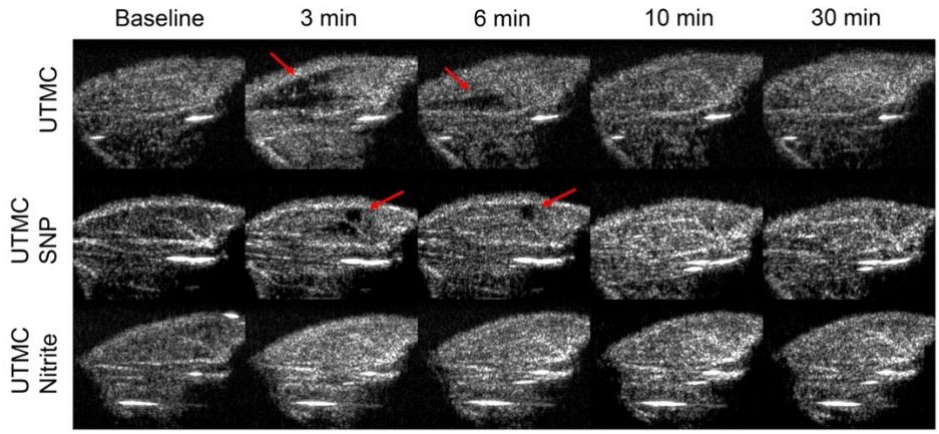

Figure 10: Contrast US imaging comparing NO donor efficacy at higher MB dose

Contrast-enhanced still-frame ultrasound images are shown after 2 min of ultrasound-targeted microbubble cavitation (UTMC) at $1\times10_9$ MB/mL at 3 mL/hr for 2 min and 1.5 MPa pressure. Images were taken 30 sec after burst in the reperfusion sequence at baseline (BL), 3, 6, 10, and 30 min after the 2 min treatment period. In the UTMC group, microvascular spasm is observed at 3 and 6 min after treatment (red arrow). This is also noted in the UTMC sodium nitroprusside (SNP) group, although spasm size is notably smaller.

7.3.4.1 Microvascular Blood Volume

Still-frame perfusion images for UTMC, UTMC with SNP, and UTMC with nitrite at baseline, 3 min, and 6 min post-treatment are shown in **Figure 10**. A higher treatment MB dosage was used to compare against results in our previous work [190].

As indicated in **Figure 11A**, at 3 min UTMC alone had significantly lower MBV relative to baseline ($p < 0.0001$). Although UTMC with SNP had higher MBV than UTMC alone at 3 min ($p < 0.05$), UTMC with nitrite had significantly higher MBV than both groups ($p < 0.005$).

7.3.4.2 NO Concentration

For NO concentration (**Figure 11B**), UTMC alone increased significantly above baseline from 26 min onward ($p < 0.0005$). UTMC with SNP increased above baseline from 18 min onward with the exception of the 26 min timepoint ($p < 0.0005$). UTMC with nitrite increased above baseline from 10 min onward ($p < 0.0005$). UTMC with SNP had significantly higher NO concentration than UTMC alone at the 8- and 10-min time points ($p < 0.05$), while UTMC with nitrite had significantly higher NO concentration than both other groups from 12 min onward ($p < 0.0005$).

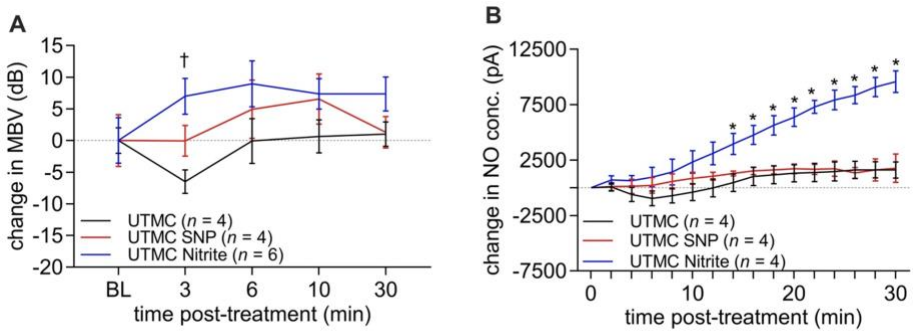

Figure 11: Effect of SNP compared to nitrite on MBV and NO concentration

Change in MBV (top) and NO concentration (bottom) are shown for UTMC and NO donor co-therapies. While a decrease in MBV with UTMC was observed at 3 min, this was mitigated with SNP and reversed with nitrite co-therapies. In addition, a significant increase in NO was only observed for UTMC with nitrite. Dagger (†) indicates all groups are significantly different ($p < 0.005$). Asterisk (*) indicates $p < 0.0005$ against other groups.

7.4 Discussion and Conclusions

Our previous work has demonstrated that UTMC restores microvascular perfusion in an *in vivo* model of MVO, with endogenous NO bioavailability playing a significant role in its efficacy [184, 190]. We sought to enhance the effects of UTMC using nitrite, an exogenous NO source, in this exploratory study. To better understand the mechanistic interactions between UTMC and nitrite, this study was performed in normal hindlimb microvasculature to prevent potential confounding factors or pathologic interference in the NO signaling pathways seen during MVO. Although we recognize that endothelial health cannot be assumed in many potential applications of UTMC, including vasculopathies, AMI, and sickle cell disease, the therapeutic interactions and synergies described here will serve as a foundation for potential future studies in such disease models.

We tested this hypothesis using a factorial design between UTMC, nitrite, and LNAME administration in a healthy rat hindlimb and found a significant three-way interaction effect of the treatment factors on microvascular perfusion and NO concentration. While UTMC and nitrite synergistically increase microvascular perfusion and NO concentration, this effect is diminished by LNAME administration, suggesting eNOS dependence. However, administration of nitrite alone resulted in significant increases in MBV regardless of LNAME administration, which supports previous characterization of nitrite as an eNOS independent contributor to NO bioavailability and vasodilation [216].

After establishing a synergistic effect between UTMC and nitrite, we then sought to characterize how US peak negative acoustic pressure and MB dosage used in UTMC nitrite co-therapy would affect MBV and NO concentration. Previously, we have demonstrated that high (1.5 MPa) US peak negative pressure led to increased clot destruction in an *in vitro* MVO flow

loop model, which solely investigated the mechanical mechanisms of UTMC and the interactions of the MB and microthrombi [187]. This increased clot destruction was ascribed to higher pressures resulting in non-linear MB expansion and collapse, with large changes in MB radius, delivering increased energy per time as well as other physical phenomenon such as microjet formation [260]. In addition, higher acoustic pressure also induced continuous cavitational activity which persisted for up to 5 ms of the US tone burst [187].

Taken together, these MB behaviors translate to increased shear force exposure of the vascular endothelium. In the current work, we demonstrated that this results in a dose response relationship between peak negative pressure and increases in MBV and NO concentration, supporting a causal relationship.

While the 0.33 MPa group saw slight, numerical increases (not statistically significant) in MBV, no increase in NO concentration was observed. At these acoustic pressures, the predicted shear stress generated by the oscillating MB should exceed the limit required to stimulate endothelial NO production (3-9 Pa). We recognize the possibility that the amount of NO produced may have been below the sensitivity of our intramuscular NO probe.

No significant effect of MB dose on MBV or NO were observed in UTMC nitrite co-therapy. All of the doses investigated resulted in similar increases in MBV and NO concentration. This observation may be due to the fact that we have exceeded a threshold concentration of MBs, beyond which further increases do not result in further enhancement of MBV or NO production. A wider range of dosages may be further characterized in future studies.

Next, we sought to characterize the effects of UTMC and UTMC nitrite therapy on various measures of reactive oxide species production and oxidative stress because these environmental factors are potentially deleterious in the setting of MVO [261]. To do so, we measured real-time

intramuscular H_2O_2 concentration and post-UTMC tissue carbonyl content as surrogate indicators of ROS production and oxidative stress [262, 263]. Both of these are well characterized and stable over the observation period of our animal model and were evaluated in the 7 min post-UTMC window [264]. A 7 minute observation period was selected because 1) an approximately 3 min transient decrease in MBV was seen in the UTMC only group suggestive of microvascular spasm and 2) recovery of MBV back toward baseline which occurs at approximately 6 minutes was blunted by the addition of LNAME to UTMC, indicating that lack of endogenous NO is a major contributor to recovery of microvascular blood volume. Thus, the mechanistic basis for this phenomenon, of which ROS production and oxidative stress are potential components, would be observed in this 7-minute time window. Increased production of ROS and oxidative stress are directly related to higher levels of NO scavenging and endothelial dysfunction [265].

However, whether this increase in ROS is the direct cause of the post-UTMC transient microvascular spasm, or a byproduct remains unclear. Our results showed that there is a nearly immediate increase in intramuscular H_2O_2 concentration after UTMC, relative to control. However, addition of nitrite to UTMC completely eliminated this increase in ROS concentration. This suggests that nitrite has protective effects on local ROS concentration after UTMC, by 1) greater clearance of local ROS from the treatment site from the enhanced microvascular perfusion, preventing its accumulation, and/or 2) greater direct conversion of ROS to other species by increased local NO.

Previous studies have also observed the formation of hydrogen peroxide after UTMC, associating it with transient permeabilization of cell membranes without jeopardizing cell viability [106, 266]. However, the study was performed under low diagnostic power US and stable MB oscillation, rather than the high-pressure US, inertial MB cavitation of our present study,

suggesting that the changes in hydrogen peroxide seen in these two studies may represent different phenomena.

To further validate the protective effects of nitrite in the setting of UTMC, we measured protein carbonylation as a marker of damage from ROS in muscle tissue samples within the same animal at both UTMC treated and untreated locations [262]. These results were congruent with those of H_2O_2 concentration, where UTMC alone resulted in a significant increase of protein carbonyl content relative to an untreated site on the same animal. Both absolute values of protein carbonyl content and animal-matched carbonyl ratios between treated and untreated sites indicated that addition of nitrite prevented any increase in carbonyl content. This together with our H_2O_2 concentration results support nitrite co-therapy as a protective measure against ROS production and oxidative stress accompanied by long-tone burst, high pressure UTMC.

To determine whether the synergistic effect between UTMC and nitrite seen in our trials is due to nitrite-specific molecular pathways or general NO donor activity, we compared nitrite administration to SNP, another exogenous NO donor which directly releases molecular NO. In this experiment, a higher dose of injected MB was used to consistently replicate the post-UTMC transient microvascular spasm previously noted and compared against our previous results featuring the same concentration [190]. Although addition of SNP prevented any transient decrease in MBV at the 3 min time point, the subsequent increase in MBV as seen with nitrite co-therapy was markedly less.

Similarly, although SNP co-therapy prevented the transient decrease in NO concentration seen with high-MB dose UTMC, it did not synergistically increase NO concentration above levels seen with UTMC alone. Although these results were obtained using a single dosage of SNP, they support that the synergistic effects seen in UTMC nitrite therapy are specific to nitrite rather than

a general exogenous NO donor. Furthermore, they reinforce that lack of NO contributes to post UTMC recovery of microvascular blood volume.

Enhancement of tissue perfusion with therapeutic US has previously been characterized in a variety of healthy and disease models over a range of US settings [267, 268]. Tissue perfusion is enhanced by focal shear stress stimulation of the microvascular endothelium caused by MB oscillation and destruction (inertial cavitation) when stimulated by US. The downstream cellular responses that occur after US stimulation include eNOS and nitric oxide-dependent changes in perfusion kinetics and purinergic signaling pathways through release of extracellular ATP [269-271].

One pathway that may be involved in the downstream signaling of UTMC cavitation events is that of AMP-activated protein kinase (AMPK) with eNOS, a potential mechanism for the synergy between UTMC and nitrite. In this proposed pathway, exogenous nitrite produces NO via two arms: 1) direct conversion of nitrite to NO via reductive mechanisms (eNOS independent) and 2) nitrite-AMPK-eNOS-NO pathway [204, 209]. That is, AMPK is activated by both nitrite and shear stress, each of which results in eNOS phosphorylation and production of NO [210, 214]. UTMC provides an external source of intravascular shear through MB oscillations which may also activate AMPK, which would result in phosphorylation of eNOS to yield even greater NO production. Additionally, AMPK may also be stimulated via calcium/calmodulin-dependent protein kinase pathways, which may also be involved in shear mechanotransductive signaling [207, 208, 212, 213]. Therefore, through shear responsiveness, the AMPK pathway could further increase NO bioavailability and explain synergism observed between nitrite and UTMC.

An additional potential explanation for the synergy between nitrite and UTMC may be that UTMC enhances the local concentration of nitrite at the treatment site. Because nitrite is not only

a source of NO but also a vasodilatory agent, this could explain the changes in MBV and NO concentration observed. To exclude this possibility, both blood and tissue nitrite concentrations were measured in rats receiving all combinations of UTMC and nitrite therapy and there were found to be no significant differences in blood or tissue nitrite concentration between rats which did and did not receive UTMC. Therefore, a UTMC-induced increase in local nitrite concentration to explain this observed synergy is unlikely.

In this study, long tone burst US at high MI was used for UTMC with nitrite co-administration. These settings were determined to be the most effective for sonothrombolysis in our previous MVO animal model with no significant adverse effects such as microvessel damage and red blood cell extravasation [184]. We have also previously characterized the imaging US used to have no effects on the outcome measures of this study [190]. Although we have made some progress toward characterizing how this may be tuned according to various ultrasound settings of UTMC, further optimization may be performed to explore a wider range of US settings, modulating other components of the US pulse, and investigating longer observation intervals to determine whether changes in NO concentration may be further sustained similar to our previous work [190]. Although previous *in vitro* studies have demonstrated the presence of inertial cavitation for US peak negative pressures above 0.6 MPa, this study did not include *in vivo* passive cavitation detection and hence confirmation of inertial cavitation [187]. Additionally, *in vivo* absolute calibration of the NO measurement system, resulting in expression of NO concentration in relative terms only.

A wider range of MB dosages may be investigated for a potentially greater effect on outcomes of NO and MBV. This study was a preliminary exploration into lower MB concentrations used for this hindlimb model, with the range ceiling guided by previous successful

dosages and the floor being an order of magnitude lower [190]. Although the highest MB dosage exceeds clinically approved concentrations, our previous histological studies for the US acoustic pressure and MB dosage used indicate there were no overt adverse effects including vessel trauma or hemorrhage [184]. Given that even the lowest concentration used showed significant increases in both MBV and NO, even lower concentrations would be warranted to fully characterize the dose-effect relationship in future work.

Although we have characterized the combination therapy effects in a healthy hindlimb setting, further development and testing in an MVO model will be necessary to determine whether these synergistic benefits are translatable to improved therapeutic efficacy. Additionally, we have demonstrated the capacity of UTMC with nitrite to increase local NO concentration. The specific biological mechanisms for the increased NO production may also be further characterized, specifically the role of the eNOS-AMPK pathway and its interactions with nitrite. Additionally, our use of LNAME to inhibit activity of all NOS isoforms may be further refined by inhibition of specific isoforms to account for the contributions of iNOS and nNOS to the increased NO concentration observed.

While we used SNP as an alternative exogenous NO donor comparison against sodium nitrite, the respective dosages of each NO donor were taken from previous studies on their application to pathological states and are not chemically equivalent [221, 272, 273]. This is also made difficult by their differing mechanistic pathways and interconversion to other species in the bloodstream. Additionally, SNP efficacy is vulnerable to systemic NO scavenging, which we attempted to account for by direct intra-arterial injection into the treated hindlimb. Additional characterization of these dosages may further inform their combination effects on UTMC therapy.

In this study, we have demonstrated the synergistic interaction between nitrite and UTMC therapy in increasing MBV and NO bioavailability. We have shown that this interaction effect is partially dependent on eNOS activity, but the specific mechanisms are yet unclear. In addition, the combination of nitrite with UTMC appears to mitigate oxidative stress. These new insights may further inform the biomechanisms of UTMC and potential application of this combination therapy to reperfusion of MVO following AMI.

8.0 Nitro-fatty Acid Microbubble Characterization and Application

8.1 Introduction

Cardiovascular disease is a leading cause of death in the United States, with over 1 million Americans estimated to have a new or recurrent acute myocardial infarction (AMI) this year [160]. Contemporary treatment for AMI is percutaneous coronary intervention (PCI), which aims to restore perfusion to the myocardium through recanalization of the epicardial vessels to effect maximal myocardial salvage [250]. Although mortality from AMI has decreased in recent years, post-MI congestive heart failure is increasing due to microvascular obstruction (MVO) and inadequate restoration of microvascular perfusion, ultimately limiting myocardial salvage [180].

MVO is a phenomenon in which myocardial tissue remains hypo-perfused after PCI even with patent upstream epicardial vessels; it occurs due to a combination of distal micro-embolization, ischemia-reperfusion injury, and activation of inflammatory cascades. Other mechanisms of MVO include tissue edema causing vessel compression and local vasospasm [162, 165, 167, 169, 170, 179, 253]. MVO occurs in up to 60% of all STEMI patients receiving PCI, and results in decreased LV function, and is an independent predictor for major adverse cardiac events, which include cardiac death, stroke, myocardial infarction, and heart failure requiring hospitalization [166, 176, 251]. MVO is also associated with increased infarct size and LV remodeling, with persistence of MVO being a stronger predictor for functional recovery than transmural infarct extension [166, 171, 172, 174, 175].

Previous strategies at treating or preventing MVO included administration of vasodilators and antiplatelet therapy, thrombus aspiration and embolic protection devices, and even use of

hyperoxemic intracoronary reperfusion therapy [178]. However, even with these various strategies, no definitive therapeutic consensus for MVO has arisen, and a number of clinical trials have yielded conflicting results [167, 176, 179]. Therefore, there is a need for an acute therapy capable of resolving MVO and its sequelae due to the unpredictable and rapidly catastrophic nature of acute cardiac events.

Use of therapeutic ultrasound for thrombolysis has become a rising subject of investigation. Our lab has previously demonstrated the efficacy of ultrasound-targeted microbubble cavitation (UTMC) in treatment of MVO and improvement of tissue perfusion [184, 190]. This technique involves image-guided ultrasound sonication of intravenously injected lipid microbubble (MB) contrast agents, resulting in microbubble oscillation (cavitation) which generates intravascular shear forces. UTMC produces both mechanical and biological effects in disrupting microthrombi to restore perfusion and activating endothelial NO pathways for local vasodilation [187, 190, 252]. In addition to thrombolysis, UTMC may also be used as a means for targeted delivery of therapeutics through use of loaded MBs, resulting in site-specific concentration of the therapeutic at higher efficiency than through systemic administration, while also reducing off-target effects [274-278]. UTMC is an ideal solution for MVO because it is a minimally invasive, theranostic technique that may visualize regions of MVO using MB contrast agents while simultaneously delivering image-guided ultrasound pulses. However, while UTMC has shown great promise in disrupting microthrombi and increasing myocardial perfusion, the numerous inflammatory mechanisms associated with MVO remain unaddressed.

To this end, nitro-fatty acids (NFAs) are endogenous signaling molecules formed from oxidative reactions between NO and nitrite-derived species and unsaturated fatty acids [232]. These molecules have been previously investigated in a wide range of inflammatory conditions

due to their role in post-translational modification of various anti-inflammatory signaling pathways [230, 233, 235-237, 245, 279, 280], resulting in decreased production of reactive oxide species, inhibition of pathogenic macrophage conversion and activation, inhibition of fibrotic and hyperplastic processes, and prevention of endothelial dysfunction [249, 281-283]. All of these effects are clinically relevant to the prevention and treatment of MVO, especially as NFAs have been demonstrated to be cardioprotective in the setting of focal cardiac ischemia [235, 284]. NFAs also present potential therapeutic interactions with UTMC from their capacity to increase nitric oxide bioavailability through multiple mechanisms. These include direct dissociation of NO molecules from the parent NFA molecule through the Nef chemical reaction, which then mediate cGMP-dependent signaling pathways [285]. In addition, NFAs have been shown to increase eNOS mRNA and protein expression as well as serine-1177 phosphorylation, resulting in increased cellular distribution and activity of eNOS [243].

Although NFAs have demonstrated their therapeutic value through previous trials featuring both longitudinal and acute systemic administration, targeted local delivery of NFAs for immediate concentration at tissue specific sites has not been explored [239]. Given their relatively rapid onset of effectiveness and lack of adverse effects from overdosing, NFAs are a strong candidate for targeted therapy in the context of MVO. The molecular structure of NFAs is also highly similar to the phospholipid species found in the lipid shell of the therapeutic MBs used in UTMC.

Another advantage of delivering NFA through loaded MBs in UTMC is the ability to concentrate payloads of NFA at the specific site of MVO. Previous literature has shown that the inhibition of various inflammatory signaling reactions by NFAs are both time-dependent and dosage-dependent in inflammatory and endothelial cells [233]. This coupled with previous successes of reducing inflammation and preserving myocardium in a myocardial ischemia model

with systemically administered NFA suggests the strong potential of further improving the efficacy of this therapy through rapidly concentrating NFAs at the site of the myocardial insult [235]. This further complements the rapid-onset and localized nature of MVO.

Therefore, the combination of NFA with therapeutic MBs used in UTMC may allow for the anti-inflammatory and cardioprotective effects of NFA to be focused at the specific location of MVO while supplementing the mechanical effects of UTMC on thrombolysis and perfusion. Site specific oscillation of NFA-loaded MBs and release of NFA within the microcirculation at the target site will create a region of concentrated NFA. Moreover, in conjunction with the increased vascular permeability and "leaky" endothelium associated with MVO, local delivery of NFA to the surrounding interstitium would be expected, although this is not necessary for effectiveness of the NFA.

We hypothesize that a novel therapeutic MB with a shell composition containing NFAs may further augment the therapeutic efficacy of UTMC for MVO. In this study we synthesized a novel NFAB agent and characterized it for successful and stable incorporation of NFAs as well as other MB contrast agent parameters including MB stability, physical characteristics, and acoustic behavior. We then applied the NFABs to our previously characterized rat hindlimb model, which mimics the microvascular structure of the heart and allows for adequate US contrast-enhanced microvascular perfusion imaging, in both a healthy state and a model of ischemia-reperfusion injury. We hypothesized that our novel NFAB agent would result not only in the significant improvements in hemodynamic parameters as previously characterized, but also improvements in outcome measures of inflammation and oxidative stress in an ischemia-reperfusion injury model.

8.2 Methods

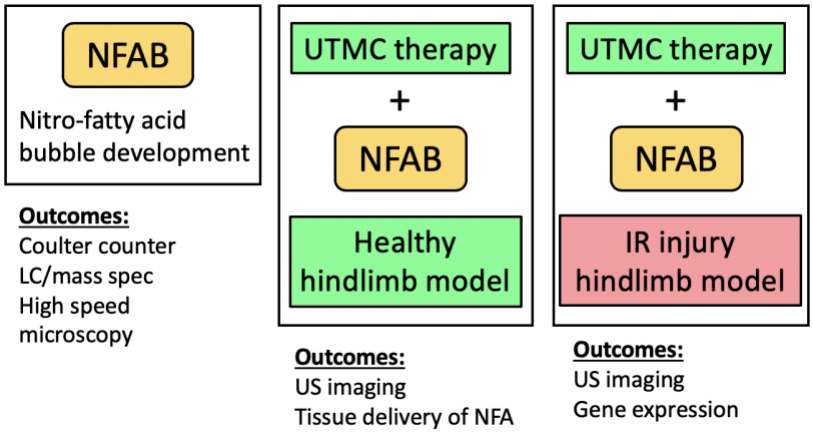

Figure 12: Simplified schematic of experimental procedures

8.2.1 Nitro-fatty Acid Microbubble Synthesis and Characterization

Nitro-fatty acid microbubbles (NFABs) were synthesized with a combination of 1,2-distearoyl-sn-glycero-3-phosphocholine (Avanti Polar Lipids Inc., Alabaster, AL), 1,2-Distearoyl-sn-Glycero-3-Phosphoethanolamine-N-(Methoxy(Polyethylene glycol)-2000) (Avanti Polar Lipids), polyoxyethylene-40 stearate (Sigma Aldrich, St. Louis, MO), and 9-nitro-oleic acid, the nitro-fatty acid. All components were combined in a glass vial with chloroform in a 29.1:5.2:43.8:21.9 molar ratio before the resulting solution was vaporized under an argon gas stream before vacuum storage. The dehydrated lipids were then rehydrated in acidic saline with a head of perfluorobutane gas prior to sonication (XL2020, Qsonica LCC, Neton, CT). The resulting NFABs were then washed 3 times in acidic saline to remove unsonicated lipids from solution before being aliquoted into sealed glass vials containing perfluorobutane.

The NFABs were characterized for concentration, size distribution, and loaded NFA content. All measurements were taken serially over up to 6 days post-synthesis to allow for tracking of stability in storage and loss of NFA content over time. Concentration and size distribution were measured using a Coulter Counter (Multisizer 3 Beckman Coulter). NFA content was measured using liquid chromatography and mass spectrometry of the final NFAB solution as well as the solution subnatant for quantification of free NFA. Free NFA was subtracted from the overall solution NFA measurement resulting in a concentration of only NFA loaded onto NFABs.

8.2.2 Other Microbubbles Used

As a comparison to the NFABs, in-house lipid MBs were synthesized using the same lipid components in absence of NFA using the same procedure and quantification for size and concentration. For contrast-enhanced US imaging, DEFINITY® MBs (Lantheus Medical Imaging, North Billerica, MA) were used without dilution. These MBs have a mean diameter of 1.1-3.3 μm and approximate concentration of 1.2×10^{10} microbubbles/mL in solution.

8.2.3 Animal Preparation

The animal studies performed in this investigation all received prior approval by the Institutional Animal Care and Use Committee at the University of Pittsburgh. The rat hindlimb model previously developed in our laboratory was used for modeling of both healthy microvasculature and microvasculature experiencing ischemia-reperfusion injury [191].

Briefly, anesthesia was induced using 2.5% inhaled isoflurane in Sprague-Dawley rats weighing 275±20 g. The right femoral artery and right internal jugular vein were then cannulated for intravascular access. The distal right femoral artery was ligated, and the infusion line was advanced to the level of the iliac bifurcation for direct access to the left femoral artery. The jugular access was used to delivery DEFINITY® MBs for contrast-enhanced US imaging undiluted at a rate of 2 mL per hr. The left femoral access was used to deliver treatment MBs and therapeutic agents. Treatment groups for the experiments included free NFA alone (with a vehicle of 85:15 polyethylene glycol to ethanol), free NFA with unmodified treatment MBs co-infusion, and NFAB infusion only.

8.2.4 Ultrasound Therapy and Perfusion Imaging

For the UTMC treatment, therapeutic US was administered using a single-element transducer operating at 1 MHz frequency (A303S, 0.5 inch, Olympus NDT, Waltham, MA). Along with the transducer, an arbitrary function generator (AFG3252, Tektronix, Beaverton, OR) and radio frequency power amplifier (800A3B, Amplifier Research, Souderton, PA) were used. This treatment transducer was fixed vertically above the gastrocnemius region of the left rat hindlimb (with the rat placed in right lateral decubitus position) at a distance of approximately 2 cm from the hindlimb surface according to the focal length of the transducer and was coupled to the hindlimb using acoustic gel.

The therapeutic US pulse itself consisted of 5000 cycles of 1 MHz tone with a peak negative acoustic pressure of 1.5 MPa. There was a 3 second interval between each pulse of 5000 cycles. The pulse was administered for 2 treatments of 10 minutes during infusion of the appropriate MB and therapeutic agent combination for each treatment group. Each individual

treatment was followed by contrast-enhanced US imaging using a clinical imaging probe (Siemens, Sequoia, 15L8 probe) and infusion of DEFINITY® MBs. It is noted that all MBs were infused using automated syringe pumps and all MB syringes were constantly rotated during administration to maintain MBs in suspension and avoid excess flotation.

Contrast-enhanced US imaging was performed using the burst-replenishment technique in contrast pulse sequence mode at 7 MHz frequency with a mechanical index of 0.2 and framerate of 5 frames per second. For the burst at the start of imaging, a 5-frame pulse with mechanical index of 1.9 was used to extinguish all contrast MBs from the field of view. After the burst, reperfusion of the hindlimb view with contrast MBs was recorded for further processing and analysis of hemodynamic parameters in cine-loops. All other US parameters including dynamic range (60 dB), gain (0 dB), and linear compression curve were kept constant throughout the studies for all treatment groups.

8.2.5 Image Acquisition and Processing

The imaging US transducer was positioned perpendicular to the longitudinal axis of the rat tibia and parallel to the working surface (also perpendicular to the treatment transducer axis). The transducer was manipulated such that the junction of the saphenous and popliteal arteries was visible in the field of view and the skin thickness was minimized. Occasional artifacts potentially representing bone reflections were permitted but ultimately excluded from any regions of analysis.

Processing of all recorded cine-loops from burst-replenishment imaging was performed using in-house code in MATLAB as described previously. Briefly, microvasculature regions of interest were selected for the gastrocnemius microvasculature such that skin, bone, and major vessels (saphenous and popliteal) were excluded. Image brightness (converted from a 16-bit scale

to 60 dB range) of the region of interest was analyzed over the appx 30 second duration of each cine-loop and fit to an exponential regression. The coefficient of the exponential regression was taken to be the plateau value for the image brightness (due to saturation of the field of view with contrast MBs after allowing adequate reperfusion) while the coefficient in front of the exponent of the regression equation was taken to be an inverse time constant (accounting for the steepness of the increase of the brightness to the plateau value over time). Hemodynamically, the plateau value was taken to be the microvascular blood volume (representing the saturated reperfusion of contrast MBs in the hindlimb view) while the inverse time constant multiplied by the plateau value resulted in the microvascular blood flow rate (units of brightness per second later converted to dB per second).

8.2.6 Healthy Hindlimb Model Experimental Protocol

Treatment groups for the healthy hindlimb model were centered around analysis of tissue delivery of the loaded NFA and included free NFA alone, NFA with co-infusion of unmodified MB UTMC, and UTMC with NFABs. Dosage of NFA in all treatment groups was equalized based on the measured amount of NFA quantified in 1E9 NFABs, which was taken to be the treatment dosage. Similarly, all treatment MBs (regardless of NFA loading) were equalized in dosage to 1E9 MBs per overall treatment (2 times 10-minute treatments). All treatment infusions (NFA or MB infusions) were administered via the femoral cannulation at 3 mL per hr. All imaging MB infusions were administered via the internal jugular cannulation at 2 mL per hr.

Placement of the therapeutic transducer over the gastrocnemius muscle was confirmed by visual inspection and one pulse of MB destruction in the field of view prior to treatment. After each 10-minute treatment, infusion of imaging MBs was performed during burst-replenishment

imaging and cine-loop recording. Rat physiologic parameters including heart rate, respiratory rate, and oxygen saturation were continuously monitored. After the second 10-minute treatment, the rat was euthanized by isoflurane overdose followed by heart excision. Following euthanasia, tissue samples were obtained from the UTMC-treated gastrocnemius muscle tissue as guided by US imaging markers. Tissue samples were also collected from the ipsilateral quadriceps femoris muscle as a control for the UTMC treatment receiving the same systemic perfusion of infused agents without targeted US stimulation. All tissue samples were then immediately frozen in liquid nitrogen and stored at minus 80 degrees Celsius.

8.2.7 Ischemia-Reperfusion Injury Model Experimental Protocol

The general protocol for the ischemia-reperfusion injury model remains the same as the healthy hindlimb model with a few exceptions. Prior to treatment, the left femoral artery was ligated using a suture, resulting in isolated hindlimb ischemia. This is distinct from the right femoral artery which was the site for cannulation into the aorta iliac bifurcation. After an hour of hindlimb ischemia, the suture was removed, allowing for reperfusion of the hindlimb for half an hour. After this half hour, treatment proceeded as with the healthy hindlimb model. After the second 10-minute treatment and perfusion imaging, a 2-hour wait was instated to allow for development of pathophysiologic changes in gene expression before the animal was sacrificed and tissue samples were collected.

8.2.8 Measurement of NFA in NFABs and Tissue Samples

For samples of NFABs, both the MBs in saline solution and samples of the saline subnatant alone were measured for NFA content. Subnatant NFA concentration was subtracted from overall MB solution NFA concentration to give concentration of incorporated NFA only. For tissue samples, skeletal muscle tissue was taken from the treatment site (gastrocnemius muscle) and a control site (quadriceps femoris muscle) on the ipsilateral hindlimb. Differential of NFA between the two sites was obtained by subtraction of their respective NFA concentrations. The protocol for NFA concentration quantification using liquid chromatography/mass spectrometry is documented in previous literature [235].

8.2.9 Measurement of Gene Expression

Skeletal muscle tissue samples from the same treatment and control locations previously described were also obtained and frozen in liquid nitrogen prior to mRNA isolation and assessment for expression using real-time PCR. Target genes included intercellular adhesion molecule 1 (ICAM-1), vascular cell adhesion molecule 1 (VCAM-1), and monocyte chemotactic protein 1 (MCP-1). These target genes have been previously validated as markers upregulated in the ischemia-reperfusion injury pathologic response and regulated by successful NFA treatment [235].

8.2.10 Statistical Analyses

All statistical analyses were performed in Prism (GraphPad Prism version 8.00, GraphPad Software, La Jolla, California, USA). Analyses were performed as either one-way ANOVAs or

two-way repeated measures ANOVAs when appropriate. Post-hoc analyses for two-way repeated measures ANOVAs were performed using Tukey's HSD while *t*-tests were used for one-way ANOVAs. For pairwise analyses, *t*-tests of the pairwise differences were performed between groups.

8.3 Results

8.3.1 Nitro-fatty Acid Microbubble Characterization

8.3.1.1 Size, Concentration, Distribution

NFAB size and distribution measurements from Coulter counter analysis are shown in Figure 13 and include results from an example batch up to 4 days post-synthesis. Quantitatively there were no significant differences in mean and standard deviation of NFAB diameter (3.0 ± 1.5 micrometers) over the 4 days measured, with NFAB concentration dropping only to 85% of the original concentration from day 1 onward. The distribution curves depict a unimodal population roughly centered at the mean similar to that observed in previous lipid MB Coulter counter measurements.

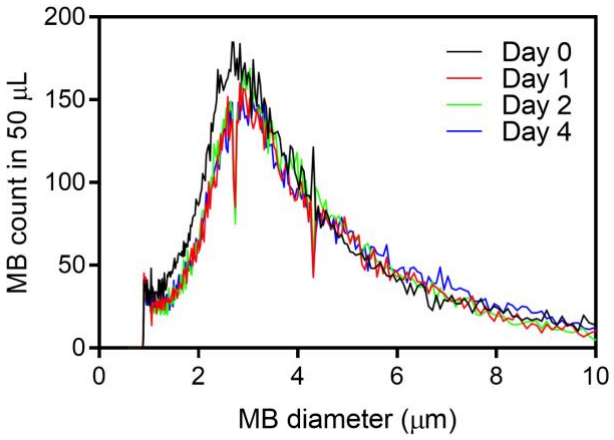

Figure 13: Coulter counter measurement of NFABs

Samples of NFABs from the same synthesis batch were serially sampled for measurement in a Coulter counter for distributions of MB counts over MB diameters, showing stability of the size and size distribution up to 4 days post-synthesis.

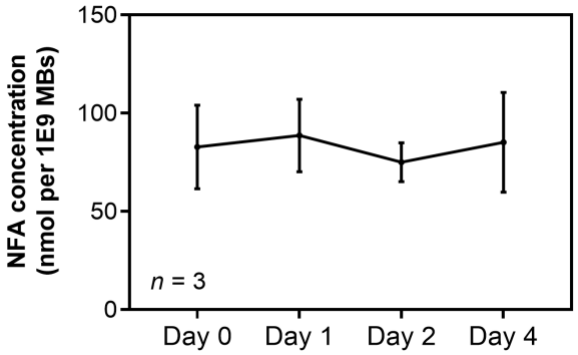

Figure 14: Quantification of loaded NFA for NFABs

Samples of NFABs in saline were quantified for NFA concentration using LC/MS methods. Subnatant samples with no NFABs were also quantified for concentration of free, unincorporated NFA which was then subtracted from total NFA concentration, resulting in the shown measurements.

8.3.1.2 Nitro-fatty Acid Content

Loaded NFA content for three batches of NFABs were serially measured up to 4 days post-synthesis in triplicate with results shown in Figure 14. The average concentration was

approximately 82.9 ± 5.8 nmol of NFA per 1E9 MBs after subtraction of the subnatant unloaded NFA content. Because the therapeutic dose for MBs previously established in the rat hindlimb model is 1E9 MBs delivered, the loaded NFA content of 1E9 MBs was taken as the equivalent dosage for free NFA infusion and free NFA with normal MB UTMC. Although statistics were not performed due to the low sample size, future experiments include increasing the replicate number for a more representative sampling of loaded NFA concentration.

8.3.1.3 High-speed Microscopy Imaging

High-speed microscopy during US stimulation of NFABs is shown in Figure 15 in the form of a still-frame series at 1.5 MPa. Given that a negative peak acoustic pressure of 1.5 MPa is well within the regime for inertial cavitation, images of the oscillating NFABs reflect these differences. For the 1.5 MPa still-frame series, several morphological changes in the oscillating NFABs are present. Namely, destruction of the MB and loss of spherical structure are immediately noticeable in each rarefactive phase visualized. In addition, separation of the expanded mother MB into several daughter MBs is also visible and is one of the potential mechanisms of efficacy for UTMC. Behavior of NFABs at 1.5 MPa suggest that these novel MBs behave similarly to other unmodified lipid MBs under US stimulation and will function appropriately in UTMC and sonothrombolysis.

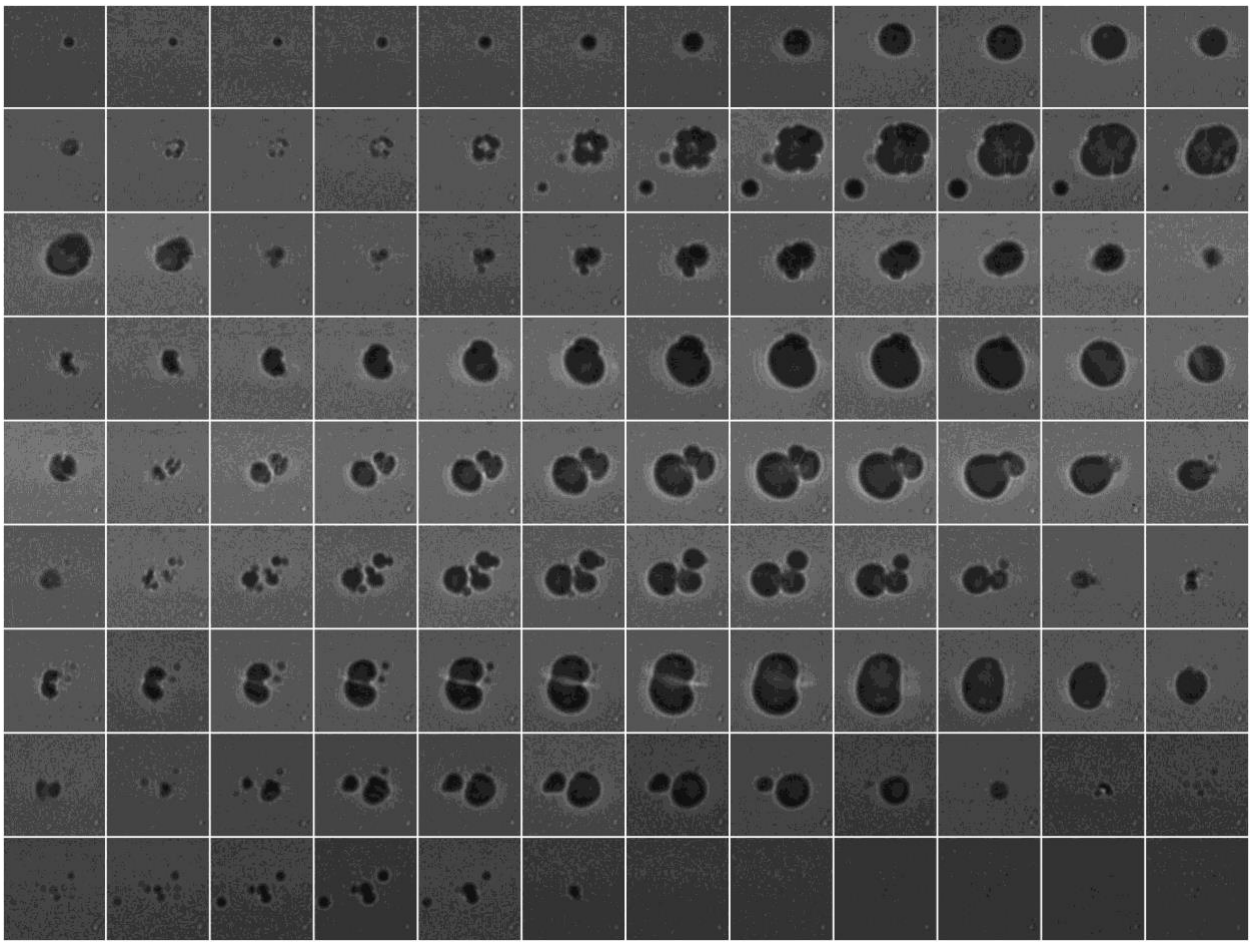

Figure 15: High speed imaging of NFABs stimulated by US at 1.5 MPa

Frame by frame analysis (10-25 million frames per second) of NFABs show typical lipid MB behaviors as expected in inertial cavitation, including collapse and formation of daughter MBs.

8.3.2 Healthy Hindlimb Model

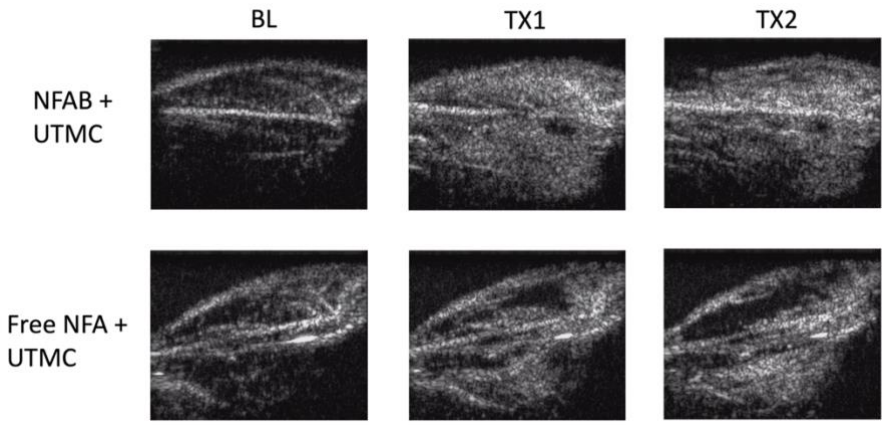

Figure 16: Burst-replenishment still-frame images from contrast-enhanced US imaging

Still-frame observational analysis at 5 seconds post-burst show drastic differences in replenishment between NFAB+UTMC and Free NFA+UTMC groups. Much of the microvascular bed is yet to be replenished in the latter, suggesting possible microvascular slowing or previously discussed microvascular spasm, while the former group shows full replenishment of the microvasculature exceeding baseline levels. TX1 for treatment 1, TX2 for treatment 2 imaging periods after a 10 minute treatment.

8.3.2.1 Perfusion Changes in Contrast-enhanced Ultrasound Imaging

Burst-replenishment imaging representative still-frames at 5 seconds post-burst for the two UTMC-treated healthy hindlimb groups are shown in Figure 16. As the main difference between these two groups is the compartment of incorporation of NFA into the MB structure versus co-infusion with unmodified MBs, differences between these groups was taken to represent the effect of incorporating NFA into the lipid MB shell.

The NFAB group showed not only a greater area coverage of contrast-visualized reperfusion as well as a greater image intensity compared to the baseline state. The free NFA co-infusion group with regular UTMC does not show greater intensity compared to baseline, as well

as incomplete reperfusion at 5 seconds post-burst. Although this is not representative of a persistent hypoperfused region given that at 30 seconds post-burst, the hypointense region was successfully reperfused, this abridged comparison further emphasizes the improved speed of microvascular reperfusion seen in the NFAB treatment group. Still-frame visualization demonstrated increased speed of microvascular perfusion of the NFAB group that was further reinforced by quantification of microvascular perfusion using region-of-interest selection.

Quantification of the hindlimb cine-loops using an exponential regression for region-of-interest image intensity is presented in Figures 17 and 18. Although both the NFAB and free NFA co-infusion with UTMC groups showed increases in microvascular blood volume, only the NFAB group demonstrated increased microvascular flow rate as well. As control, free NFA alone did not affect hindlimb microvascular perfusion. These results suggest that while UTMC itself had a significant effect on increasing blood volume, the incorporation of NFA into the MB shells offered additional hemodynamic benefits.

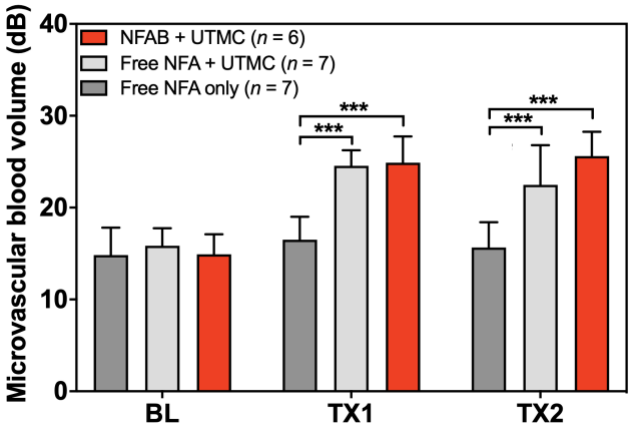

Figure 17: Changes in microvascular blood volume

Changes in microvascular blood volume show similar increases from baseline for both NFA+UTMC and free NFA + UTMC groups after treatments 1 and 2. Three asterisks indicates $p<0.001$ between the bracketed groups. TX1 for treatment 1, TX2 for treatment 2 imaging periods after a 10 minute treatment.

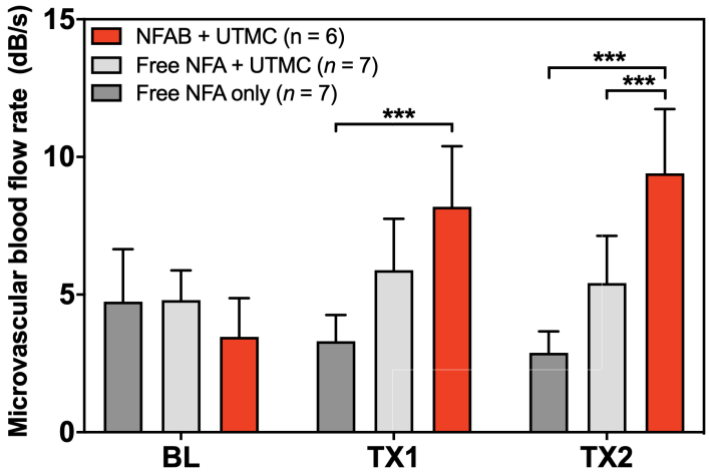

Figure 18: Change in microvascular flow rate

Only the NFAB+UTMC group demonstrated significantly increased microvascular blood flow rate compared to other treatment groups. Three asterisks indicate $p<0.001$. TX1 for treatment 1, TX2 for treatment 2 imaging periods after a 10 minute treatment.

8.3.2.2 Tissue Delivery of Nitro-fatty Acid

Tissue concentrations of NFA at both US treated and untreated sites for the three groups are shown in Figure 19 as differences in concentration between the two sites. Free NFA alone showed no difference in concentration (as no UTMC was applied to the hindlimb in this group), while NFA co-infusion with regular UTMC and NFAB UTMC showed sequentially increasing differences in concentration. Incorporation of NFA into the lipid MB resulted in approximately twice the increase in tissue delivery of NFA compared to NFA administration as a co-infusion with standard MBs.

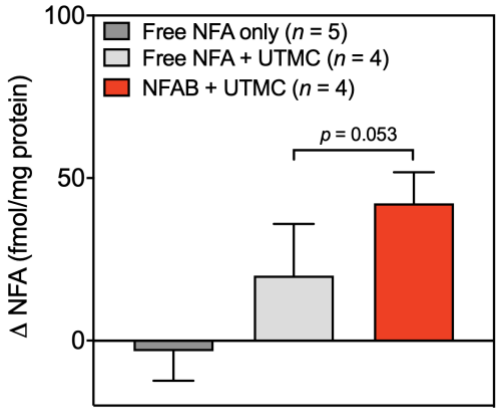

Figure 19: Change in tissue concentration of NFA

Change in NFA concentration was taken as a difference between US treated and untreated regions on the ipsilateral hindlimb on the same animal. All samples were analyzed as pairwise differences of treated minus untreated concentrations of NFA.

8.3.3 Ischemia-reperfusion Injury Model

8.3.3.1 Perfusion Changes in Contrast-enhanced Ultrasound Imaging

Still-frames from the burst-replenishment cine-loops are shown in Figure 20 for the NFAB and NFA co-infusion with standard UTMC groups. The NFAB group showed significant increases in perfusion compared to the post-IR state while the NFA co-infusion group showed no improvements with potentially even decreases in perfusion.

Quantitative analysis of hindlimb perfusion showed that only the NFAB group had significant increases in microvascular blood volume as well as microvascular blood flow after each treatment (Figures 21 and 22). In addition, the free NFA only group and the NFA co-infusion group showed decreased mean microvascular blood flow after each treatment below the flow rate immediately after ischemia-reperfusion injury.

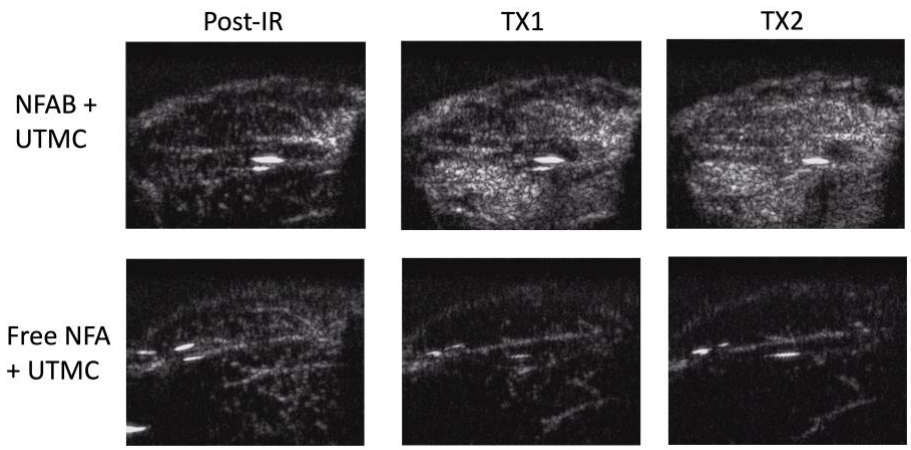

Figure 20: Contrast-enhanced US still-frame images

TX1 for treatment 1, TX2 for treatment 2 imaging periods after a 10 minute treatment. Still-frame images were taken from burst-replenishment contrast-enhanced cine-loops at 5 seconds post-burst. Note the complete replenishment of microvasculature in the NFAB+UTMC group while the free NFA+UTMC group shows a decrease in microvascular perfusion.

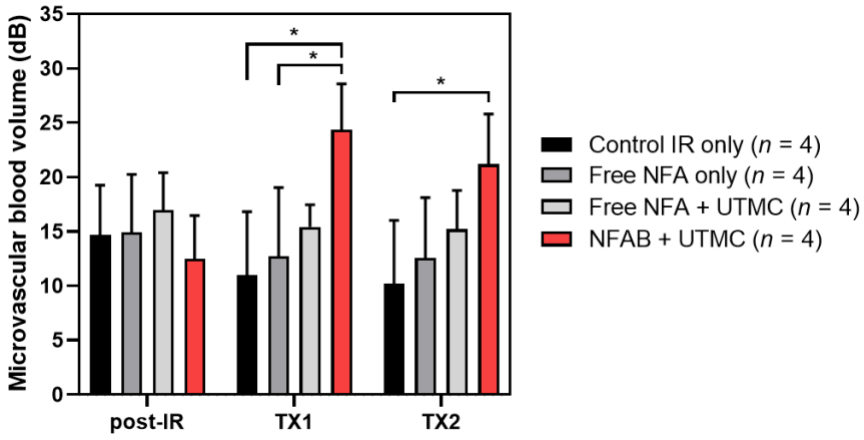

Figure 21: Changes in microvascular blood volume in the IR model

Significant increases in microvascular blood volume are only seen in the NFAB+UTMC group for the IR model after each treatment. Compared to the healthy hindlimb model, no significant increases in microvascular blood volume were seen in the free NFA+UTMC group after the post-IR imaging interval. Asterisk indicates $p<0.05$ for bracketed groups. TX1 for treatment 1, TX2 for treatment 2 imaging periods after a 10 minute treatment.

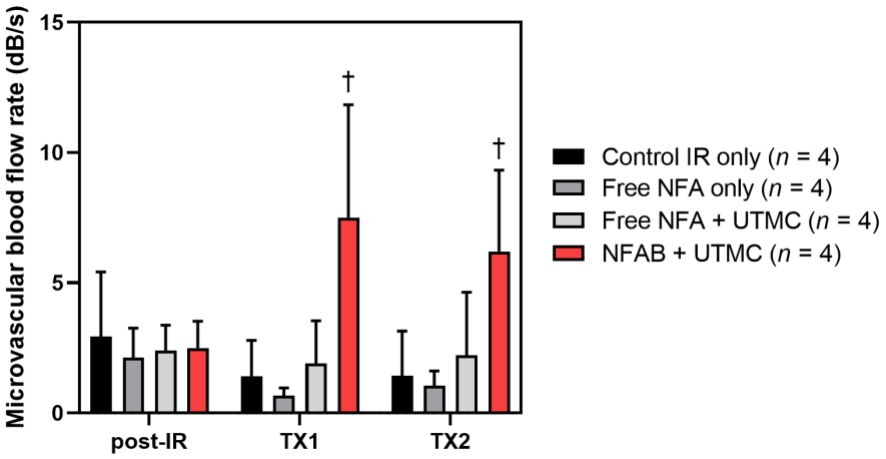

Figure 22: Changes in microvascular blood flow rate in the IR model

Similar to microvascular blood volume, only the NFAB+UTMC group showed significant increases in microvascular blood flow rate compared to all other groups. Dagger indicates $p<0.05$ against all other groups. TX1 for treatment 1, TX2 for treatment 2 imaging periods after a 10 minute treatment.

8.3.3.2 Gene Expression Changes

Results of gene expression analysis for all target genes are shown in Figure 23. For I-CAM1, V-CAM1, MCP, and TNF-α, only the NFAB group resulted in significantly lower gene expression in the treatment sample compared to the control sample. In addition, the treated NFAB sample showed a lower level of gene expression than treated samples from all other groups. Although the NFA only and NFA co-infusion groups showed lower mean relative treatment group I-CAM1 expression compared to their respective control groups, these differences were not statistically significant.

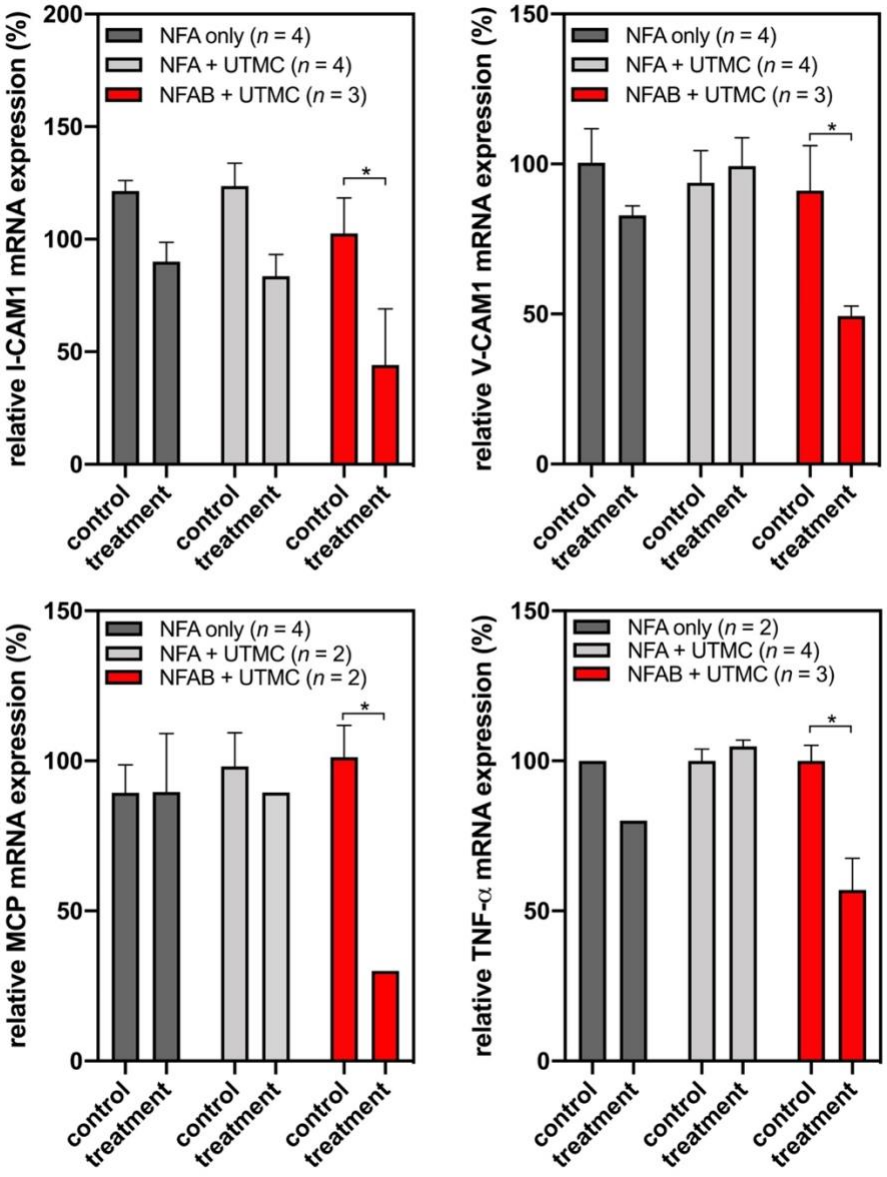

Figure 23: Gene expression changes with NFAB UTMC treatment

Changes in gene expression for key genes in inflammation and recruitment of leukocytes are shown for skeletal muscle tissue samples taken from control (no US treatment) and US treated sites on the ipsilateral hindlimb from the same animal. Only the NFAB+UTMC group showed significant reductions in mRNA expression for the target genes in the treatment site compared to the other groups. Both control and treatment sites were subjected to the same IR injury. Asterisk indicates $p<0.05$ between bracketed groups.

8.4 Discussion and Conclusions

In this study a newly developed NFA microbubble agent was characterized and applied in UTMC therapy in both healthy and disease hindlimb models. To our knowledge this is the first MB functionalization of NFAs as well as the first application of NFAs in UTMC therapy. Not only was the novel NFAB agent shown to be stable in terms of MB properties and loading of the NFA, ultra-high-speed microscopy analysis of the NFABs showed similar acoustic responses under US stimulation as previous lipid MB agents. Results from the healthy hindlimb model showed that not only did NFAB UTMC result in increased microvascular flow rate compared to a co-infusion of free NFA with standard MB UTMC, it also resulted in increased skeletal muscle tissue concentration of NFA in the treatment site. For the ischemia-reperfusion injury hindlimb model, NFAB UTMC again resulted in significantly improved hemodynamic parameters compared to all other treatment groups, as well as reduced levels of gene expression for signaling mediators of inflammation and oxidative stress, demonstrating the improved efficacy of NFAB UTMC in delivering targeted benefits of NFAs over NFA co-infusion with standard lipid MBs.

In comparing the contrast-enhanced perfusion US imaging results of this study with previous investigations of UTMC, similarities were noted with our previous study using nitrite in adjunctive administration with UTMC [191]. However, while nitrite is a known reservoir of nitric oxide bioavailability and has several identified mechanisms of chemical conversion to nitric oxide especially in environments of hypoxia and acidosis, NFAs have been noted to only directly serve as a nitric oxide donor in strongly aqueous environments that are not similar to the biological vascular environment [217, 226]. Therefore, the mechanism of enhanced perfusion by NFAs is unlikely to result from direct donation of nitric oxide.

This is also supported by our results showing that infusion of free NFA alone had no significant effects on hindlimb perfusion. However, previous investigations have shown that NFAs may have other mechanisms of enhancing nitric oxide bioavailability. These include upregulation of heme oxygenase-1 (HO-1) and endothelial nitric oxide synthase (eNOS) gene expression and increased phosphorylation of eNOS at several sites including the Ser1177 site, which is known to regulate enzymatic activity [243, 244]. HO-1 serves to metabolize hemoglobin, which scavenges free NO as well [241]. Given that previous studies on *in vitro* endothelial NO production after NFA administration already showed significant increases at 2 hours post-treatment, these mechanisms of gene expression upregulation and post-translational modification of eNOS are more likely feasible in the timescale of the treatments in this investigation.

In addition, our previous studies suggest that UTMC plays a role in increasing NO bioavailability through interactions with endogenous NO production given the blunting effect of eNOS inhibitors on UTMC-associated increases in perfusion [190]. In addition, nitrite was also shown to have positive interactions with eNOS NO production, which served as a mechanistic explanation for the synergy in both NO production and increased perfusion when administered with UTMC [191]. Similar to this precedent, both UTMC and NFAs may have positive interactions on eNOS activity for increased NO bioavailability. Future studies may investigate the specific mechanisms further including measurement of eNOS phosphorylation and various protein kinase phosphorylation as well as *in vivo* measurement of NO bioactivity.

Comparison of the NFAB UTMC results against the free NFA co-infusion with standard MB UTMC showed significant increases in perfusion with NFABs. Because the total dosage of NFA between these two groups was equalized against the quantified amount of NFA loaded onto the NFABs, the differences between these two groups is most likely attributed to the mechanistic

advantages of NFA incorporation into the lipid shell itself. Previous studies on MB-based therapeutic delivery have shown that attachment of the therapeutic agent on MBs themselves does result in improved localization in the UTMC target site [275, 276, 286]. However, because this study is the first to our knowledge utilizing bioactive therapeutic lipids, we can only assume from previous MB delivery treatments that similar principles would apply in this context. Therefore, mechanisms including sonoporation and sono-printing may apply with this application. Given that NFAs have known mechanisms of incorporation into biological membranes leading to nuclear translocation and alteration of gene expression, said mechanisms of UTMC may suffice for successful delivery and signal transduction of the NFAs. However, to fully analyze the effects of UTMC on facilitating effects of NFA co-infusion as well as to isolate the effects of UTMC alone, further experimental groups of normal UTMC alone, NFA vehicle alone, and a non-nitrated fatty acid such as oleic acid alone are needed and planned for future study.

With regards to alterations in gene expression, we have demonstrated that NFAB UTMC resulted in significantly decreased expression of several gene targets relevant to inflammation and ischemia-reperfusion injury, especially compared against the NFA co-infusion with standard UTMC, which did not show significant changes in levels of gene expression between treatment and control sites within the same animal. Although this is further evidence for the improved efficacy of NFAs when incorporated into NFABs, our results for NFA alone and NFA co-infusion show significantly reduced therapeutic efficacy that is likely due to our experimental design when compared against previous studies evaluating the effects of NFAs on gene expression.

Specifically, a previous study on focal cardiac ischemia analyzing effects of nitro-oleic acid on several similar target genes as in the present investigation implemented a period of 24 hours between treatment and tissue sample collection [235]. Given that our protocol only waited

2 hours between conclusion of treatments and tissue collection, the increased time in the previous study may have allowed for significantly more therapeutic activity of the NFAs as well as incubation of further pathologic gene expression changes in the untreated tissue samples.

However, because our treatment groups included several groups which all involved administration of the same cumulative NFA dose, a shorter incubation time in this investigation was used to improve sensitivity between these groups in detecting significant group effects. In addition, given the ease with which nitro-fatty acids may traverse between multiple biological compartments, reducing the incubation time further reduces the equilibration effect of NFA diffusion, which was also potentially significant in detecting changes in NFA tissue concentration between groups with the same NFA dosage.

Although this study has yielded results demonstrating the potential therapeutic value of NFABs in UTMC, there were several limitations. Regarding NFAB characterization, cavitation detection *in vivo* was not implemented, although cavitation was visually confirmed with ultra-high-speed microscopy and frequency decomposition analysis. Additional optimization of NFAB design and composition may be performed. For NFAB UTMC therapy, additional observation intervals may be implemented both to improve characterization of short and long-term tissue loading kinetics as well as extend characterization of gene expression and hemodynamic parameter changes. Stability of NFABs in the circulatory environment was not assessed, although satisfactory visualization of NFABs on contrast-enhanced US imaging was confirmed. Mechanistic analyses identifying the source of hemodynamic changes were also not performed and may include live *in vivo* detection of changes in NO concentration. Future work includes additional measures and genetic targets characterizing oxidative stress and inflammation and application of NFAB UTMC in animal models of cardiac pathology such as an MVO model with microthrombi injection.

In all, NFAB UTMC is a combination of two treatments leading to greatly expanded therapeutic potential. Although this study was limited to a hindlimb model of ischemia-reperfusion, previous mechanistic studies of NFAs have demonstrated its value in treatment of other types of cardiovascular pathology. Given that the strength of UTMC lies in not only in delivering and concentrating other therapeutic agents at a target site in a rapid manner but also eliciting mechanotransductive intravascular responses, other applications of NFAB UTMC specifically may include treatment of myocardial infarction, microvascular obstruction, and during post-infarct recovery. Localized inflammatory vascular pathologies such as peripheral vascular disease, atherosclerosis, and restenosis may also benefit from NFAB UTMC given the many anti-inflammatory and vasodilatory functions of this therapy.

Bibliography

1. Chan, V. and A. Perlas, *Basics of ultrasound imaging*, in *Atlas of ultrasound-guided procedures in interventional pain management*. 2011, Springer. p. 13-19.

2. Cootney, R.W., *Ultrasound Imaging: Principles and Applications in Rodent Research.* ILAR Journal, 2001. **42**(3): p. 233-247.

3. Aldrich, J.E., *Basic physics of ultrasound imaging.* Critical care medicine, 2007. **35**(5): p. S131-S137.

4. Kossoff, G., *Basic physics and imaging characteristics of ultrasound.* World J Surg, 2000. **24**(2): p. 134-42.

5. Wells, P.N., *Ultrasound imaging.* Physics in Medicine & Biology, 2006. **51**(13): p. R83.
6. Park, R., et al., *B-mode gray-scale ultrasound: imaging artifacts and interpretation principles.* Veterinary Radiology, 1981. **22**(5): p. 204-210.

7. Ortiz, S.H.C., T. Chiu, and M.D. Fox, *Ultrasound image enhancement: A review.* Biomedical Signal Processing and Control, 2012. **7**(5): p. 419-428.

8. Ng, A. and J. Swanevelder, *Resolution in ultrasound imaging.* Continuing Education in Anaesthesia Critical Care & Pain, 2011. **11**(5): p. 186-192.

9. Jensen, J.A., *Medical ultrasound imaging.* Progress in biophysics and molecular biology, 2007. **93**(1-3): p. 153-165.

10. Alvarez-Sánchez, M.-V. and B. Napoléon, *Contrast-enhanced harmonic endoscopic ultrasound imaging: Basic principles, present situation and future perspectives.* World J. Gastroenterol.: WJG, 2014. **20**(42): p. 15549.

11. Shapiro, R.S., et al., *Tissue harmonic imaging sonography: evaluation of image quality compared with conventional sonography.* AJR Am., 1998. **171**(5): p. 1203-1206.

12. Ziegler, L. and R.T. O'Brien, *Harmonic ultrasound: a review.* Veterinary Radiol Ultrasound, 2002. **43**(6): p. 501-509.

13. Ter Haar, G., *Therapeutic ultrasound.* Ultraschall Med., 1999. **9**(1): p. 3-9.

14. Robertson, V.J. and K.G. Baker, *A review of therapeutic ultrasound: effectiveness studies.* Physical therapy, 2001. **81**(7): p. 1339-1350.

15. van der Windt, D.A., et al., *Ultrasound therapy for musculoskeletal disorders: a systematic review.* Pain, 1999. **81**(3): p. 257-271.

16. Baker, K.G., V.J. Robertson, and F.A. Duck, *A review of therapeutic ultrasound: biophysical effects.* Physical therapy, 2001. **81**(7): p. 1351-1358.

17. Cullum, N., et al., *Systematic reviews of wound care management:(5) beds;(6) compression;(7) laser therapy, therapeutic ultrasound, electrotherapy and electromagnetic therapy.* 2001.

18. Speed, C., *Therapeutic ultrasound in soft tissue lesions.* Rheumatology, 2001. **40**(12): p. 1331-1336.

19. Bailey, M., et al., *Physical mechanisms of the therapeutic effect of ultrasound (a review).* Acoustical Physics, 2003. **49**(4): p. 369-388.

20. Yu, T., Z. Wang, and T.J. Mason, *A review of research into the uses of low level ultrasound in cancer therapy.* Ultrasonics sonochemistry, 2004. **11**(2): p. 95-103.

21. Lindner, J.R., *Microbubbles in medical imaging: current applications and future directions.* Nature Reviews Drug Discovery, 2004. **3**(6): p. 527.

22. Sites, B.D., et al., *Artifacts and pitfall errors associated with ultrasound-guided regional anesthesia: Part I: Understanding the basic principles of ultrasound physics and machine operations.* 2007.

23. Goldberg, B.B., J.-B. Liu, and F. Forsberg, *Ultrasound contrast agents: a review.* Ultrasound Med Biol, 1994. **20**(4): p. 319-333.

24. Cosgrove, D., *Ultrasound contrast agents: an overview.* Eur. J. Radiol., 2006. **60**(3): p. 324-330.

25. Calliada, F., et al., *Ultrasound contrast agents: basic principles.* Eur. J. Radiol., 1998. **27**: p. S157-S160.

26. Frinking, P.J., et al., *Ultrasound contrast imaging: current and new potential methods.* Ultrasound Med Biol, 2000. **26**(6): p. 965-975.

27. Correas, J.-M., et al., *Ultrasound contrast agents: properties, principles of action, tolerance, and artifacts.* Eur. Radiol., 2001. **11**(8): p. 1316-1328.

28. Deng, C.X. and F.L. Lizzi, *A review of physical phenomena associated with ultrasonic contrast agents and illustrative clinical applications.* Ultrasound Med Biol, 2002. **28**(3): p. 277-286.

29. Burns, P.N. and S.R. Wilson, *Microbubble contrast for radiological imaging: 1. Principles.* Ultrasound quarterly, 2006. **22**(1): p. 5-13.

30. Cosgrove, D. and R. Eckersley, *Contrast-Enhanced Ultrasound: Basic Physics and Technology Overview*, in *Enhancing the Role of Ultrasound with Contrast Agents*, R. Lencioni, Editor. 2006, Springer Milan: Milano. p. 3-14.

31. Stride, E., *Physical principles of microbubbles for ultrasound imaging and therapy.* Cerebrovasc Dis, 2009. **27**(Suppl. 2): p. 1-13.

32. Azmin, M., et al., *How do microbubbles and ultrasound interact? Basic physical, dynamic and engineering principles.* Current pharmaceutical design, 2012. **18**(15): p. 2118-2134.

33. Stride, E. and C. Coussios, *Cavitation and contrast: the use of bubbles in ultrasound imaging and therapy.* P I MECH ENG H, 2010. **224**(2): p. 171-191.

34. Liu, Y., H. Miyoshi, and M. Nakamura, *Encapsulated ultrasound microbubbles: therapeutic application in drug/gene delivery.* J CONTROL RELEASE, 2006. **114**(1): p. 89-99.

35. Klibanov, A.L., *Ultrasound molecular imaging with targeted microbubble contrast agents.* Journal of Nuclear Cardiology, 2007. **14**(6): p. 876.

36. Klibanov, A.L., *Ligand-carrying gas-filled microbubbles: ultrasound contrast agents for targeted molecular imaging.* Bioconjugate chemistry, 2005. **16**(1): p. 9-17.

37. Lee, M., et al., *Stabilization and fabrication of microbubbles: applications for medical purposes and functional materials.* Soft matter, 2015. **11**(11): p. 2067-2079.

38. Sirsi, S. and M. Borden, *Microbubble Compositions, Properties and Biomedical Applications.* Bubble Sci Eng Technol, 2009. **1**(1-2): p. 3-17.

39. Teraphongphom, N., et al., *Nanoparticle Loaded Polymeric Microbubbles as Contrast Agents for Multimodal Imaging.* Langmuir, 2015. **31**(43): p. 11858-67.

40. Christiansen, C., et al., *Physical and biochemical characterization of Albunex, a new ultrasound contrast agent consisting of air-filled albumin microspheres suspended in a solution of human albumin.* Biotechnology and applied biochemistry, 1994. **19**(3): p. 307-320.

41. AH, M., et al., *Structure and organization of albumin molecules forming the shell of air-filled microspheres: evidence for a monolayer of albumin molecules of multiple orientations stabilizing the enclosed air.* Biotechnology and applied biochemistry, 1996. **24**(2): p. 145-153.

42. Grinstaff, M.W. and K.S. Suslick, *Air-filled proteinaceous microbubbles: synthesis of an echo-contrast agent.* Proceedings of the National Academy of Sciences, 1991. **88**(17): p. 7708-7710.

43. Dayton, P.A., et al., *Optical and acoustical observations of the effects of ultrasound on contrast agents.* IEEE transactions on ultrasonics, ferroelectrics, and frequency control, 1999. **46**(1): p. 220-232.

44. Podell, S., et al., *Physical and biochemical stability of Optison®, an injectable ultrasound contrast agent.* Biotechnology and applied biochemistry, 1999. **30**(3): p. 213-223.

45. Cavalieri, F., et al., *Ultrasonic synthesis of stable, functional lysozyme microbubbles.* Langmuir, 2008. **24**(18): p. 10078-10083.

46. Korpanty, G., et al., *Targeting vascular endothelium with avidin microbubbles.* Ultrasound Med Biol, 2005. **31**(9): p. 1279-1283.

47. Wang, W., C.C. Moser, and M.A. Wheatley, *Langmuir trough study of surfactant mixtures used in the production of a new ultrasound contrast agent consisting of stabilized microbubbles.* J Phys Chem, 1996. **100**(32): p. 13815-13821.

48. Singhal, S., C. Moser, and M. Wheatley, *Surfactant-stabilized microbubbles as ultrasound contrast agents: stability study of Span 60 and Tween 80 mixtures using a Langmuir trough.* Langmuir, 1993. **9**(9): p. 2426-2429.

49. Dressaire, E., et al., *Interfacial polygonal nanopatterning of stable microbubbles.* Science, 2008. **320**(5880): p. 1198-1201.

50. D'Arrigo, J., *Stable gas-in-liquid emulsions: production in natural waters and artificial media*. 2011: Elsevier.

51. Notter, R.H. and Z. Wang, *Pulmonary surfactant: physical chemistry, physiology, and replacement.* Rev Chem Eng, 1997. **13**(4): p. 1-118.

52. Duncan, P.B. and D. Needham, *Test of the Epstein− Plesset Model for gas microparticle dissolution in aqueous media: effect of surface tension and gas undersaturation in solution.* Langmuir, 2004. **20**(7): p. 2567-2578.

53. Epstein, P.S. and M.S. Plesset, *On the stability of gas bubbles in liquid-gas solutions.* J Chem Phys, 1950. **18**(11): p. 1505-1509.

54. Kim, D.H., et al., *Mechanical properties and microstructure of polycrystalline phospholipid monolayer shells: Novel solid microparticles.* Langmuir, 2003. **19**(20): p. 8455-8466.

55. Stride, E. and M. Edirisinghe, *Novel microbubble preparation technologies.* Soft matter, 2008. **4**(12): p. 2350-2359.

56. Borden, M.A., et al., *Surface phase behavior and microstructure of lipid/PEG-emulsifier monolayer-coated microbubbles.* Colloids Surf B Biointerfaces, 2004. **35**(3-4): p. 209-23.

57. Borden, M.A., et al., *Lateral phase separation in lipid-coated microbubbles.* Langmuir, 2006. **22**(9): p. 4291-4297.

58. Wheatley, M.A., B. Schrope, and P. Shen, *Contrast agents for diagnostic ultrasound: development and evaluation of polymer-coated microbubbles.* Biomaterials, 1990. **11**(9): p. 713-717.

59. Bjerknes, K., et al., *Air-filled polymeric microcapsules from emulsions containing different organic phases.* J microencapsul, 2001. **18**(2): p. 159-171.

60. Cui, W., et al., *Preparation and evaluation of poly (L-lactide-co-glycolide)(PLGA) microbubbles as a contrast agent for myocardial contrast echocardiography.* J Biomed Mater Res, 2005. **73**(1): p. 171-178.

61. Cavalieri, F., et al., *Stable polymeric microballoons as multifunctional device for biomedical uses: synthesis and characterization.* Langmuir, 2005. **21**(19): p. 8758-8764.

62. Böhmer, M.R., et al., *Preparation of monodisperse polymer particles and capsules by ink-jet printing.* Colloids Surf, 2006. **289**(1-3): p. 96-104.

63. Borden, M.A., et al., *DNA and polylysine adsorption and multilayer construction onto cationic lipid-coated microbubbles.* Langmuir, 2007. **23**(18): p. 9401-9408.

64. Lentacker, I., et al., *Ultrasound-responsive polymer-coated microbubbles that bind and protect DNA.* Langmuir, 2006. **22**(17): p. 7273-7278.

65. Shchukin, D.G., et al., *Metallized polyelectrolyte microcapsules.* Adv Mater, 2005. **17**(4): p. 468-472.

66. Dayton, P.A. and K.W. Ferrara, *Targeted imaging using ultrasound.* J Magn, 2002. **16**(4): p. 362-377.

67. Ferrara, K., R. Pollard, and M. Borden, *Ultrasound microbubble contrast agents: fundamentals and application to gene and drug delivery.* Annu. Rev. Biomed. Eng., 2007. **9**: p. 415-447.

68. Klibanov, A.L., *Targeted delivery of gas-filled microspheres, contrast agents for ultrasound imaging.* Adv Drug Deliv Rev, 1999. **37**(1-3): p. 139-157.

69. Borden, M.A., et al., *A stimulus-responsive contrast agent for ultrasound molecular imaging.* Biomaterials, 2008. **29**(5): p. 597-606.

70. Zhao, S., et al., *Radiation-force assisted targeting facilitates ultrasonic molecular imaging.* Molecular imaging, 2004. **3**(3): p. 15353500200404115.

71. Sboros, V., *Response of contrast agents to ultrasound.* Adv Drug Deliv Rev, 2008. **60**(10): p. 1117-1136.

72. Nishikawa, M. and L. Huang, *Nonviral vectors in the new millennium: delivery barriers in gene transfer.* Human gene therapy, 2001. **12**(8): p. 861-870.

73. Shohet, R.V., et al., *Echocardiographic destruction of albumin microbubbles directs gene delivery to the myocardium.* Circulation, 2000. **101**(22): p. 2554-2556.

74. Kipshidze, N.N., et al., *Novel site-specific systemic delivery of Rapamycin with perfluorobutane gas microbubble carrier reduced neointimal formation in a porcine coronary restenosis model.* Catheterization and cardiovascular interventions, 2005. **64**(3): p. 389-394.

75. Teupe, C., et al., *Vascular gene transfer of phosphomimetic endothelial nitric oxide synthase (S1177D) using ultrasound-enhanced destruction of plasmid-loaded microbubbles improves vasoreactivity.* Circulation, 2002. **105**(9): p. 1104-1109.

76. Bielinska, A., *Kukowska) Latallo JF, Baker JR Jr. The interaction of plasmid DNA with polyamidoamine dendrimers: mechanism of complex formation and analysis of alterations induced in nuclease sensitivity and transcriptional activity of the complexed DNA.* Biochim Biophys Acta, 1997. **1353**(2): p. 180.

77. Boussif, O., *F. Lezoualc h, MA Zanta, MD Mergny, D. Scherman, B. Demeneix, JP Behr.* Proc. Natl. Acad. Sci. USA, 1995. **92**: p. 7297-7301.

78. Midoux, P., et al., *Polymer-based gene delivery: a current review on the uptake and intracellular trafficking of polyplexes.* Current gene therapy, 2008. **8**(5): p. 335-352.

79. Bekeredjian, R., P.A. Grayburn, and R.V. Shohet, *Use of ultrasound contrast agents for gene or drug delivery in cardiovascular medicine.* J Am Coll Cardiol, 2005. **45**(3): p. 329-335.

80. Unger, E.C., et al., *Therapeutic applications of microbubbles.* Eur. J. Radiol., 2002. **42**(2): p. 160-168.

81. Unger, E.C., et al., *Acoustically active lipospheres containing paclitaxel: a new therapeutic ultrasound contrast agent.* Invest Radiol, 1998. **33**(12): p. 886-892.

82. Tartis, M.S., et al., *Therapeutic effects of paclitaxel-containing ultrasound contrast agents.* Ultrasound Med Biol, 2006. **32**(11): p. 1771-1780.

83. Christiansen, J.P., et al., *Targeted tissue transfection with ultrasound destruction of plasmid-bearing cationic microbubbles.* Ultrasound Med Biol, 2003. **29**(12): p. 1759-1767.

84. Kheirolomoom, A., et al., *Acoustically-active microbubbles conjugated to liposomes: characterization of a proposed drug delivery vehicle.* J Control Release, 2007. **118**(3): p. 275-284.

85. Mehier-Humbert, S., et al., *Ultrasound-mediated gene delivery: influence of contrast agent on transfection.* Bioconj chem, 2007. **18**(3): p. 652-662.

86. Seemann, S., et al., *Pharmaceutical evaluation of gas-filled microparticles as gene delivery system.* Pharm res, 2002. **19**(3): p. 250-257.

87. Niu, C., et al., *Doxorubicin loaded superparamagnetic PLGA-iron oxide multifunctional microbubbles for dual-mode US/MR imaging and therapy of metastasis in lymph nodes.* Biomaterials, 2013. **34**(9): p. 2307-17.

88. Janib, S.M., A.S. Moses, and J.A. MacKay, *Imaging and drug delivery using theranostic nanoparticles.* Adv Drug Deliv Rev, 2010. **62**(11): p. 1052-1063.

89. Mahalingam, S., et al., *Formation of protein and protein–gold nanoparticle stabilized microbubbles by pressurized gyration.* Langmuir, 2015. **31**(2): p. 659-666.

90. Garg, S., A.A. Thomas, and M.A. Borden, *The effect of lipid monolayer in-plane rigidity on in vivo microbubble circulation persistence.* Biomaterials, 2013. **34**(28): p. 6862-70.

91. Kwan, J.J. and M.A. Borden, *Lipid monolayer collapse and microbubble stability.* Adv Colloid Interface Sci, 2012. **183-184**: p. 82-99.

92. Myrset, A.H., et al., *Design and characterization of targeted ultrasound microbubbles for diagnostic use.* Ultrasound Med Biol, 2011. **37**(1): p. 136-50.

93. Wrenn, S.P., M. Mleczko, and G. Schmitz, *Phospholipid-stabilized microbubbles: Influence of shell chemistry on cavitation threshold and binding to giant uni-lamellar vesicles.* Applied Acoustics, 2009. **70**(10): p. 1313-1322.

94. Shen, Y., R.L. Powell, and M.L. Longo, *Interfacial and stability study of microbubbles coated with a monostearin/monopalmitin-rich food emulsifier and PEG40 stearate.* J Colloid Interface Sci, 2008. **321**(1): p. 186-94.

95. Wu, S.Y., et al., *Effects of the microbubble shell physicochemical properties on ultrasound-mediated drug delivery to the brain.* J Control Release, 2015. **212**: p. 30-40.

96. Helfield, B., et al., *Biophysical insight into mechanisms of sonoporation.* Proc Natl Acad Sci U S A, 2016. **113**(36): p. 9983-8.

97. Helfield, B.L., et al., *Mechanistic Insight into Sonoporation with Ultrasound-Stimulated Polymer Microbubbles.* Ultrasound Med Biol, 2017. **43**(11): p. 2678-2689.

98. Chen, X., et al., *Ultra-fast bright field and fluorescence imaging of the dynamics of micrometer-sized objects.* Rev Sci, 2013. **84**(6): p. 063701.

99. Chen, X., et al., *Dynamic behavior of microbubbles during long ultrasound tone-burst excitation: Mechanistic insights into ultrasound-microbubble mediated therapeutics using high-speed imaging and cavitation detection.* Ultrasound Med Biol, 2016. **42**(2): p. 528-538.

100. Helfield, B., et al., *Individual lipid encapsulated microbubble radial oscillations: Effects of fluid viscosity.* J Acoust Soc Am, 2016. **139**(1): p. 204-14.

101. Helfield, B., et al., *Fluid Viscosity Affects the Fragmentation and Inertial Cavitation Threshold of Lipid-Encapsulated Microbubbles.* Ultrasound Med Biol, 2016. **42**(3): p. 782-94.

102. Lentacker, I., et al., *Understanding ultrasound induced sonoporation: definitions and underlying mechanisms.* Adv Drug Deliv Rev, 2014. **72**: p. 49-64.

103. De Cock, I., et al., *Sonoprinting and the importance of microbubble loading for the ultrasound mediated cellular delivery of nanoparticles.* Biomaterials, 2016. **83**: p. 294-307.

104. Van Wamel, A., et al., *Vibrating microbubbles poking individual cells: drug transfer into cells via sonoporation.* J Control Release, 2006. **112**(2): p. 149-155.

105. Burks, S.R., et al., *Investigation of cellular and molecular responses to pulsed focused ultrasound in a mouse model.* PLoS one, 2011. **6**(9): p. e24730.

106. Juffermans, L.J., et al., *Transient permeabilization of cell membranes by ultrasound-exposed microbubbles is related to formation of hydrogen peroxide.* Am J Physiol Heart Circ Physiol, 2006. **291**(4): p. H1595-601.

107. Begley, D.J., *Delivery of therapeutic agents to the central nervous system: the problems and the possibilities.* Pharmacol Ther, 2004. **104**(1): p. 29-45.

108. Hynynen, K., et al., *Local and reversible blood–brain barrier disruption by noninvasive focused ultrasound at frequencies suitable for trans-skull sonications.* Neuroimage, 2005. **24**(1): p. 12-20.

109. Hynynen, K., et al., *Focal disruption of the blood–brain barrier due to 260-kHz ultrasound bursts: a method for molecular imaging and targeted drug delivery.* J Neurosurg, 2006. **105**(3): p. 445-454.

110. Jordao, J.F., et al., *Antibodies targeted to the brain with image-guided focused ultrasound reduces amyloid-beta plaque load in the TgCRND8 mouse model of Alzheimer's disease.* PLoS one, 2010. **5**(5): p. e10549.

111. Burgess, A., et al., *Alzheimer disease in a mouse model: MR imaging–guided focused ultrasound targeted to the hippocampus opens the blood-brain barrier and improves pathologic abnormalities and behavior.* Radiology, 2014. **273**(3): p. 736-745.

112. Leinenga, G. and J.J.S.t.m. Götz, *Scanning ultrasound removes amyloid-β and restores memory in an Alzheimer's disease mouse model.* Sci Trans Med, 2015. **7**(278): p. 278ra33-278ra33.

113. Lin, W.T., et al., *Protective effects of low-intensity pulsed ultrasound on aluminum-induced cerebral damage in Alzheimer's disease rat model.* Sci Rep, 2015. **5**: p. 9671.

114. McMahon, D., R. Bendayan, and K. Hynynen, *Acute effects of focused ultrasound-induced increases in blood-brain barrier permeability on rat microvascular transcriptome.* Sci Rep, 2017. **7**: p. 45657.

115. Deng, J., et al., *The role of caveolin-1 in blood–brain barrier disruption induced by focused ultrasound combined with microbubbles.* J Mol Neurosci, 2012. **46**(3): p. 677-687.

116. O'Reilly, M.A., et al., *Investigation of the Safety of Focused Ultrasound-Induced Blood-Brain Barrier Opening in a Natural Canine Model of Aging.* Theranostics, 2017. **7**(14): p. 3573-3584.

117. Lipsman, N., et al., *Blood-brain barrier opening in Alzheimer's disease using MR-guided focused ultrasound.* Nat Commun, 2018. **9**(1): p. 2336.

118. Suzuki, J.-i., et al., *Ultrasound-microbubble–mediated intercellular adhesion molecule-1 small interfering ribonucleic acid transfection attenuates neointimal formation after arterial injury in mice.* J Am Coll Cardiol, 2010. **55**(9): p. 904-913.

119. Xu, Y.-L., et al., *Myocardium-targeted transplantation of mesenchymal stem cells by diagnostic ultrasound-mediated microbubble destruction improves cardiac function in myocardial infarction of New Zealand rabbits.* Int J Cardiol, 2010. **138**(2): p. 182-195.

120. Unger, E., et al., *Cardiovascular drug delivery with ultrasound and microbubbles.* Adv Drug Deliv Rev, 2014. **72**: p. 110-26.

121. Sutton, J.T., et al., *Ultrasound-mediated drug delivery for cardiovascular disease.* Expert Opin Drug Deliv, 2013. **10**(5): p. 573-92.

122. Raake, P., et al., *Cardio-specific long-term gene expression in a porcine model after selective pressure-regulated retroinfusion of adeno-associated viral (AAV) vectors.* Gene Therapy, 2008. **15**(1): p. 12-17.

123. Peng, C.A., *Analysis of gene transfer rate with immobilized retroviral vectors.* Ann NY Acad Sci, 2009. **1161**(1): p. 26-33.

124. Beronja, S., et al., *Rapid functional dissection of genetic networks via tissue-specific transduction and RNAi in mouse embryos.* Nat Med, 2010. **16**(7): p. 821.

125. Yao, X.-L., et al., *Optimization and internalization mechanisms of PEGylated adenovirus vector with targeting peptide for cancer gene therapy.* Biomacromolecules, 2012. **13**(8): p. 2402-2409.

126. Fabrice Prunier, M., M. Yoshiaki Kawase, and B. Davide Gianni, *Prevention of ventrieular arrhythmias with sarcoplasmie reticulum Ca^ 2+ ATPase pump over expression in a porcine model of ischemia rcpefusion.* Circulation, 2008. **118**: p. 614-624.

127. Cavazzana-Calvo, M. and A. Fischer, *Gene therapy for severe combined immunodeficiency: are we there yet?* J Clin Invest, 2007. **117**(6): p. 1456-1465.

128. Nayerossadat, N., T. Maedeh, and P.A. Ali, *Viral and nonviral delivery systems for gene delivery.* Adv biomed res, 2012. **1**.

129. Park, H.-J., F. Yang, and S.-W. Cho, *Nonviral delivery of genetic medicine for therapeutic angiogenesis.* Adv Drug Deliv Rev, 2012. **64**(1): p. 40-52.

130. Ko, Y., et al., *Gene delivery into ischemic myocardium by double-targeted lipoplexes with anti-myosin antibody and TAT peptide.* Gene therapy, 2009. **16**(1): p. 52-59.

131. Charoensit, P., et al., *Enhanced growth inhibition of metastatic lung tumors by intravenous injection of ATRA-cationic liposome/IL-12 pDNA complexes in mice.* Cancer gene therapy, 2010. **17**(7): p. 512-522.

132. Ye, J., et al., *Ultrasound-mediated targeted microbubbles: a new vehicle for cancer therapy.* Front Chem Sci Eng, 2013. **7**(1): p. 20-28.

133. Arvanitis, C.D., et al., *Cavitation-enhanced extravasation for drug delivery.* Ultrasound Med Biol, 2011. **37**(11): p. 1838-1852.

134. Chen, Z., et al., *Enhancement of survivin gene downregulation and cell apoptosis by a novel combination: liposome microbubbles and ultrasound exposure.* Med Onc, 2009. **26**(4): p. 491-500.

135. Wang, Y., et al., *Delivery of TFPI-2 using SonoVue and adenovirus results in the suppression of thrombosis and arterial re-stenosis.* Exp Biol Med, 2010. **235**(9): p. 1072-1081.

136. Chen, S., et al., *Stimulation of adult resident cardiac progenitor cells by durable myocardial expression of thymosin beta 4 with ultrasound-targeted microbubble delivery.* Gene therapy, 2013. **20**(2): p. 225-233.

137. Müller, O., et al., *Augmentation of AAV-mediated cardiac gene transfer after systemic administration in adult rats.* Gene therapy, 2008. **15**(23): p. 1558-1565.

138. Beeri, R., et al., *New efficient catheter-based system for myocardial gene delivery.* Circulation, 2002. **106**(14): p. 1756-1759.

139. Naka, T., et al., *Ultrasound enhances retrovirus-mediated gene transfer.* Prep biochem biotech, 2007. **37**(2): p. 87-99.

140. Chen, S., et al., *Optimization of ultrasound parameters for cardiac gene delivery of adenoviral or plasmid deoxyribonucleic acid by ultrasound-targeted microbubble destruction.* J Am Coll Cardiol, 2003. **42**(2): p. 301-308.

141. Howard, C.M., et al., *Ultrasound guided site specific gene delivery system using adenoviral vectors and commercial ultrasound contrast agents.* J Cell Phys, 2006. **209**(2): p. 413-421.

142. Taylor, S.L., et al., *Targeted retroviral gene delivery using ultrasound.* J Gene Med, 2007. **9**(2): p. 77-87.

143. Geers, B., et al., *Elucidating the mechanisms behind sonoporation with adeno-associated virus-loaded microbubbles.* Mol Pharm, 2011. **8**(6): p. 2244-2251.

144. Culp, W.C. and T.C. McCowan, *Ultrasound augmented thrombolysis.* Curr Med Imaging Rev, 2005. **1**(1): p. 5-12.

145. Cintas, P., et al., *Enhancement of enzymatic fibrinolysis with 2-MHz ultrasound and microbubbles.* J Thromb Haemost, 2004. **2**(7): p. 1163-6.

146. Porter, T.R. and F. Xie, *Ultrasound, microbubbles, and thrombolysis.* Prog Cardiovasc Dis, 2001. **44**(2): p. 101-10.

147. Luo, H., et al., *Transcutaneous ultrasound augments lysis of arterial thrombi in vivo.* Circulation, 1996. **94**(4): p. 775-778.

148. Harpaz, D., et al., *Ultrasound accelerates urokinase-induced thrombolysis and reperfusion.* Am Heart J, 1994. **127**(5): p. 1211-1219.

149. Tsivgoulis, G., et al., *Safety and efficacy of ultrasound-enhanced thrombolysis: a comprehensive review and meta-analysis of randomized and nonrandomized studies.* Stroke, 2010. **41**(2): p. 280-7.

150. Hitchcock, K.E. and C.K. Holland, *Ultrasound-assisted thrombolysis for stroke therapy: better thrombus break-up with bubbles.* Stroke, 2010. **41**(10 Suppl): p. S50-3.

151. Alexandrov, A.V., et al., *Ultrasound-enhanced systemic thrombolysis for acute ischemic stroke.* N Engl J Med, 2004. **351**(21): p. 2170-8.

152. Zafar, A., et al., *MRI-Guided High-Intensity Focused Ultrasound as an Emerging Therapy for Stroke: A Review.* J Neuroimaging, 2019. **29**(1): p. 5-13.

153. Burgess, A., et al., *High-intensity focused ultrasound (HIFU) for dissolution of clots in a rabbit model of embolic stroke.* PLoS one, 2012. **7**(8).

154. Engelhardt, T.C., et al., *Catheter-directed ultrasound-accelerated thrombolysis for the treatment of acute pulmonary embolism.* Thromb Res, 2011. **128**(2): p. 149-154.

155. Garcia, M.J. *Endovascular management of acute pulmonary embolism using the ultrasound-enhanced ekosonic system*. in *Sem Intervent Rad*. 2015. Thieme Medical Publishers.

156. Kucher, N., et al., *Randomized, controlled trial of ultrasound-assisted catheter-directed thrombolysis for acute intermediate-risk pulmonary embolism.* Circulation, 2014. **129**(4): p. 479-486.

157. Chatterjee, S., et al., *Thrombolysis for pulmonary embolism and risk of all-cause mortality, major bleeding, and intracranial hemorrhage: a meta-analysis.* JAMA, 2014. **311**(23): p. 2414-2421.

158. Mostafa, A., et al., *Ultrasound accelerated thrombolysis in patients with acute pulmonary embolism: a systematic review and proportion meta-analysis.* Int J Cardiol, 2016. **211**: p. 27-30.

159. Engelberger, R.P. and N. Kucher, *Ultrasound-assisted thrombolysis for acute pulmonary embolism: a systematic review.* Eur Heart J, 2014. **35**(12): p. 758-64.

160. Benjamin, E.J., et al., *Heart Disease and Stroke Statistics-2018 Update: A Report From the American Heart Association.* Circulation, 2018. **137**(12): p. e67-e492.

161. Eeckhout, E. and M.J. Kern, *The coronary no-reflow phenomenon: a review of mechanisms and therapies.* Eur Heart J, 2001. **22**(9): p. 729-39.

162. Bekkers, S.C., et al., *Microvascular obstruction: underlying pathophysiology and clinical diagnosis.* J Am Coll Cardiol, 2010. **55**(16): p. 1649-60.

163. Nakano, M., et al., *Microvascular obstruction is caused by atherothrombosis in patients with acute coronary syndrome undergoing percutaneous coronary intervention*. 2011, Am Heart Assoc.

164. Schwartz, R.S., et al., *Microemboli and microvascular obstruction in acute coronary thrombosis and sudden coronary death: relation to epicardial plaque histopathology.* J Am Coll Cardiol, 2009. **54**(23): p. 2167-2173.

165. Gupta, S. and M.M. Gupta, *No reflow phenomenon in percutaneous coronary interventions in ST-segment elevation myocardial infarction.* Indian Heart J, 2016. **68**(4): p. 539-51.

166. Bouleti, C., N. Mewton, and S. Germain, *The no-reflow phenomenon: State of the art.* Arch Cardiovasc Dis, 2015. **108**(12): p. 661-74.

167. Niccoli, G., et al., *Myocardial no-reflow in humans.* J Am Coll Cardiol, 2009. **54**(4): p. 281-92.

168. Durante, A. and P.G. Camici, *Novel insights into an "old" phenomenon: the no reflow.* Int J Cardiol, 2015. **187**: p. 273-280.

169. Jaffe, R., et al., *Microvascular obstruction and the no-reflow phenomenon after percutaneous coronary intervention.* Circulation, 2008. **117**(24): p. 3152-6.

170. Kaul, S., *The "no reflow" phenomenon following acute myocardial infarction: mechanisms and treatment options.* J Cardiol, 2014. **64**(2): p. 77-85.

171. Hamirani, Y.S., et al., *Effect of microvascular obstruction and intramyocardial hemorrhage by CMR on LV remodeling and outcomes after myocardial infarction: a systematic review and meta-analysis.* JACC Cardiovasc Imaging, 2014. **7**(9): p. 940-52.

172. de Waha, S., et al., *Relationship between microvascular obstruction and adverse events following primary percutaneous coronary intervention for ST-segment elevation myocardial infarction: an individual patient data pooled analysis from seven randomized trials.* Eur Heart J, 2017. **38**(47): p. 3502-3510.

173. de Waha, S., et al., *Impact of early vs. late microvascular obstruction assessed by magnetic resonance imaging on long-term outcome after ST-elevation myocardial infarction: a comparison with traditional prognostic markers.* Eur Heart J, 2010. **31**(21): p. 2660-2668.

174. Ndrepepa, G., et al., *5-year prognostic value of no-reflow phenomenon after percutaneous coronary intervention in patients with acute myocardial infarction.* J Am Coll Cardiol, 2010. **55**(21): p. 2383-2389.

175. Khorramirouz, R., et al., *Microvascular obstruction in non-infarct related coronary arteries is an independent predictor of major adverse cardiovascular events in patients with ST segment-elevation myocardial infarction.* Int J Cardiol, 2018.

176. Mazhar, J., M. Mashicharan, and A. Farshid, *Predictors and outcome of no-reflow post primary percutaneous coronary intervention for ST elevation myocardial infarction.* Int J Cardiol Heart Vasc, 2016. **10**: p. 8-12.

177. Wu, K.C., et al., *Prognostic significance of microvascular obstruction by magnetic resonance imaging in patients with acute myocardial infarction.* Circulation, 1998. **97**(8): p. 765-772.

178. Rezkalla, S.H., et al., *Management of No-Reflow Phenomenon in the Catheterization Laboratory.* JACC Cardiovasc Interv, 2017. **10**(3): p. 215-223.

179. Jaffe, R., A. Dick, and B.H. Strauss, *Prevention and treatment of microvascular obstruction-related myocardial injury and coronary no-reflow following percutaneous coronary intervention: a systematic approach.* JACC Cardiovasc Interv, 2010. **3**(7): p. 695-704.

180. Ibáñez, B., et al., *Evolving therapies for myocardial ischemia/reperfusion injury.* J Am Coll Cardiol, 2015. **65**(14): p. 1454-1471.

181. Trifunovic, D., et al., *Management of No-Reflow*, in *Microcirculation*. 2020, Springer. p. 237-251.

182. Yadava, M., et al., *Therapeutic Ultrasound Improves Myocardial Blood Flow and Reduces Infarct Size in a Canine Model of Coronary Microthromboembolism*. J Am Soc Echocardiogr, 2019.

183. Roos, S.T., et al., *Sonothrombolysis in acute stroke and myocardial infarction: a systematic review.* 2014. **4**: p. 1-6.

184. Pacella, J.J., et al., *Treatment of microvascular micro-embolization using microbubbles and long-tone-burst ultrasound: an in vivo study.* 2015. **41**(2): p. 456-464.

185. Slikkerveer, J., et al., *Therapeutic application of contrast ultrasound in ST elevation myocardial infarction: Role in coronary thrombosis and microvascular obstruction.* Eur Heart J: Acute Cardiovascular Care, 2019. **8**(1): p. 45-53.

186. Mathias, W., et al., *Diagnostic ultrasound impulses improve microvascular flow in patients with STEMI receiving intravenous microbubbles.* J Am Coll Cardiol, 2016. **67**(21): p. 2506-2515.

187. Leeman, J.E., et al., *Effect of acoustic conditions on microbubble-mediated microvascular sonothrombolysis.* Ultrasound in Medicine and Biology, 2012. **38**(9): p. 1589-1598.

188. Cohen, M.G., et al., *Transcutaneous ultrasound-facilitated coronary thrombolysis during acute myocardial infarction.* Am J Cardiol, 2003. **92**(4): p. 454-457.

189. Hudson, M., et al., *Adjunctive transcutaneous ultrasound with thrombolysis: results of the PLUS (Perfusion by ThromboLytic and UltraSound) trial.* JACC: Cardiovascular Interventions, 2010. **3**(3): p. 352-359.

190. Yu, F.T., et al., *The Role of Nitric Oxide during Sonoreperfusion of Microvascular Obstruction.* Theranostics, 2017. **7**(14): p. 3527.

191. Gary, Z.Y., et al., *Ultrasound-Targeted Microbubble Cavitation with Sodium Nitrite Synergistically Enhances Nitric Oxide Production and Microvascular Perfusion.* Ultrasound Med Biol, 2019.

192. Istvanic, F., et al., *Sonoreperfusion therapy for microvascular obstruction: A step toward clinical translation.* Ultrasound Med Biol, 2020.

193. Roos, S.T., et al., *Unexpected high incidence of coronary vasoconstriction in the reduction of microvascular Injury using sonolysis (ROMIUS) Trial.* Ultrasound Med Biol, 2016. **42**(8): p. 1919-1928.

194. Moncada, S. and E. Higgs, *Endogenous nitric oxide: physiology, pathology and clinical relevance.* Eur J Clin Invest, 1991. **21**(4): p. 361-374.

195. Fleming, I. and R. Busse, *Molecular mechanisms involved in the regulation of the endothelial nitric oxide synthase.* Am J Physiol Regul Integr Comp Physiol, 2003. **284**(1): p. R1-R12.

196. Ignarro, L., *Nitric oxide as a unique signaling molecule in the.* J Physiol Pharm, 2002. **53**(4): p. 503-514.

197. Loscalzo, J. and G. Welch, *Nitric oxide and its role in the cardiovascular system.* Prog Cardiovasc Dis, 1995. **38**(2): p. 87-104.

198. Lei, J., et al., *Nitric oxide, a protective molecule in the cardiovascular system.* Nitric Oxide, 2013. **35**: p. 175-185.

199. Kourembanas, S., et al., *Nitric oxide regulates the expression of vasoconstrictors and growth factors by vascular endothelium under both normoxia and hypoxia.* J Clin Invest, 1993. **92**(1): p. 99-104.

200. Albrecht, E.W., et al., *Protective role of endothelial nitric oxide synthase.* J Path, 2003. **199**(1): p. 8-17.

201. Kubes, P., et al., *Nitric oxide synthesis inhibition induces leukocyte adhesion via superoxide and mast cells.* The FASEB Journal, 1993. **7**(13): p. 1293-1299.

202. Arndt, H., et al., *Mediators of leukocyte adhesion in rat mesenteric venules elicited by inhibition of nitric oxide synthesis.* Gastroenterology, 1993. **105**(3): p. 675-680.

203. Schulz, R., M. Kelm, and G. Heusch, *Nitric oxide in myocardial ischemia/reperfusion injury.* Cardiovasc Res, 2004. **61**(3): p. 402-13.

204. Fisslthaler, B. and I. Fleming, *Activation and signaling by the AMP-activated protein kinase in endothelial cells.* Circ Res, 2009. **105**(2): p. 114-27.

205. Shaul, P.W., *Regulation of endothelial nitric oxide synthase: location, location, location.* Ann Rev Physiol, 2002. **64**(1): p. 749-774.

206. Lira, V.A., et al., *Nitric oxide increases GLUT4 expression and regulates AMPK signaling in skeletal muscle.* Am J Physiol Endocrinol Metab, 2007. **293**(4): p. E1062-8.

207. Harrison, D., et al., *Endothelial mechanotransduction, nitric oxide and vascular inflammation.* J Intern Med 2006. **259**(4): p. 351-363.

208. Kuchan, M. and J.A. Frangos, *Role of calcium and calmodulin in flow-induced nitric oxide production in endothelial cells.* Am J Physiol, 1994. **266**(3): p. C628-C636.

209. Zhang, Y., et al., *AMP-activated protein kinase is involved in endothelial NO synthase activation in response to shear stress.* Arterioscler Thromb Vasc Biol, 2006. **26**(6): p. 1281-7.

210. Miyamoto, L., et al., *Nitrite Activates 5' AMP-Activated Protein Kinase-Endothelial Nitric Oxide Synthase Pathway in Human Glomerular Endothelial Cells.* Biol Pharm Bull, 2017. **40**(11): p. 1866-1872.

211. Taylor, C.A., et al., *In vivo quantification of blood flow and wall shear stress in the human abdominal aorta during lower limb exercise.* Ann Biomed Eng, 2002. **30**(3): p. 402-408.

212. Levine, Y.C., G.K. Li, and T. Michel, *Agonist-modulated regulation of AMP-activated protein kinase (AMPK) in endothelial cells. Evidence for an AMPK -> Rac1 -> Akt -> endothelial nitric-oxide synthase pathway.* J Biol Chem, 2007. **282**(28): p. 20351-64.

213. Reihill, J.A., et al., *AMP-activated protein kinase mediates VEGF-stimulated endothelial NO production.* Biochem Biophys Res Commun, 2007. **354**(4): p. 1084-8.

214. Zhang, J., et al., *Identification of nitric oxide as an endogenous activator of the AMP-activated protein kinase in vascular endothelial cells.* J Biol Chem, 2008. **283**(41): p. 27452-61.

215. Deshmukh, A.S., et al., *Nitric oxide increases cyclic GMP levels, AMP-activated protein kinase (AMPK)alpha1-specific activity and glucose transport in human skeletal muscle.* Diabetologia, 2010. **53**(6): p. 1142-50.

216. Cosby, K., et al., *Nitrite reduction to nitric oxide by deoxyhemoglobin vasodilates the human circulation.* Nat Med, 2003. **9**(12): p. 1498-505.

217. Lundberg, J.O., E. Weitzberg, and M.T. Gladwin, *The nitrate-nitrite-nitric oxide pathway in physiology and therapeutics.* Nat Rev Drug Discov, 2008. **7**(2): p. 156-67.

218. Gladwin, M.T., et al., *The emerging biology of the nitrite anion.* Nat Chem Biol, 2005. **1**(6): p. 308-314.

219. Kim-Shapiro, D.B. and M.T. Gladwin, *Mechanisms of nitrite bioactivation.* Nitric Oxide, 2014. **38**: p. 58-68.

220. Webb, A.J., et al., *Mechanisms underlying erythrocyte and endothelial nitrite reduction to nitric oxide in hypoxia: role for xanthine oxidoreductase and endothelial nitric oxide synthase.* Circ Res, 2008. **103**(9): p. 957-964.

221. Baker, J.E., et al., *Nitrite confers protection against myocardial infarction: role of xanthine oxidoreductase, NADPH oxidase and K(ATP) channels.* J Mol Cell Cardiol, 2007. **43**(4): p. 437-44.

222. Shiva, S., et al., *Nitrite augments tolerance to ischemia/reperfusion injury via the modulation of mitochondrial electron transfer.* J Exp Med, 2007. **204**(9): p. 2089-102.

223. Dezfulian, C., et al., *Nitrite therapy is neuroprotective and safe in cardiac arrest survivors.* Nitric Oxide, 2012. **26**(4): p. 241-50.

224. Pluta, R.M., et al., *Nitrite infusions to prevent delayed cerebral vasospasm in a primate model of subarachnoid hemorrhage.* JAMA, 2005. **293**(12): p. 1477-1484.

225. Blood, A.B., et al., *Inhaled nitrite reverses hemolysis-induced pulmonary vasoconstriction in newborn lambs without blood participation.* Circulation, 2011. **123**(6): p. 605-612.

226. Duranski, M.R., et al., *Cytoprotective effects of nitrite during in vivo ischemia-reperfusion of the heart and liver.* J Clin Invest, 2005. **115**(5): p. 1232-40.

227. Gonzalez, F.M., et al., *Nitrite anion provides potent cytoprotective and antiapoptotic effects as adjunctive therapy to reperfusion for acute myocardial infarction.* Circulation, 2008. **117**(23): p. 2986-94.

228. Jones, D.A., et al., *Randomized phase 2 trial of intracoronary nitrite during acute myocardial infarction.* Circ Res, 2015. **116**(3): p. 437-447.

229. Pluta, R.M., et al., *Safety and feasibility of long-term intravenous sodium nitrite infusion in healthy volunteers.* PLoS one, 2011. **6**(1): p. e14504.

230. Freeman, B.A., et al., *Nitro-fatty acid formation and signaling.* J Biol Chem, 2008. **283**(23): p. 15515-9.

231. Buchan, G.R., et al., *Nitro-fatty acid formation and metabolism.* Nitric Oxide, 2018. **79** p.38-44.

232. Woodcock, S.R., et al., *Nitrated fatty acids: synthesis and measurement.* Free Radic Biol Med, 2013. **59**: p. 14-26.

233. Villacorta, L., et al., *Nitro-fatty acids in cardiovascular regulation and diseases: characteristics and molecular mechanisms.* Front Biosci, 2016. **21**: p. 873.

234. Nadtochiy, S.M., et al., *Mitochondrial nitroalkene formation and mild uncoupling in ischaemic preconditioning: implications for cardioprotection.* Cardiovasc Res, 2009. **82**(2): p. 333-40.

235. Rudolph, V., et al., *Endogenous generation and protective effects of nitro-fatty acids in a murine model of focal cardiac ischaemia and reperfusion.* Cardiovasc Res, 2010. **85**(1): p. 155-66.

236. Kansanen, E., et al., *Nrf2-dependent and -independent responses to nitro-fatty acids in human endothelial cells: identification of heat shock response as the major pathway activated by nitro-oleic acid.* J Biol Chem, 2009. **284**(48): p. 33233-41.

237. Rubbo, H., *Nitro-fatty acids: novel anti-inflammatory lipid mediators.* Braz J Med Biol Res, 2013. **46**(9): p. 728-34.

238. Rom, O., et al., *Inflammatory signaling and metabolic regulation by nitro-fatty acids.* Nitric Oxide, 2018. **78**: p. 140-145.

239. Schopfer, F.J., et al., *Nitro-fatty acids: new drug candidates for chronic inflammatory and fibrotic diseases.* Nitric Oxide, 2018. **79**: p. 31-37.

240. Mollenhauer, M., D. Mehrkens, and V. Rudolph, *Nitrated fatty acids in cardiovascular diseases.* Nitric Oxide, 2018.

241. Vijayan, V., et al., *Heme oxygenase-1 as a therapeutic target in inflammatory disorders of the gastrointestinal tract.* World J. Gastroenterol, 2010. **16**(25): p. 3112.

242. Ma, Q., *Role of nrf2 in oxidative stress and toxicity.* Ann Rev Pharm Toxicol, 2013. **53**: p. 401-426.

243. Khoo, N.K., et al., *Activation of vascular endothelial nitric oxide synthase and heme oxygenase-1 expression by electrophilic nitro-fatty acids.* Free Radic Biol Med, 2010. **48**(2): p. 230-9.

244. Shin, E., et al., *Nitrooleate mediates nitric oxide synthase activation in endothelial cells.* Lipids, 2014. **49**(5): p. 457-66.

245. Schopfer, F.J., et al., *Nitrolinoleic acid: an endogenous peroxisome proliferator-activated receptor gamma ligand.* Proc Natl Acad Sci U S A, 2005. **102**(7): p. 2340-5.

246. Rudolph, T.K., et al., *Nitro-fatty acids reduce atherosclerosis in apolipoprotein E-deficient mice.* Arterioscler Thromb Vasc Biol, 2010. **30**(5): p. 938-45.

247. Zhang, J., et al., *Nitro-oleic acid inhibits angiotensin II-induced hypertension.* Circ Res, 2010. **107**(4): p. 540-8.

248. Villacorta, L., et al., *Electrophilic nitro-fatty acids inhibit vascular inflammation by disrupting LPS-dependent TLR4 signalling in lipid rafts.* Cardiovasc Res, 2013. **98**(1): p. 116-24.

249. Rudolph, T.K., et al., *Nitrated fatty acids suppress angiotensin II-mediated fibrotic remodelling and atrial fibrillation.* Cardiovasc Res, 2016. **109**(1): p. 174-84.

250. Smith, S.C., et al., *ACC/AHA/SCAI 2005 guideline update for percutaneous coronary intervention: a report of the American College of Cardiology/American Heart Association Task Force on Practice Guidelines (ACC/AHA/SCAI writing committee to update the 2001 guidelines for percutaneous coronary intervention).* J Am Coll Cardiol, 2006. **47**(1): p. e1-e121.

251. Galli, A. and F. Lombardi, *Postinfarct Left Ventricular Remodelling: A Prevailing Cause of Heart Failure.* Cardiol Res Pract, 2016. **2016**: p. 2579832.

252. Chen, X., et al., *New insights into mechanisms of sonothrombolysis using ultra-high-speed imaging.* Ultrasound Med Biol, 2014. **40**(1): p. 258-262.

253. Reffelmann, T. and R.A.J.B.r.i.c. Kloner, *The no-reflow phenomenon: a basic mechanism of myocardial ischemia and reperfusion.* Basic Res Cardiol, 2006. **101**(5): p. 359-372.

254. Tousoulis, D., et al., *The role of nitric oxide on endothelial function.* Curr Vasc Pharm, 2012. **10**(1): p. 4-18.

255. Bolli, R., *Cardioprotective function of inducible nitric oxide synthase and role of nitric oxide in myocardial ischemia and preconditioning: an overview of a decade of research.* J Mol Cell Cardiol, 2001. **33**(11): p. 1897-918.

256. Wei, K., et al., *Quantification of myocardial blood flow with ultrasound-induced destruction of microbubbles administered as a constant venous infusion.* Circulation, 1998. **97**(5): p. 473-483.

257. Hudson, J.M., R. Karshafian, and P.N. Burns, *Quantification of flow using ultrasound and microbubbles: a disruption replenishment model based on physical principles.* Ultrasound Med Biol, 2009. **35**(12): p. 2007-2020.

258. MacArthur, P.H., S. Shiva, and M.T. Gladwin, *Measurement of circulating nitrite and S-nitrosothiols by reductive chemiluminescence.* J Chromatogr B, 2007. **851**(1-2): p. 93-105.

259. Pelletier, M.M., et al., *The measurement of blood and plasma nitrite by chemiluminescence: pitfalls and solutions.* Free Rad Biol Med, 2006. **41**(4): p. 541-548.

260. Postema, M., et al., *Ultrasound-induced encapsulated microbubble phenomena.* Ultrasound Med Biol, 2004. **30**(6): p. 827-840.

261. Higashi, Y., et al., *Endothelial function and oxidative stress in cardiovascular diseases.* Circ J, 2009. **73**(3): p. 411-418.

262. Reznick, A.Z. and L. Packer, *Oxidative damage to proteins: spectrophotometric method for carbonyl assay*, in *Methods in enzymology*. 1994, Elsevier. p. 357-363.

263. Halliwell, B., *Reactive oxygen species in living systems: source, biochemistry, and role in human disease.* Am J Med, 1991. **91**(3): p. S14-S22.

264. Dalle-Donne, I., et al., *Protein carbonyl groups as biomarkers of oxidative stress.* Clin Chim Act, 2003. **329**(1-2): p. 23-38.

265. Li, C. and R.M. Jackson, *Reactive species mechanisms of cellular hypoxia-reoxygenation injury.* Am J Physiol, 2002. **282**(2): p. C227-C241.

266. Juffermans, L.J., et al., *Ultrasound and microbubble-induced intra- and intercellular bioeffects in primary endothelial cells.* Ultrasound Med Biol, 2009. **35**(11): p. 1917-27.

267. Belcik, J.T., et al., *Augmentation of Limb Perfusion and Reversal of Tissue Ischemia Produced by Ultrasound-Mediated Microbubble Cavitation.* Circ Cardiovasc Imag, 2015. **8**(4): p. e002979.

268. Xie, F., et al., *Coronary and microvascular thrombolysis with guided diagnostic ultrasound and microbubbles in acute ST segment elevation myocardial infarction.* J Am Soc Echocardiogr, 2011. **24**(12): p. 1400-1408.

269. Belcik, J.T., et al., *Augmentation of Muscle Blood Flow by Ultrasound Cavitation Is Mediated by ATP and Purinergic Signaling.* Circulation, 2017. **135**(13): p. 1240-1252.

270. Suchkova, V.N., et al., *Ultrasound improves tissue perfusion in ischemic tissue through a nitric oxide dependent mechanism.* Thromb Haemost, 2002. **87**(05): p. 865-870.

271. Siegel, R.J., et al., *Ultrasound energy improves myocardial perfusion in the presence of coronary occlusion.* J Am Coll Cardiol, 2004. **44**(7): p. 1454-1458.

272. Kuroki, I., et al., *Effect of sodium nitroprusside on ischemia-reperfusion injuries of the rat liver*. Hepto-gastroenterol, 2004. **51**(59): p. 1404-1407.

273. Johanning, R.J., et al., *A retrospective study of sodium nitroprusside use and assessment of the potential risk of cyanide poisoning.* Pharmacotherapy, 1995. **15**(6): p. 773-777.

274. Carson, A.R., et al., *Gene therapy of carcinoma using ultrasound-targeted microbubble destruction.* Ultrasound Med Biol 2011. **37**(3): p. 393-402.

275. Carson, A.R., et al., *Ultrasound-targeted microbubble destruction to deliver siRNA cancer therapy.* Cancer research, 2012.

276. Kopechek, J.A., et al., *Ultrasound targeted microbubble destruction-mediated delivery of a transcription factor decoy inhibits STAT3 signaling and tumor growth.* Theranostics, 2015. **5**(12): p. 1378.

277. Kopechek, J.A., et al., *Cardiac gene expression knockdown using small inhibitory RNA-loaded microbubbles and ultrasound.* PLoS one, 2016. **11**(7): p. e0159751.

278. Yu, F.T., et al., *Low Intensity Ultrasound Mediated Liposomal Doxorubicin Delivery Using Polymer Microbubbles.* Mol Pharm, 2016. **13**(1): p. 55-64.

279. Cui, T., et al., *Nitrated fatty acids: Endogenous anti-inflammatory signaling mediators.* J Biol Chem, 2006. **281**(47): p. 35686-98.

280. Baker, P.R., et al., *Fatty acid transduction of nitric oxide signaling: multiple nitrated unsaturated fatty acid derivatives exist in human blood and urine and serve as endogenous peroxisome proliferator-activated receptor ligands.* J Biol Chem, 2005. **280**(51): p. 42464-75.

281. Cole, M.P., et al., *Nitro-fatty acid inhibition of neointima formation after endoluminal vessel injury.* Circ Res, 2009. **105**(10): p. 965-72.

282. Koudelka, A., et al., *Nitro-Oleic Acid Prevents Hypoxia- and Asymmetric Dimethylarginine-Induced Pulmonary Endothelial Dysfunction.* Cardiovasc Drugs Ther, 2016. **30**(6): p. 579-586.

283. Ambrozova, G., et al., *Nitro-oleic acid modulates classical and regulatory activation of macrophages and their involvement in pro-fibrotic responses.* Free Radic Biol Med, 2016. **90**: p. 252-260.

284. Nadtochiy, S.M., et al., *Nitroalkenes confer acute cardioprotection via adenine nucleotide translocase 1*. J Biol Chem, 2012. **287**(5): p. 3573-80.

285. Schopfer, F.J., et al., *Fatty acid transduction of nitric oxide signaling Nitrolinoleic acid is a hydrophobically stabilized nitric oxide donor*. J Biol Chem, 2005. **280**(19): p. 19289-19297.

286. Yu, F.T., et al., *Low intensity ultrasound mediated liposomal doxorubicin delivery using*